Analysis of mass variations in Greenland by a novel variant of the mascon approach

Ran, Jiangjun

Important note
To cite this publication, please use the final published version (if applicable).
Please check the document version above.

Analysis of mass variations in Greenland by a novel variant of the mascon approach

Jiangjun RAN

Analysis of mass variations in Greenland by a novel variant of the mascon approach

Proefschrift

ter verkrijging van de graad van doctor
aan de Technische Universiteit Delft,
op gezag van de Rector Magnificus prof.ir. K.C.A.M Luyben,
voorzitter van het College voor Promoties,
in het openbaar te verdedigen op donderdag 6 juli 2017 om 12:30 uur

door

Jiangjun RAN

Bachelor of Engineering in Surveying and Mapping Engineering
Southwest Jiaotong University, China
geboren te Chongqing, China

Dit proefschrift is goedgekeurd door de

promotor: Prof. Dr. -Ing. habil. R. Klees
copromotor: Dr. ir. P.G. Ditmar

Samenstelling promotiecommissie:

Rector Magnificus,	voorzitter
Prof. Dr. -Ing. habil. R. Klees,	Technische Universiteit Delft
Dr. ir. P.G. Ditmar,	Technische Universiteit Delft

Onafhankelijke leden:

Prof.Dr. M.R. van den Broeke,	Utrecht University
Prof.Dr.-Ing. J. Kusche,	Universität Bonn
Prof.Dr.-Ing. N. Sneeuw,	Universität Stuttgart
Prof.Dr.ir. R.F. Hanssen,	Technische Universiteit Delft
Prof. M. Zhong,	Institute of Geodesy and Geophysics, Chinese Academy of Sciences
Prof.Dr. L.L.A. Vermeersen,	Technische Universiteit Delft, reservelid

To my parents

Summary

The Greenland ice sheet (GrIS) is currently losing mass, as a result of complex mechanisms of ice-climate interaction that need to be understood for reliable projections of future sea level rise. The thesis focuses on the estimation of mass anomalies in Greenland using data from the GRACE satellite gravity mission. Monthly GRACE gravity field solutions are post-processed using a new variant of the "mascon approach". Greenland is covered with multiple distinctive "mascons", assuming the mass anomalies within each one are laterally-homogeneous.

Gravity disturbances at mean satellite altitude are synthesized from the GRACE spherical harmonic coefficients. They are used as pseudo-observations to estimate the mascon mass anomalies using weighted least-squares techniques. No regularization is applied. The full noise covariance matrix of gravity disturbances is propagated from the full noise covariance matrix of spherical harmonic coefficients using the law of covariance propagation. Those matrices represent a complete stochastic description of random noise in the data, provided that it is Gaussian. The inverse noise covariance matrix is used as a weight matrix in the weighted least-squares estimate of the mascon mass anomalies. The limited spectral content of the gravity disturbances is accounted for by applying a low-pass filter to the design matrix providing a spectrally consistent functional model.

Using numerical experiments with simulated signal and data, we demonstrate the importance of the data weighting and of the spectral consistency between the mascon model and the pseudo-observations. The developed methodology is applied to process real GRACE data using CSR RL05 monthly gravity field solutions with full noise covariance matrices. We distinguish five GrIS drainage systems. The obtained mass anomaly estimates per mascon are integrated over individual drainage systems, as well as over entire Greenland. We find that using a weighted least-squares estimator reduces random noise in the estimates by factors ranging from 1.5 to 3.0, depending on the drainage system. Furthermore, we compare the de-trended mascon mass anomaly time-series with similar time-series from the Regional Atmospheric Climate Model (RACMO 2.3), which describes the Surface Mass Balance (SMB). We show that the weighted least-squares estimate reduces the discrepancies between the time-series by 24%–47%.

Then, we combine GRACE mass anomaly estimates, SMB model outputs, and ice discharge data to systematically analyze the mass budget of Greenland at various temporal and spatial scales. Among others, we reveal a substantial seasonal meltwater storage, which peaks in July, reaching in total 100 ± 20 Gt. Meltwater storage is particularly intense in the northern, northwestern and southeastern drainage systems. An analysis of outlet glacier velocities shows that the contribution of ice discharge to the seasonal mass variations is minor, at a level of only a few Gt. In addition, we propose a simple way

to use GRACE data for validating SMB model outputs in winter, based on the fact that ice discharge cannot be negative.

Finally, we use numerical simulations and real data to identify the optimal GRACE data processing strategy (primarily the size of the mascons) for three temporal scales of interest: monthly mass anomalies, mean mass anomalies per calendar month, and long-term linear trends. We show that the two major contributors to the error budgets are random errors and parameterization (model) errors; the latter are caused by a spatial variability of actual mass anomalies within individual mascons. We find that the errors in long-term linear trend estimates are mainly caused by the parameterization errors, and that accurate estimates require small size mascons in combination with the ordinary least-squares estimator. The error budget of mean mass anomalies per calendar month is dominated by the parameterization error when the size of mascons is large and by random errors otherwise. Hence, accurate estimates require mascons of intermediate size in combination with a weighted least-squares estimator. Finally, we find that random errors are the dominant error source in monthly mass anomalies. We advise to use in this case large mascons and a weighted least-squares estimator.

Our new variant of the mascon approach and the results of this thesis can be used in support of future research on GrIS hydrology, glacier dynamics, and surface mass balance, as well as their mutual interactions.

Contents

1

Introduction

1.1. Background

Earth's climate is rapidly changing, causing, among others, the sea level rise, with potentially severe impacts on coastal areas all over the world. One major contribution to sea level rise is the melting of ice of the Greenland ice sheet (GrIS) and the Antarctic ice sheet (AIS). In the last 10 years, the GrIS has become one of the largest contributors to sea level rise, with 0.7-1.1 mm/yr out of 3.2 mm/yr (see e.g., *Shepherd et al.*, 2012; *Jacob et al.*, 2012; *Stocker et al.*, 2013; *Moon et al.*, 2014; *Khan et al.*, 2015).

The GrIS, whose area is about 1, 710, 000 square kilometers, is smaller than the AIS, but its mass loss rate is much larger than that of the AIS. More importantly, there are indications that the GrIS mass loss is accelerating in the last 15 years (*Velicogna and Wahr*, 2006; *Velicogna*, 2009; *Velicogna et al.*, 2014; *Schrama et al.*, 2014; *Chen et al.*, 2006). If this tendency continues, its contribution to the overall sea level budget will be even more significant in the future. Therefore, the status of the GrIS is receiving increasing attention in the scientific community (*Khan et al.*, 2015).

The mass loss of the GrIS is a combined effect of ice discharge and changes in surface mass balance (SMB). Ice discharge refers to the dynamic ice loss via outlet glaciers. It is usually derived from ice flow velocities provided by satellite interferometric synthetic-aperture radar (InSAR) data and ice thickness measurements at flux gates. It can also be simulated by ice flow models, e.g., the Ice Sheet System Model (ISSM) (*Larour et al.*, 2012). Ice discharge manifests itself as a long-term trend with small seasonal variations (*van den Broeke et al.*, 2009). SMB is defined as the residual of total precipitation (rain and snow), meltwater runoff, and sublimation. SMB-related mass changes of the GrIS vary temporally and spatially. Most of them concentrate in the narrow coastal areas of Greenland and show strong inter- and intra-annual variations. SMB-related mass changes can be simulated by a climate model, e.g., the Regional Atmospheric Climate Model (RACMO 2.3) (*Noël et al.*, 2015) and the Community Earth System Model (CESM) (*Gent et al.*, 2011). Future projections of both ice discharge and SMB-related mass changes are based on models. Even a small bias in a model may have a large impact on future projections. Therefore, the proper validation and calibration of the models are critical.

To that purpose, satellite gravimetry is one of the best sources of independent information about changes in mass of the GrIS, as it is the only method which directly

measures mass changes over time, with just a limited number of assumptions. In this thesis, satellite gravimetry refers to measurements by the Gravity Recovery And Climate Experiment (GRACE) satellite gravity mission, as it is the only satellite gravity mission which can continuously monitor Earth's mass variations with relatively high spatial and temporal resolutions. Typically, GRACE data are used to compute monthly gravity field solutions consisting of Spherical Harmonic Coefficients (SHCs) complete to some maximum degree, e.g., 96 for the CSR RL05 solutions (*Bettadpur*, 2012) or 90 for GFZ RL05 solutions (*Dahle et al.*, 2012). Alternatively, monthly gravity solutions in terms of mass anomalies per mass concentration block ("mascon") have also been released by Jet Propulsion Laboratory (JPL) (*Watkins et al.*, 2015), Goddard Space Flight Center (GSFC) (*Luthcke et al.*, 2013) and CSR (*Save et al.*, 2016). To clean monthly SHCs for the contribution of high-frequency mass variations, an ocean tide model (e.g., EOT11a (*Savcenko and Bosch*, 2010)), a model of non-tidal components of the atmospheric and oceanic mass variations (e.g., the Atmosphere and Ocean De-aliasing model (AOD) (*Dobslaw et al.*, 2013)), and other background models are routinely being used. Since the sensitivity of GRACE is anisotropic, monthly SHCs are strongly contaminated by north-south "stripes". The amplitude of the "stripes" depends on the latitude with smaller amplitudes in polar areas and larger amplitudes around the equator.

The conversion of gravity field variations into mass anomalies at the Earth's surface can be performed by a proper scaling of the SHCs (*Wahr et al.*, 1998). In order to suppress stripes and high-frequency noise in the solutions, low-pass filters and/or de-striping schemes are frequently used (*Jekeli*, 1981; *Wahr et al.*, 1998; *Swenson and Wahr*, 2006). Among the problems caused by spatial filtering are a reduction of the spatial resolution, distortions of the derived mass anomalies, and signal leakage to areas surrounding the area where the mass change occurred (*Bonin and Chambers*, 2013).

Alternatively to the estimation of SHCs, mass anomalies can be estimated for a set of pre-defined regions, which are called "mascons". Low-pass filters and de-striping can be avoided in the mascon approach. High-frequency noise in the SHCs is suppressed by using some realistic assumptions, like the one that a mass anomaly as a function of geographical coordinates is constant within a given mascon. Furthermore, the geometry of the mascons can be chosen to take into account available physical constraints, like the geometry of the coastal line. All this mitigates signal distortions and may allow a relatively high spatial resolution to be achieved. A side effect of the mascon approach, however, is that it comes with a parameterization error, i.e., a mismatch between the assumption of uniformly mass distribution inside each mascon and the continuous mass change signal in reality.

Originally, the mascon representation was proposed by *Muller and Sjogren* (1968) in their efforts to model the static gravity field of the Moon. *Luthcke et al.* (2006a) used this idea to derive mass anomalies from GRACE K-band Ranging (KBR) data. Variants of the mascon approach which use monthly solutions in terms of SHCs as input were proposed by *Forsberg and Reeh* (2007), *Baur and Sneeuw* (2011) and *Schrama and Wouters* (2011). According to them, monthly SHCs are used to synthesize gravity data (e.g., gravity

disturbances, water thickness values). After that, the mass anomalies per mascon are derived by means of a least-squares adjustment.

In the course of last 10 years, GRACE data have been widely utilized to investigate the mass balance of GrIS. *Velicogna and Wahr* (2005) was the first to derive the ice loss rate in 2002-2004, which was $-75 \pm 26\ Gt/yr$. After this, *Velicogna and Wahr* (2006) and *Chen et al.* (2006) reported that GrIS was losing mass with an acceleration in the southern part. In 2003-2013, the linear mass loss trends of GrIS estimated by both *Velicogna et al.* (2014) and *Schrama et al.* (2014) were around -280 Gt/yr, which is equivalent to ~ 0.8 mm/yr sea level rise. The mass loss is concentrated in the northwest and southeast parts of Greenland.

1.2. Research motivation

Even though previous works have provided much new information on the GrIS mass balance, there are still many open issues which need further investigations. Firstly, by now, most of the studies on the mass balance of the GrIS using GRACE focus on either the long-term trend or the acceleration (see e.g., *Wouters et al.*, 2008, 2013; *Shepherd et al.*, 2012; *Velicogna et al.*, 2014; *van den Broeke et al.*, 2009; *Schrama et al.*, 2014; *Chen et al.*, 2006; *Jacob et al.*, 2012; *Baur and Sneeuw*, 2011). In order to better understand mass changes of the GrIS and related control mechanisms, an investigation of the intra-annual mass variation of GrIS is required.

Secondly, mass anomalies obtained by the existing variants of the mascon approach are statistically sub-optimal, in the sense that spatial correlations of random noise in SHCs are not taken into account. This random noise is strongly correlated due to the aforementioned anisotropic sensitivity of GRACE. However, so far, it is not known yet to what extent mass anomalies of the GrIS are improved when taking the noise correlations into account.

Furthermore, the spectrum of the synthesized GRACE-based gravity data is limited to the maximum spherical harmonic degree of the monthly solutions, whereas the mascon representation is more flexible in that sense. However, when using mascons, one has to force explicitly a spectral consistency between the monthly GRACE solution and the functional model. This has not been done yet.

Finally, when using mascons, the estimated mass anomalies strongly depend on the chosen parameterization, i.e, number and the geometry of the mascons. In the past, two typical approaches to the parameterization were used. A commonly-used "geophysical" approach is based on the geometry of GrIS drainage systems. In that case, each mascon is formed as a combination of several neighboring drainage systems. For instance, *Luthcke et al.* (2006a) divided GrIS into 6 mascons. Each mascon was further split into two parts: above and below 2000-m elevation. A disadvantage of this approach is that it is not sufficiently flexible. The mascon size is defined a priori and can hardly be adjusted in line with the actual spatial resolution of GRACE data. Another common approach

is "geometrical": the GrIS is split into blocks of a regular shape (e.g., equal-angular or equal-area) (*Rowlands et al.*, 2005; *Luthcke et al.*, 2013; *Schrama et al.*, 2014; *Baur and Sneeuw*, 2011). In this case, however, it is problematic to take into account the geometry of the coast line. An additional disadvantage of equal-angular blocks is that their areas depend on the latitude: the blocks in the north of Greenland are much smaller than those in the south of Greenland. This does not allow the choice of a parameterization of the GrIS which is optimally adapted to the spatial resolution of GRACE data. Therefore, the optimal parameterization of the GrIS still needs further investigations.

1.3. Research objectives

The primary objective of this thesis is to better understand the mass balance of the GrIS at high spatial resolution using satellite gravimetry, supported with satellite altimetry, a regional climate model, and InSAR data. To that end, we

- investigate the intra-annual mass variations for the whole GrIS and for individual drainage systems, by combing GRACE- and SMB- based estimates.

- derive statistically-optimal mass anomalies from monthly GRACE level-2 products. For this purpose, an adjusted mascon approach is to be developed based on the mascon variants proposed by *Forsberg and Reeh* (2007) and *Baur and Sneeuw* (2011), which uses the full noise covariance matrix of monthly SHCs and propagates them into full noise variance covariance matrices of the synthesized gravity data using the law of covariance propagation. The latter are used when estimating the mascon coefficients using weighted least-squares techniques.

- re-formulate the functional model of the mascon approach in order to make it spectrally consistent with monthly SHCs.

- understand the performance of the proposed methodology, by conducting a well-designed numerical study and validating the results using independent data.

- propose a parameterization of the GrIS, which better exploits the resolution of GRACE data, by taking appropriate physical constraints into account.

- investigate the optimal choice of the mascon size depending on temporal scale.

1.4. Outline

The thesis is organized as follows.

In Chapter 2, we briefly describe the types and distribution of glaciers of the GrIS. After that, the methods currently used to estimate the mass anomalies of the GrIS, i.e., satellite altimetry, the Input-Output method and satellite gravimetry, are briefly discussed. More importantly, the state-of-the-art of the mass balance of the GrIS estimated by different methods is discussed as well. It is worth to mention that this Chapter is dedicated to a

1

general review of what is known about the state of the GrIS. More detailed introductions of different research questions are given in later Chapters.

Chapter 3 focuses on a review of the mascon approach and its variants, which aim to estimate the mass variations of the GrIS from GRACE data with a high spatial resolution. In particular, the advantages and disadvantages of each variant are discussed in details.

In order to produce statistically-optimal mass anomaly estimates of GrIS from monthly SHCs, an adjusted mascon approach is developed in Chapter 4. Novel elements include the optimal data weighting, a scheme for an automatic division of the GrIS into equal area mascons, and the spectral consistency of the functional model with monthly SHCs. Then GrIS mass anomalies obtained with this approach are validated with independent estimates produced by RACMO 2.3.

Using the optimal data processing scheme, the seasonal mass anomalies of the GrIS are obtained from GRACE in Chapter 5. In particular, it is discussed to what extent the SMB contributes to the total mass variations observed by GRACE at intra-annual scales. Furthermore, using ice discharge observations at multi-year scale, this Chapter presents an attempt to close the budgets of long-term linear trends and accelerations of GrIS mass variations. Based on the monthly ice discharge computed by ice velocities and ice thickness values of outlet glaciers, the contribution of ice discharge seasonality to variations of the Greenland mass balance during summer is quantified.

In order to understand the optimal parameterization, Chapter 6 analyzes the impact of parameterization on the mass anomaly estimates from GRACE at different temporal scales, i.e., monthly, intra-annual and multi-year scales.

In Chapter 7, we conclude by emphasizing the main findings and identifying topics for future research.

2

GrIS mass variation: an overview

2.1. Introduction

On-going mass loss of the GrIS has drawn the attention of the scientific community, among others due to its potential to exacerbate sea level rise in the future. In this Chapter, we will firstly review the types of glaciers in Greenland and their distribution. Next, an introduction into the GrIS mass balance is given. After that, the methods used to estimate GrIS mass variations are discussed. Note that this chapter aims to give a basic overview of GrIS mass balance. Further information related to each specific research question is presented in the introduction section of later chapters.

2.2. GrIS Glaciers

Outlet glaciers of the GrIS can be divided into land-terminating glaciers, ice-shelf-terminating glaciers, and marine-terminating glaciers (cf. Fig. 2.1). A land-terminating glacier has a terminus on land. On Greenland, the land-terminating glaciers are mainly located in the southwest, though a few are also located in the northeast. Their velocities are around 10-100 m/yr (*Moon et al.*, 2012). An ice-shelf-terminating glacier means a glacier with floating tongue in the ocean. There are only a few large ice-shelf-terminating glaciers on Greenland, which are primarily located in the northern part of Greenland. Mean velocities of ice-shelf-terminating glaciers are generally around 300-1670 m/yr. Marine-terminating glaciers, like ice-shelf-terminating glaciers, have termini in the ocean, but do not form floating tongues (cf. Fig. 2.2). Figure 2.2 shows an extra floating tongue for the ice-shelf-terminating glacier outside the grounding line, compared with the marine-terminating glacier. Note that the grounding line is the boundary where the floating tongue begins. Most glaciers in GrIS are marine-terminating glaciers and are common in the northwest and southeast of Greenland. The mean velocities of the marine-terminating glaciers are 2830 m/yr and 1630 m/yr, respectively (*Moon et al.*, 2012). Some glaciers in the northern part of Greenland are marine-terminating, as well. However, their flow velocities are quite small, i.e., <200 m/yr.

2.3. Mass balance of the Greenland ice sheet

This section is dedicated to the mass balance of the GrIS, which can be divided into two parts, i.e., the surface mass balance and the ice discharge. As shown in Fig. 2.3, the GrIS gains mass from snow fall (~94%) and rain fall (~6%) (*Ettema et al.*, 2009a).
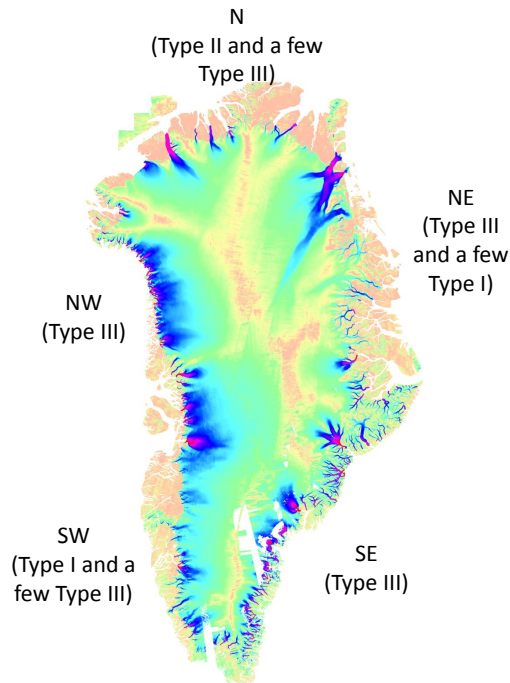
Figure 2.1: Schematic view of three types of GrIS outlet glaciers. Type I stands for land-terminating glaciers, whereas Type II and III refer to ice-shelf-terminating glaciers and marine-terminating glaciers, respectively. The velocity map over 2007-2010 by *Moon et al.* (2012) is shown as a background.
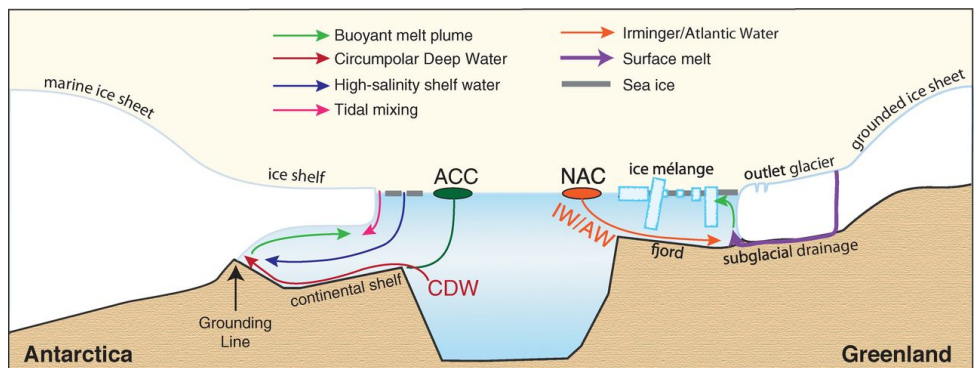
Figure 2.2: Schematic view at an ice-shelf-terminating glacier (left) and a marine-terminating glacier (right) (*Joughin et al.*, 2012)

Part of the rain water runs off, while the other penetrates to deeper layers. The snow at the top of a glacier gradually becomes firn, and finally is compacted as ice. The surface mass balance also depends on the processes related to ablation, e.g., runoff (~90%) and

sublimation/evaporation (~10%) (*Ettema et al.*, 2009a). During periods with positive air temperature and strong solar radiation, a part of snow/ice melts and becomes liquid water. The melt water is divided into two parts. One part forms surface runoff. The other part penetrates down to deeper layers, where much of the water is refrozen or retained. In addition, there is still water that penetrates to the ice-bedrock interface and forms deep runoff.

2
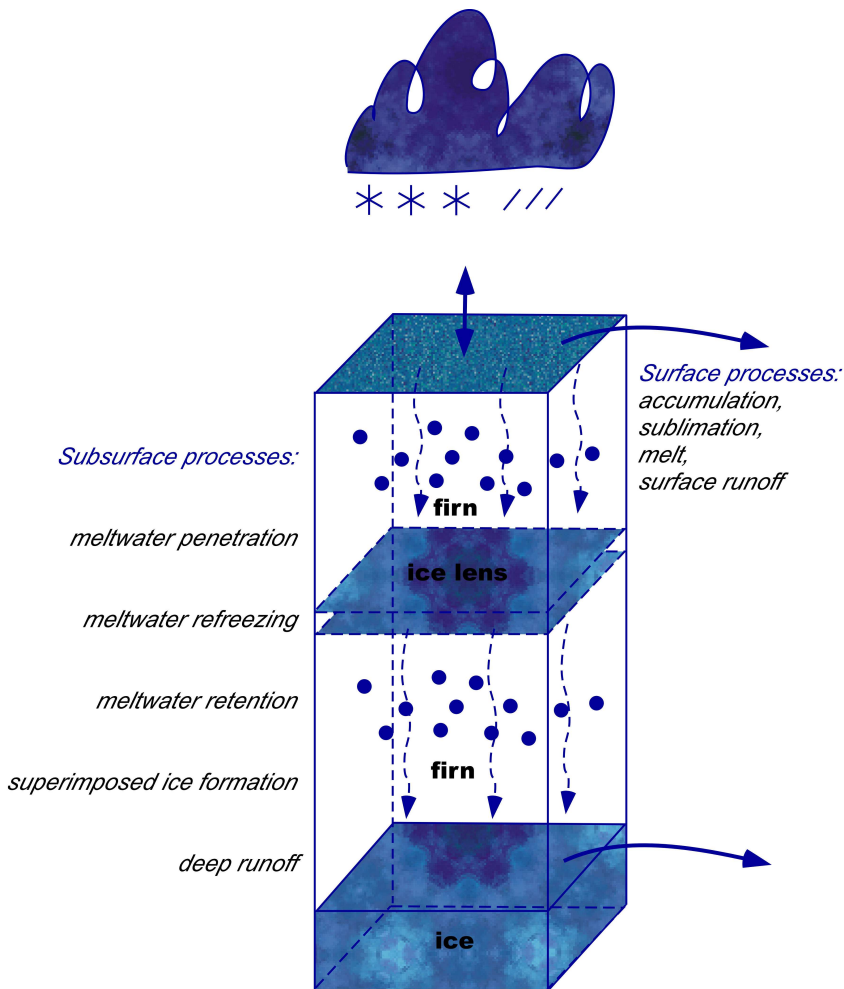
Figure 2.3: Processes represented by the surface mass balance model (*Ettema et al.*, 2009a)

In summary, the GrIS accumulates mass via snow fall (SN) and rain fall (RA) and loses mass by melt water runoff (RU), sublimation (SU), evaporation (EV), and ice discharge (ID). By comparing the input and output using Eq. (2.1), the mass balance of the GrIS,

$\frac{dM}{dt}$, can be written as

$$\frac{dM}{dt} = SN + RA - SU - RU - EV - ID. \tag{2.1}$$

2.4. GrIS mass variation estimation

The widely used tools to estimate the mass balance of the GrIS are satellite altimetry, the Input-Output Method (IOM), and satellite gravimetry (see e.g., *Zwally*, 2002; *van den Broeke et al.*, 2009; *Tapley et al.*, 2004). A brief introduction of the three methods is given below.

2.4.1. Altimetry

Since 1978, space-borne radar missions have been widely used to derive the surface elevation changes of polar ice sheets (*Wingham et al.*, 1998; *Davis*, 1998). The only dedicated ice radar altimetry missions are Envisat (2002-2012) and Cryosat-2 (2010-). The only laser altimetry satellite mission so far was ICESat. A short description of ICESat is provided below as data of that mission are used in this thesis.

ICESat was launched in 2003 and terminated in 2010. Its major scientific target was to investigate the mass variations of the GrIS and the AIS, as well as their contributions to global sea level rise (*Zwally*, 2002). By using the on-board Geoscience Laser Altimeter System (GLAS), ICESat could accurately measure the two-way travel time of the pulse sent by one of the three lasers (see Fig. 2.4), and thus the distance between the satellite and the surface.

(a) Signal transmitter   (b) Signal receiver
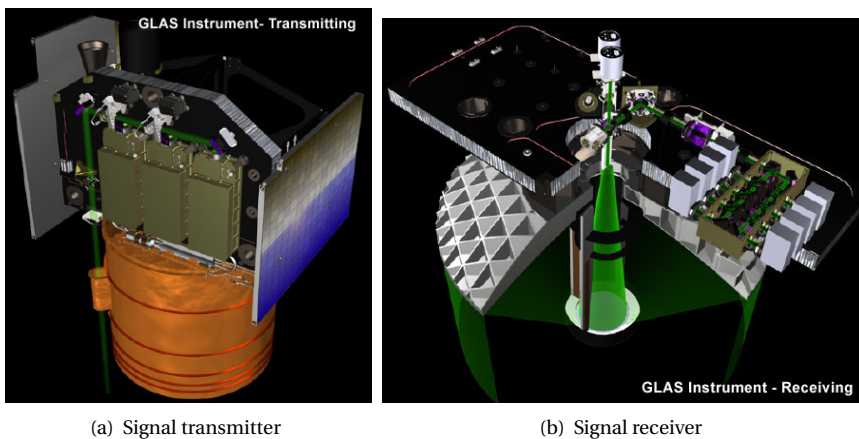
Figure 2.4: The on-board Geoscience Laser Altimeter System (GLAS) of ICESat (Credit: NASA)

Satellite laser altimetry is able to detect long-term surface elevation changes of the ice sheet. Mass changes are derived by multiplying the surface elevation changes with the firn/ice mass densities. The advantage of satellite laser altimetry is that it can reach a relatively high spatial resolution of a few kilometers. However, there are several shortcomings. Firstly, when converting the surface elevation changes to mass changes, the densities of the components (i.e., snow, firn, and ice) at the location where the elevation changes are measured need to be known. They are, however, difficult to determine accurately. Secondly, the compaction of snow and firn causes elevation changes as well, but is not related to any mass change. Therefore, corrections for compaction need to be applied. Thirdly, laser altimetry is not able to collect data in the presence of cloud cover. Finally, the temporal coverage of the ICESat mission was rather limited.

Multi-year mass loss of the GrIS has been investigated in many studies based on ICESat data. For instance, *Sørensen et al.* (2011) reported that the ICESat-based mass balance estimates over 2003-2008 are in the range of -191±23 Gt/yr to -240±28 Gt/yr, depending on different processing schemes. However, a much smaller estimate, -139±68 Gt/yr in 2003-2007, was obtained by *Slobbe et al.* (2009). More recently, *Shepherd et al.* (2012) estimated a linear mass change trend for the whole GrIS of -185 ± 24 Gt/yr over the period October 2003 to December 2008.

2.4.2. The Input-Output method

The IOM obtains the mass balance by examining the surface mass balance (SMB) and ice discharge separately. In order to quantify the SMB, a surface mass balance (SMB) model is widely used to account for the input and the output, as shown in Fig. 2.5. One of the most popular surface mass balance models is the regional atmospheric climate model (RACMO) (*Ettema et al.*, 2009a), whose output is used to describe the SMB-based mass variation of GrIS in this thesis. Based on RACMO, *Velicogna et al.* (2014) obtained a contribution of SMB to the long-term trend of the GrIS of -180 ± 33 Gt/yr over the years 2003-2012 relative with respect to the reference period 1961-1990.

Ice discharge can be derived from ice flow velocities $\mathbf{V}$ and ice thickness T at the flux gates of outlet glaciers,

$$ID = \int_p \mathbf{V}T\mathbf{dp}, \tag{2.2}$$

where $\mathbf{dp} = \mathrm{dp} \cdot \mathbf{n}$, $\mathbf{n}$ is the unit normal vector of the flux gate. A flux gate p stands for a cross-section of a glacier that is used to evaluate the glacier's ice discharge. Many attempts have been made to estimate the mass balance of the GrIS using IOM, after the pioneering study conducted by *Thomas et al.* (2000). For instance, *van den Broeke et al.* (2009) estimated the mean GrIS mass loss rate over the years 2003-2008 as -237±20 Gt/yr. Recently, by using the image data of the Landsat 7 Enhanced Thematic Mapper Plus and the Advanced Space-borne Thermal and Reflectance Radiometer (ASTER), *Enderlin et al.* (2014) derived the ice flow velocities for around 178 outlet glaciers. After combining this information with the ice thickness profiles (*Korona et al.*, 2009), they estimated the
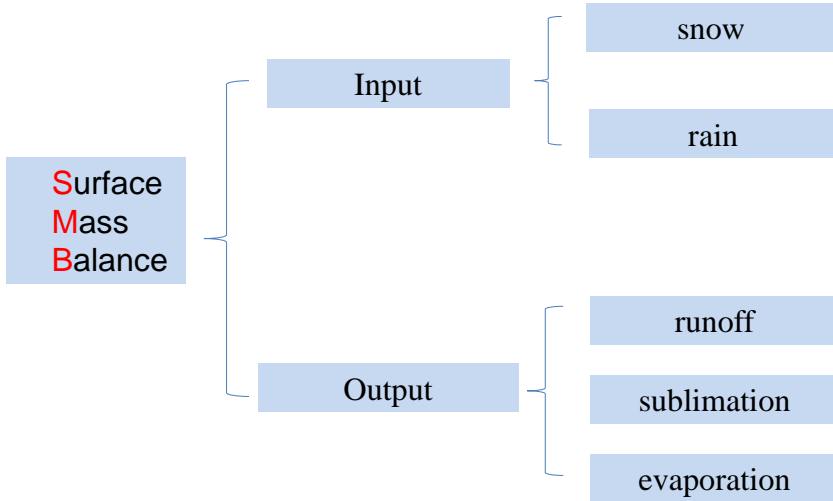
Figure 2.5: Surface mass balance components

annual ice discharge of the GrIS to be at the mean level of around 535 Gt/yr from 2005 to 2012. By combining this estimate with the SMB-based mass changes from RACMO, they found that the mass change trend of the GrIS was -378 Gt/yr over the period 2009-2012. The difference with the estimate by *van den Broeke et al.* (2009) may be caused by an on-going acceleration of GrIS mass anomalies.

2.4.3. Satellite gravimetry

In 2002, the Gravity Recovery and Climate Experiment (GRACE) satellite mission was launched to measure the gravity field of the Earth. Its results are widely utilized in this dissertation to investigate the mass variations of the GrIS. The GRACE mission consists of two identical satellites flying in the same orbit separated by about 200-km. GRACE is the first satellite gravimetry mission which utilizes an accurate inter-satellite ranging system to measure variations in the distance between the two satellites at micrometer accuracy level (Fig. 2.6). In addition, the on-board accelerometers can measure the non-gravitational accelerations of the satellites with an accuracy of about $3.0 \times 10^{-10} m/s^2$. These two instruments make GRACE capable for sensing the Earth's mass re-distribution with an unprecedented accuracy and spatial-temporal resolution of about ~ 300 by 300 km and one month, respectively.
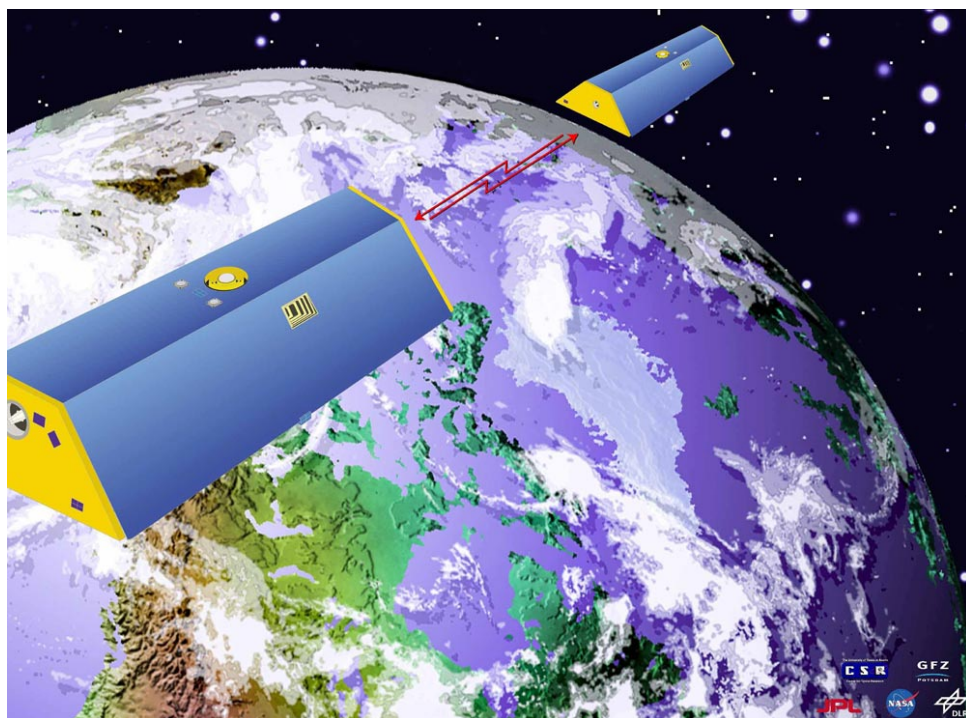
Figure 2.6: GRACE mission (Credit: NASA)

GRACE directly measures the total mass variations of the GrIS without any additional assumptions about the density of the firn. However, GRACE can not distinguish GrIS mass anomalies from the Glacial Isostatic Adjustment (GIA) signal, which is triggered by the non-elastic rebound of the Earth caused by a relief of ice load, from the mass variations of GrIS. Usually the effect of GIA is corrected by models (*A et al.*, 2013; *Simpson et al.*, 2009).

In the early time, there were some differences among the linear trends estimated by different researchers, e.g., -219±21 Gt/yr over 2002-2005 by *Chen et al.* (2006), -230±33 Gt/yr over 2002-2009 by *Velicogna* (2009), -179±25 Gt/yr over 2003-2008 by *Wouters et al.* (2008), etc. However, by now, the differences have been largely eliminated. For instance, *Velicogna et al.* (2014) and *Schrama et al.* (2014) provided very similar estimates of a linear mass change trend of GrIS over the period 2003 - 2013 as -280 ± 59 Gt/yr and -278 ± 19 Gt/yr, respectively. Most of the mass loss took place in the southeast and northwest parts of Greenland, whereas little mass gain was observed in the interior of Greenland. It is also worth mentioning that there is evidence from GRACE data that the GrIS is losing mass with an acceleration of ~ 31 Gt/yr^2, which concentrates in the southeast and northwest of Greenland (*Schrama et al.*, 2014; *Velicogna et al.*, 2014).

2.4.4. The intercomparison of GrIS mass anomalies estimated by different methods

The three methods mentioned above, i.e., IOM, satellite laser altimetry, and gravimetry, have their own strengths and weaknesses. In general, the mass anomalies obtained by those methods show some agreements (*Slobbe et al.*, 2009; *Ettema et al.*, 2009a; *van den Broeke et al.*, 2009; *Sørensen et al.*, 2011; *Velicogna et al.*, 2014; *Enderlin et al.*, 2014; *Schrama et al.*, 2014). For instance, all of them observed large mass variations in the coastal areas of Greenland, whereas relatively small mass gains were found in the inner part. Furthermore, the northwest and southeast parts of Greenland were identified by all methods as the two largest contributors to the total GrIS mass loss, while the northern, southwest and northeast parts contribute less.

However, some differences were also observed among the mass estimations of GrIS by the three methods. The inter-comparison study conducted by *Shepherd et al.* (2012) provided a good opportunity to understand the differences of GrIS mass anomalies estimated by different methods. The chosen time interval was the period from October 2003 to December 2008 for the reason that both laser altimetry satellite and gravimetry satellites were operating optimally during that period (*Shepherd et al.*, 2012). The trends of GrIS mass anomalies derived by IOM, satellite laser altimetry, and gravimetry were -284±65 Gt/yr, -185±24 Gt/yr, and -228±30 Gt/yr, respectively (*Shepherd et al.*, 2012). Note that the mass loss trend observed by GRACE was produced by averaging the estimates obtained by different groups (*Shepherd et al.*, 2012). The trend inferred from laser altimetry data is the smallest one; it is 19% and 35% smaller than the estimates from IOM and gravimetry, respectively. This might be caused by the large uncertainty of firn density, which has been used to convert the volume changes into mass changes.

2.5. Summary

There are three types of glaciers in GrIS, land-terminating glaciers, ice-shelf-terminating glaciers and marine-terminating glaciers. At present, the mass variations of GrIS are estimated using three methods, i.e., satellite altimetry, IOM and satellite gravimetry. Surface elevation changes with a high spatial resolution are provided by satellite altimetry. However, when converting the elevation changes into mass changes, a model of ice/firn densities is needed, and model errors contribute to the overall error budget. The IOM models the physical surface processes, which helps to understand the mechanism of GrIS mass variations. Nevertheless, information about ice thickness and flow velocities is needed, which is usually difficult to obtain in practice. Satellite gravimetry is capable to measure the mass changes directly without any assumptions, whereas its spatial resolution is limited to around 300 km, and corrections for GIA need to be applied.

<div style="text-align: right">

3

</div>

GRACE post-processing methodologies: an overview

3.1. Introduction

Monthly gravity field solutions delivered by GRACE are one of the most valuable sources of information about mass variations of the GrIS (see e.g., *Velicogna and Wahr*, 2006; *Chen et al.*, 2006; *Velicogna*, 2009; *Velicogna et al.*, 2014; *Schrama et al.*, 2014). Unfortunately, monthly GRACE SHCs are strongly contaminated by random noise. It is caused by the fact that GRACE measures mass variations anisotropically, i.e., GRACE data are more sensitive to mass variations in the along-track direction than to those in the cross-track direction. To minimize errors in the estimation of mass anomalies, many post-processing approaches have been proposed, e.g., the de-striping scheme (*Swenson and Wahr*, 2006), the basin-averaging technique (*Velicogna*, 2009), and the mascon approach (*Forsberg and Reeh*, 2007; *Baur and Sneeuw*, 2011; *Schrama and Wouters*, 2011; *Schrama et al.*, 2014). Because of the ability of reaching higher spatial resolution and reduced signal leakage, the mascon approach has become one of the most popular methods of GRACE data post-processing. In this Chapter, the mascon approach and its variants are reviewed, and their pros and cons are discussed.

3.2. Towards high spatial resolution methodologies

The mascon approach typically assumes that the mass variation is uniform inside each mascon. This idea originates from *Muller and Sjogren* (1968), who modelled the static gravity field of the Moon. Then, it was applied to estimate surface mass variations of the GrIS from GRACE Level 1B data (*Luthcke et al.*, 2006a). After that, the mascon approach was developed further to deal with GRACE Level 2 data, i.e., monthly SHCs, by *Forsberg and Reeh* (2007), *Sasgen et al.* (2010), *Baur and Sneeuw* (2011), *Schrama and Wouters* (2011) and *Schrama et al.* (2014). A summary of each mascon approach variant is given in Sections 3.2.1 to 3.2.5.

3.2.1. The mascon approach by Luthcke et al. (2006a)

Let's assume that a mass variation takes place in a mascon W at time t at the Earth surface. Then, the mass variation can be represented by a set of differential SHCs $(\Delta \bar{C}_{lm}^{(W)}(t), \Delta \bar{S}_{lm}^{(W)}(t))$ relatively to a prior mean static gravity field model (*Luthcke et al.*,

2006a; *Rowlands et al.*, 2010). The relation between differential SHCs and the surface density $\sigma^{(W)}(t)$ of mascon W is

$$\Delta \bar{C}_{lm}^{(W)}(t) = \frac{\sigma^{(W)}(t)(1+k_l)a^2}{(2l+1)M} \int_W \bar{P}_{lm}(\sin\phi)\cos m\lambda d\Omega$$
$$\Delta \bar{S}_{lm}^{(W)}(t) = \frac{\sigma^{(W)}(t)(1+k_l)a^2}{(2l+1)M} \int_W \bar{P}_{lm}(\sin\phi)\sin m\lambda d\Omega,$$

(3.1)

where M is the mass of the Earth; k_l is the loading Love number of degree l; a is the semi-major axis of the reference ellipsoid; $d\Omega$ is a surface element of the unit sphere; (r, ϕ, λ) are spherical coordinates; $\bar{P}_{lm}$ is the fully normalized associated Legendre function of degree l and order m.

After converting the surface mass density $\sigma^{(W)}(t)$ to the commonly used Equivalent Water Height (EWH) $H^{(W)}(t)$, Eq. (3.1) becomes

$$\Delta \bar{C}_{lm}^{(W)}(t) = H^{(W)}(t)\frac{\rho_w(1+k_l)a^2}{(2l+1)M} \int_W \bar{P}_{lm}(\sin\phi)\cos m\lambda d\Omega$$
$$\Delta \bar{S}_{lm}^{(W)}(t) = H^{(W)}(t)\frac{\rho_w(1+k_l)a^2}{(2l+1)M} \int_W \bar{P}_{lm}(\sin\phi)\sin m\lambda d\Omega,$$

(3.2)

where ρ_w is the density of water. By combing Eq. (3.2) with the variational equations approach, which links SHCs to the raw satellite-to-satellite tracking data, surface densities of mascons can be estimated using least-square techniques (*Luthcke et al.*, 2006b; *Rowlands et al.*, 2010). In order to stabilize the normal matrix, additional constraint in space and time are incorporated into the estimation process. The constraint equation for any mascon pair (I, J) is (*Rowlands et al.*, 2010)

$$H^{(I)} - H^{(J)} = 0.$$

(3.3)

The weight of the constraint equation is defined as

$$\text{WT}^{(IJ)} = S \cdot \exp(2 - d^{(IJ)}/D - t^{(IJ)}/T),$$

(3.4)

where $d^{(IJ)}$ is the distance between the centers of mascon I and J; D is the correlation distance, and T is time; $t^{(I)}$ and $t^{(J)}$ are the time tags of the mass variations taking place in the mascon I and J, respectively; $t^{(IJ)}$ is the difference of $t^{(I)}$ and $t^{(J)}$; S is a scale factor to adjust the weight of the constrain equation. For more details, we refer to *Rowlands et al.* (2010).

It is worth to mention that two new variants of the mascon approach, which estimate mass anomalies from GRACE Level 1B data as well, were recently developed by *Watkins et al.* (2015) and *Save et al.* (2016). However, since the basic ideas are similar to the variant by *Luthcke et al.* (2006a), we do not discuss them in more detail. But their major differences compared with *Luthcke et al.* (2006a) are briefly described below. The major difference of *Watkins et al.* (2015) is to analytically link KBRR with the unknown mascon parameters, instead of taking SHCs as an intermediate. The innovation of *Save et al.* (2016) is to utilize different spatial constraints which are purely extracted from GRACE information. For more detail, we refer to *Watkins et al.* (2015) and *Save et al.* (2016).

3.2.2. The mascon approach by Luthcke et al. (2013)

Luthcke et al. (2013) made an attempt to estimate solutions with higher accuracy, compared with the mascon approach by *Luthcke et al.* (2006a). The major methodological difference of the two variants is that the latter applies multiple iterations in the least-square approach, by defining the cost function

$$J(\Delta\mathbf{h_k}) = (\mathbf{n} - \mathbf{AL}\Delta\mathbf{h_k})^T\mathbf{W}(\mathbf{n} - \mathbf{AL}\Delta\mathbf{h_k}) + \mu(\tilde{\mathbf{h}}_k + \Delta\mathbf{h_k})^T\mathbf{P_{hh}}(\tilde{\mathbf{h}}_k + \Delta\mathbf{h_k}), \qquad (3.5)$$

where $\tilde{\mathbf{h}}_k$ is the vector of unknown parameters at step $k-1$, i.e., the mass anomaly per mascon in meters of EWH, k is the iteration index, $\Delta\mathbf{h_k}$ is the correction of $\tilde{\mathbf{h}}_k$, $\mathbf{n}$ is the residual between the GRACE KBRR observations and a model prediction generated by $\mathbf{h_k}$, $\mathbf{A}$ is the matrix of partial derivatives of KBRR observations with respect to the Stokes coefficients $(\Delta\bar{C}_{lm}, \Delta\bar{S}_{lm})$ in Eq. (3.2), $\mathbf{L}$ is the matrix of partial derivatives of differential Stokes coefficients with respect to $\mathbf{h_k}$, $\mathbf{W}$ is the data weight matrix, $\mathbf{P_{hh}}$ is the mascon regularization matrix as defined by Eq. (3.4), and μ is the regularization factor, which controls the amount of regularization.

Then the iterated mascon solution $\tilde{\mathbf{h}}_{k+1}$ is given by $\tilde{\mathbf{h}}_{k+1} = \tilde{\mathbf{h}}_k + \Delta\mathbf{h_k}$, where

$$\Delta\mathbf{h_k} = (\mathbf{L}^T\mathbf{A}^T\mathbf{WAL} + \mu\mathbf{P_{hh}})^{-1}(\mathbf{L}^T\mathbf{A}^T\mathbf{Wn} + \mu\mathbf{P_{hh}}\mathbf{h_k}). \qquad (3.6)$$

According to *Luthcke et al.* (2013), the iterated variant of the mascon approach strengthens the signal amplitude. Moreover, unlike applying a uniform statio-temporal constraint to any mascon pair globally as in *Luthcke et al.* (2006a), *Luthcke et al.* (2013) apply anisotropic constraints by dividing the Earth's surface into seven regions: Greenland coastal area (< 2000 m elevation), Greenland inner area (> 2000 m elevation), Antartica coastal area (< 2000 m elevation), Antartica inner area (> 2000 m elevation), Gulf of Alaska, land and ocean.

The mascon approaches of *Luthcke et al.* (2006a), *Watkins et al.* (2015), *Save et al.* (2016) and *Luthcke et al.* (2013) are able to derive mass variations from GRACE data with high spatial and temporal resolutions and cause less signal distortions, compared with the mass anomalies represented in terms of SHCs. Directly operating on GRACE Level 1B data (i.e., K-band rage-rate observations, orbit data, accelerometer data, etc.), makes these approaches very complex, and the implementation and further improvement of them is almost impossible for others (*Baur and Sneeuw*, 2011).

3.2.3. The mascon approach by Sasgen et al. (2010)

Sasgen et al. (2010) propose a variant of the mascon approach to estimate the mass loss trend in the Amundsen Sea sector from GRACE Level 2 data. Using time series of GRACE monthly spherical harmonic coefficients, they fit an analytic model consisting of a linear trend, a bias, and annual and semiannual components for each spherical harmonic coefficient. The fitted trend is converted into gridded geoid heights, which form the observations to estimate a model of total mass change for the Amundsen Sea section.

This model comprises 8 parameters corresponding to a subdivision of the Amundsen Sea sector into 8 drainage systems. Each parameter, say, m_k represents the total mass change over the drainage system k. The distribution of the total mass change over the drainage system is given by a spatially varying function w_k, which is proportional to the observed ice flow velocities from InSAR inside the drainage system k and zero outside. If w_k is normalized to

$$\int_{\sigma_R} w_k(x)\, d\sigma_R = 1, \tag{3.7}$$

where x is a point on the surface of the sphere σ_R of radius R, we may expand $w(x)$ in surface spherical harmonics,

$$w(x) = \sum_{n,m} w_{nm}^{(k)} \bar{Y}_{nm}(\hat{x}), \tag{3.8}$$

where $\bar{Y}_{nm}$ is a surface spherical harmonic of degree n and order m and $\hat{x} = \frac{x}{|x|}$ is a point on the unit sphere. Then, the geoid height signal of a unit total mass change over the drainage system k can be written as

$$\bar{N}_k(x) = \frac{GM}{Rg_0} \sum_{n_{min}}^{n_{max}} \frac{4\pi R^2}{2n+1}(1+q_n) \sum_m w_{nm}^{(k)} \bar{Y}_{nm}(\hat{x}), \tag{3.9}$$

where G is the universal gravitational constant, g_0 is a representative value of gravity at the Earth's surface (e.g., 9.81 m/s^2), and $\{q_n\}$ are the elastic-compressive surface load Love numbers. *Sasgen et al.* (2010) suggest a value of $n_{min} = 7$ to suppress signal leakage from outside Antarctica. n_{max} is set equal to 55. The functional model which relates the pseudo-observations with the model parameters follows then from the superposition principle,

$$N(x) = \sum_{k=1}^{8} \zeta_k(x)\, m_k. \tag{3.10}$$

An estimate of the model parameters $\{m_k\}$ is then obtained using weighted least-squares techniques with regularization.

This variant of the mascon approach provides a reasonable estimation of the trend in mass variations at the Amundsen Sea sector at the drainage system scale. It allows for spatial variations of mass changes inside each drainage system, instead of assuming an uniform mass distribution.

3.2.4. The mascon approach by Schrama and Wouters (2011)

In *Schrama and Wouters* (2011) and *Bonin and Chambers* (2013), a unit basin function is introduced for each mascon to represent the spatial pattern of the signal at the Earth surface. Every basin function is equal to 1 inside its domain and 0 outside on a pre-defined grid which covers not only Greenland, but also the neighbouring areas. Then a spherical harmonic synthesis (complete to degree 60) is applied to each basin function separately. Because of the finite spatial resolution provided by GRACE monthly solutions, a Gaussian smoothing is applied to the converted harmonic coefficients of

each mascon. Then, for each mascon, a set of smoothly changing leakage weights between 0 and 1 on the grid is produced and denoted as $w(\phi, \lambda)$. Let's denote $\alpha_{\mathbf{j}}$ as unknown parameter to represent an uniform signal amplitude of mascon j. Then the full modelled signal h (EWH in units of metres) could be represented as a linear combination of the product of each mascon amplitude and its spatially smoothed leakage weights.

$$h(\phi, \lambda) = \sum_{j=1}^{N} \alpha_j w_j(\phi, \lambda), \tag{3.11}$$

where N is the number of mascons. Then, Eq. (3.11) could also be rewritten in matrix form

$$\mathbf{h} = \mathbf{S}\alpha, \tag{3.12}$$

where $\mathbf{S}$ is the design matrix formed by $w_j(\phi, \lambda)$ and α is the vector of unknown parameters to be estimated using a least-square adjustment

$$\alpha = (\mathbf{S}^\mathbf{T}\mathbf{S})^{-1}\mathbf{S}^\mathbf{T}\mathbf{h}. \tag{3.13}$$

To stabilize the normal matrix, Tikhonov regularisation with regularization matrix $\mathbf{W}^{-1}$ is used, i.e., (3.13)

$$\alpha = (\mathbf{S}^\mathbf{T}\mathbf{S} + \mathbf{W}^{-1})^{-1}\mathbf{S}^\mathbf{T}\mathbf{h}. \tag{3.14}$$

Similar to the variant of the mascon approach by *Sasgen et al.* (2010), this method also works with GRACE Level 2 data. However, *Schrama and Wouters* (2011) forced an uniform mass re-distribution inside each mascon as was also done by *Luthcke et al.* (2006a).

3.2.5. The "mascon" approach by Baur and Sneeuw (2011)

Inspired by *Forsberg and Reeh* (2007), *Baur and Sneeuw* (2011) relate individual point mass variations at the Earth surface to gravitational disturbances at satellite altitude. Their functional model can be written as

$$\delta g_i = G \sum_{j=1}^{N} \delta m_j (r_{s_i}^2 + r_{p_j}^2 - 2r_{s_i} r_{p_j} \cos \Psi_{ij})^{-\frac{3}{2}} (r_{s_i} - r_{p_j} \cos \Psi_{ij}), \tag{3.15}$$

where δg_i is the gravity disturbance at point S_i at satellite altitude (e.g., 500 km), δm_j is the mass variation at point P_j, Ψ_{ij} is the spherical distance between S_i and P_j, and r_{s_i} and r_{p_j} are the spherical radii of point S_i and P_j. The point masses are located at a mean Earth sphere of radius a.

The gravity disturbance at point S_i is synthesized from the GRACE Level 2 data as

$$\delta g = \frac{GM}{r^2} \sum_{l=1}^{L} \frac{l+1}{1+k'_l} (\frac{a}{r})^l \sum_{m=0}^{l} \bar{P}_{lm}(sin\phi)(\Delta C_{lm} \cos m\lambda + \Delta S_{lm} \sin m\lambda), \tag{3.16}$$

where GM is the geocentric constant. Then, the mass variations at the Earth surface can be estimated using least-squares.
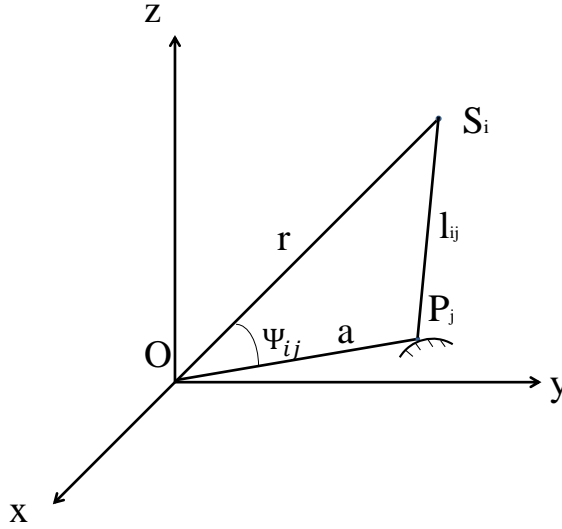
Figure 3.1: Schematic plot of the mascon approach proposed by *Baur and Sneeuw* (2011). P_j and S_i are used for data points at the satellite altitude and the point masses at the Earth surface, respectively.

In contrast to the variant by *Sasgen et al.* (2010) and *Schrama and Wouters* (2011), the mascon approach proposed by *Baur and Sneeuw* (2011) links the mass variations at the Earth surface to the gravity disturbances synthesized from GRACE level-2 data at a mean satellite altitude. This makes data noise less subject to artificial manipulations (such as downward continuation and low-pass filtering). However, they use ordinary least-squares, though the noise covariance matrix of the gravity disturbances is a full matrix.

3.3. Summary

In this Chapter, we provided a short review of the most important mascon approaches suggested in the literature. The approaches of *Luthcke et al.* (2006a), *Luthcke et al.* (2013), *Watkins et al.* (2015), and *Save et al.* (2016) directly operate on GRACE Level 1B data, which makes them very complex and difficult to reproduce by others. The approaches of *Forsberg and Reeh* (2007), *Sasgen et al.* (2010), *Baur and Sneeuw* (2011), and *Schrama and Wouters* (2011) use GRACE monthly spherical harmonic models as input. From them, pseudo-observations are synthesized, e.g., geoid heights (*Sasgen et al.*, 2010), low-pass filtered EWHs (*Schrama and Wouters*, 2011), and gravity disturbances at mean satellite altitude (*Forsberg and Reeh*, 2007; *Baur and Sneeuw*, 2011). These approaches are much easier to implement.

The mascon variant of *Forsberg and Reeh* (2007) and *Forsberg and Reeh* (2007) is chosen as the basis of further developments in the framework of this thesis (cf. Chaper 4). We consider this variant as more natural as the synthesized data in that case better resemble

original satellite observations, without the need to apply a low-pass filter as in *Schrama and Wouters* (2011).

3

Statistically optimal estimation of Greenland mass variations from GRACE monthly solutions using an improved mascon approach

4.1. Introduction

The objective of this Chapter is to develop a statistically-optimal variant of the mascon approach applicable to the estimation of mass anomalies in Greenland. We suggest a number of improvements upon *Forsberg and Reeh* (2007) and *Baur and Sneeuw* (2011). Firstly, we properly propagate the full error covariance matrices of monthly SHCs into gravity disturbances at altitude using the law of covariance propagation. These noise covariance matrices of gravity disturbances are used in the subsequent least-squares adjustment. We expect a noticeable improvement of the estimated mass anomalies and their uncertainties, as noise in SHCs is highly correlated (*Swenson and Wahr*, 2006), among others due to the anisotropic sensitivity of the GRACE KBR data. To address the ill-conditioning of the propagated noise covariance matrices, we develop an approximate inversion scheme based on an eigenvalue decomposition. Secondly, we ensure a spectral consistency between the GRACE-based gravity disturbances and the unknown mascon parameters. The spectrum of the GRACE-based gravity disturbances is limited by the maximum spherical harmonic degree of the monthly sets of SHCs, whereas the mascon representation implies that gravity disturbances contain energy at higher frequencies, too. The spectral consistency has not been considered in previous studies, which use exclusively scaled unit matrices to describe the noise in the data. Then, a spectral inconsistency between model and data has a minor effect on the solution. When using full noise covariance matrices as in this study, the spectral consistency between model and data is indispensable to obtain high-quality solutions.

Typically, the mascon approach makes use of regularization or other spatial constraints to suppress noise at the price of introducing a bias in the solution. The zero-order and first-order Tikhonov regularizations are widely utilized to stabilize the normal matrix. The zero-order regularization, however, which minimizes the L2-norm of the unknown function, may heavily damp long-term trends and other strong signals. The first-order regularization, which minimizes the gradient of the unknown function (in our case, the differences between mass anomalies at neighboring mascons), smears the signals.

24

4. Statistically optimal estimation of Greenland mass variations from GRACE monthly solutions using an improved mascon approach

The resulting signal leakage makes the interpretation of results more problematic, since the estimated mass anomalies cannot be attributed solely to a specific mascon or even drainage system. In this study, no spatial constraints in the form of regularization are used. Instead, the size of the mascons is chosen carefully in order to control the noise.

To demonstrate the performance of the proposed methodology, we make use of both synthetic and real data. In the latter case, we exploit GRACE Release-05 monthly solutions provided by CSR. To investigate the importance of proper data weighting and for validation, we compare the estimated mass anomalies with Surface Mass Balance (SMB) estimates from the Regional Atmospheric Climate Model (RACMO 2.3) (*Noël et al.*, 2015). However a direct comparison of GRACE-based and SMB-based mass anomalies due to the presence of ice discharge signal in the former time-series is not possible. To solve that problem, we estimate and remove linear trends from both time-series. This is justified because seasonal mass variations over Greenland are dominated by SMB variations (*van den Broeke et al.*, 2009).

The remaining part of this Chapter is organized as follows. In Section 4.2, we present the improved mascon approach. Its performance is demonstrated using simulated data, which is the subject of Section 4.3. Particularly, we investigate to what extent the estimates are improved when incorporating the full noise covariance matrices and ensuring the spectral consistency between the data and the mascon parameters. In Section 4.4, we present the results of real data processing and validate them against SMB time-series. Finally, we provide a summary and the main conclusions in Section 4.5.

4.2. Methodology

We propose an improved mascon approach compared to earlier studies by *Forsberg and Reeh* (2007) and *Baur and Sneeuw* (2011). Section 4.2.1 describes the exploited functional model, which is forced to be spectrally consistent with monthly GRACE spherical harmonic models. In Section 4.2.2, we discuss a practical way to divide the territory of Greenland into almost equal-area patches of irregular shape. The proper choice of the area over which gravity disturbances at satellite altitude are generated, is discussed in Section 4.2.3. Section 4.2.4 describes the statistically-optimal inversion of gravity disturbances into mass anomalies per mascon.

4.2.1. Gravity disturbances

Monthly sets of gravity disturbances at mean satellite altitude are computed from monthly GRACE SHCs using a spherical harmonic synthesis. Then, they are linked to the gravitational attraction of the mascons. Finally, mascon parameters are estimated using weighted least-squares techniques.

GRACE-based gravity disturbances

In the context of this study, a gravity disturbance δg is understood as the negative radial derivative of the gravitational potential V, generated by a mass anomaly:

$$\delta g = -\frac{\partial V}{\partial r}. \tag{4.1}$$

They are linked to a set of GRACE SHCs ΔC_{lm} and ΔS_{lm} complete to degree L as

$$\delta g_p = \frac{GM}{r_p^2} \sum_{l=1}^{L} \frac{l+1}{1+k_l'} \left(\frac{a}{r_p}\right)^l \sum_{m=0}^{l} \bar{P}_{lm}(\sin\phi_p)(\Delta C_{lm}\cos m\lambda_p + \Delta S_{lm}\sin m\lambda_p), \tag{4.2}$$

where GM is the geocentric constant; a is the semi-major axis of the reference ellipsoid; (r_p, ϕ_p, λ_p) are spherical coordinates of a data point p, which in this study is assumed to be located at an altitude of 500 km above a mean Earth sphere; L is the maximum degree of the monthly GRACE solutions; and $\bar{P}_{lm}$ is the normalized associated Legendre function of degree l and order m. Notice that the expression contains the load Love numbers k_l', which are introduced to account for the effect of the elastic response of the Earth to a load, which is included in the SHCs. The lateral distribution of data points is discussed in Section 4.2.3.

4

Gravity disturbances generated by a set of mascons

Suppose we have N mascons M_i ($i = 1, 2, ..., N$). The surface density (mass per unit area) of mascon i is denoted as ρ_i. Then, Eq. (4.1) can be re-written as

$$\delta g_p = -\frac{\partial}{\partial r}\left(G\sum_{i=1}^{N}\rho_i \int_{M_i} \frac{ds}{l_p}\right) = -\frac{\partial}{\partial r}\left(G\sum_{i=1}^{N}\rho_i I_{i,p}\right), \tag{4.3}$$

where G is the universal gravitational constant, and

$$I_{i,p} = \int_{M_i} \frac{ds}{l_p} \tag{4.4}$$

with l_p being the distance between an integration point and the data point p.

$I_{i,p}$ has to be computed using numerical integration. Here, we use a composed Newton-Cotes formula. The nodes are located on a Fibonacci grid (*González*, 2010). The number of nodes of mascon i is denoted K_i. Then,

$$I_{i,p} \approx \sum_{j=1}^{K_i} w_{ij} \frac{1}{l_{ij,p}}, \tag{4.5}$$

where $w_{ij} = S_i/K_i$ with S_i the surface area of mascon i. The distance $l_{ij,p}$ between a Fibonacci point with spherical coordinates $(r_{ij}, \phi_{ij}, \lambda_{ij})$ and the data point p with spherical coordinates(r_p, ϕ_p, λ_p) can be computed as

$$l_{ij,p} = (r_{ij}^2 + r_p^2 - 2r_{ij}r_p\cos\Psi_{ij,p})^{\frac{1}{2}}, \tag{4.6}$$

26

4. Statistically optimal estimation of Greenland mass variations from GRACE monthly solutions using an improved mascon approach

where $\cos\Psi_{ij,p} = \sin\phi_p \sin\phi_{ij} + \cos\phi_p \cos\phi_{ij} \cos(\lambda_p - \lambda_{ij})$.

Then,

$$\delta g_p \approx G \sum_{i=1}^{N} \rho_i \sum_{j=1}^{K_i} w_{ij}(r_{ij}^2 + r_p^2 - 2r_{ij}r_p \cos\Psi_{ij,p})^{-\frac{3}{2}}(r_{ij} - r_p \cos\Psi_{ij,p}). \qquad (4.7)$$

Eq. (4.7) represents the functional model that relates the gravity disturbances and the surface densities of the mascons. In matrix-vector form, Eq. (4.7) can be written as

$$\mathbf{d} \approx \mathbf{A}'\mathbf{x}, \qquad (4.8)$$

where $\mathbf{x}$ is the vector of surface densities, $\mathbf{d}$ is the vector of gravity disturbances, and $\mathbf{A}'$ is the design matrix. The vector $\mathbf{x}$ is estimated from the vector of gravity disturbances $\mathbf{d}$ using weighted least-squares techniques.

The gravity disturbances of Eq. (4.2) have a limited bandwidth because the monthly GRACE solutions are limited to a certain maximum spherical harmonic degree. However, the gravity disturbances of Eq. (4.7) are not band-limited. Hence, the functional model, Eq. (4.8) is, not correct as there is a spectral inconsistency between the data and the model. To obtain a spectrally consistent functional model, we need to apply a lowpass filter to the design matrix $\mathbf{A}'$, i.e., $\mathbf{A}'$ needs to be replaced by $\mathbf{A}$, where

$$\mathbf{A} = \mathbf{Y}\mathbf{A}', \qquad (4.9)$$

and $\mathbf{Y}$ represents the lowpass filter. Without such a lowpass filter, the short-wavelengths of the estimated mascon solution would be biased towards zero.

To define a suitable lowpass filter, we need to remember that each column of the design matrix $\mathbf{A}'$ represents a set of gravity disturbances caused by a single mascon of unit surface density. Therefore, the filter operation can be implemented as follows. Firstly, gravity disturbances caused by a single mascon of unit surface density are computed on an equal-angular global grid. They are used as input to estimate a SH model of gravity disturbances complete to some maximum degree $L > L_G$ using a spherical harmonic analysis (L_G is the maximum degree of the monthly GRACE spherical harmonic models). The SH model is truncated at the maximum degree L_G, and successively used to synthesise a column of the design matrix $\mathbf{A}$, which corresponds to the single mascon. This procedure has to be followed for every mascon. The result is a design matrix $\mathbf{A}$, which is spectrally consistent with the information content in the data and the data noise covariance matrix.

The spectrally consistent analog of Eq. (4.8) is written as

$$\mathbf{d} = \mathbf{A}\mathbf{x} + \mathbf{n}, \qquad (4.10)$$

where the vector $\mathbf{n}$ is introduced to account for noise in the GRACE-based gravity disturbances. This noise is assumed to be zero-mean and Gaussian. Furthermore, we assume that

$$D\{\mathbf{n}\} = \mathbf{C_d}, \qquad (4.11)$$

where $D\{\cdot\}$ is the dispersion operator, and $\mathbf{C_d}$ is the data noise covariance matrix. The latter is computed on a month-by-month basis from the full noise covariance matrix of the monthly SHCs using the law of covariance propagation.

Then, the best-linear unbiased estimate (BLUE) of the mass anomalies is

$$\widehat{\mathbf{x}} = (\mathbf{A}^T\mathbf{C_d}^{-1}\mathbf{A})^{-1}\mathbf{A}^T\mathbf{C_d}^{-1}\mathbf{d}. \tag{4.12}$$

The BLUE, Eq. (4.12), is referred to as the "statistically optimal estimator" in this study.

4.2.2. Parameterization

The proper choice of the size of a mascon is important to mitigate noise amplification during the data inversion. To facilitate experiments with different mascon sizes, we developed a procedure for an automatic division of the territory of Greenland into nearly equal-area mascons of a desired size. The procedure consists of two steps. In the first step, Greenland is split into latitudinal strips of equal width, which is chosen to be as close to the desired size as possible. In the second step, each strip is split into individual mascons of an approximately desired size using straight segments in the rectangular projection. The orientation of the segments is adapted to follow the orientation of the west and east borders of the current strip. Examples of the resulting parameterizations are shown in Fig 4.1. Note that the geometry of the mascons located along the Greenland coast follow the coastal line.

We also define 9 mascons outside Greenland to reduce leakage of signal from outside Greenland into the Greenland mascons. These mascons cover Iceland, Svalbard, and the Canada's Arctic Archipelago glaciers, see Fig 4.2. It is worth mentioning that we do not parameterize the nearby ocean areas, due to a minor impact of oceanic mascons, e.g., at the level of 7 Gt/yr for the trend over 2003-2013, when the optimal data weighting is applied.

4.2.3. Distribution of data points

When choosing the altitude of the data grid, we followed the suggestion of *Baur and Sneeuw* (2011): 500 km. Another option is to use mean altitudes per monthly GRACE solution to address the decrease in orbital altitude of the GRACE satellites, as was done by *Forsberg et al.* (2017). Numerical studies (not shown here) reveal that this leads to similar estimates (within 10 Gt/yr in terms of trend over 2003-2013) when the data weighting is switched on. We attribute the observed minor differences to the fact that the applied data processing strategy, including the truncation of the spectrum of the matrix Cd, was fine-tuned for the grid altitude of 500 km. We expect that fine-tuning of the data processing for grid altitudes chosen consistently with actual GRACE orbits would reduce these differences further. We consider this refinement as a minor aspect, which is out of the scope of this thesis.
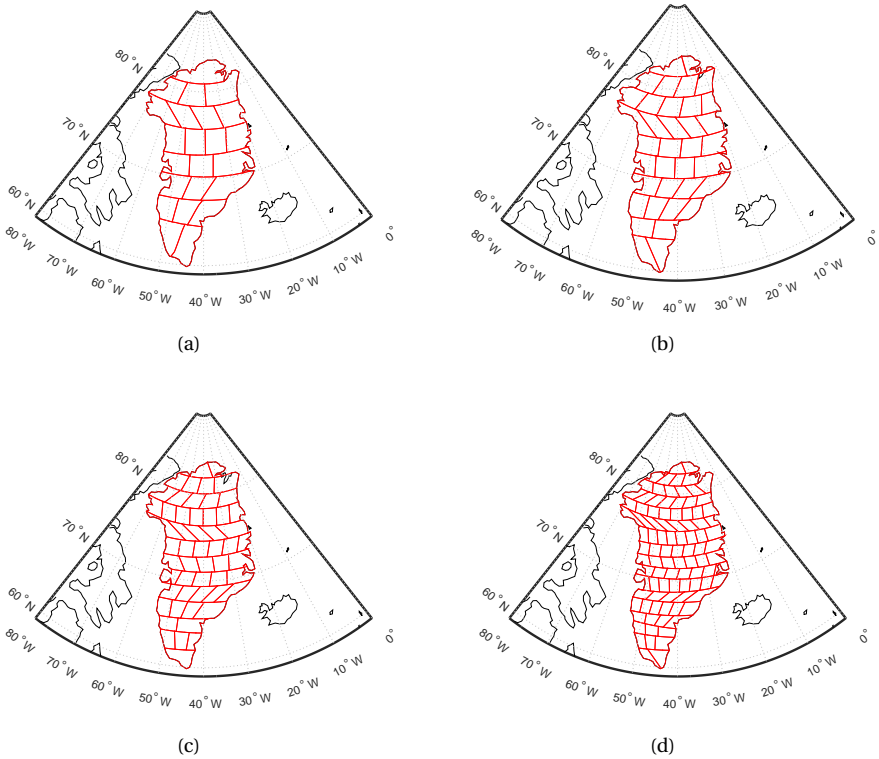
28

4. **Statistically optimal estimation of Greenland mass variations from GRACE monthly solutions using an improved mascon approach**

(a)

(b)

(c)

(d)

Figure 4.1: Partitioning of Greenland into 23 (size about 300 × 300 km), 36 (size about 250 × 250 km), 54 (size about 200 × 200 km), and 95 (size about 150 × 150 km) mascons, respectively.

The data area comprises Greenland and a buffer zone of 800 km around Greenland. The use of a buffer zone is justified by the fact that each gravity disturbance at satellite altitude is sensitive to a mass re-distribution in a neighbourhood of a few hundred kilometres around that point (*Baur and Sneeuw*, 2011). Thus, defining the data area in such a way ensures a more comprehensive representation of the target signals. The data points are located on a Fibonacci grid with a mean distance of 37.5 km. Additional data points on the oceans, but outside the data area are introduced for reasons discussed in Section 4.3.2. They are located on a Fibonacci grid with a mean distance of 2000 km. The total number of data points is 6953 with 6867 points inside the data area and 86 points in ocean areas outside the data area.

4.2.4. Data inversion

The full noise covariance matrix of the GRACE-based gravity disturbances, $\mathbf{C_d}$, is ill-conditioned and possesses a gradually decreasing eigenvalue spectrum with many
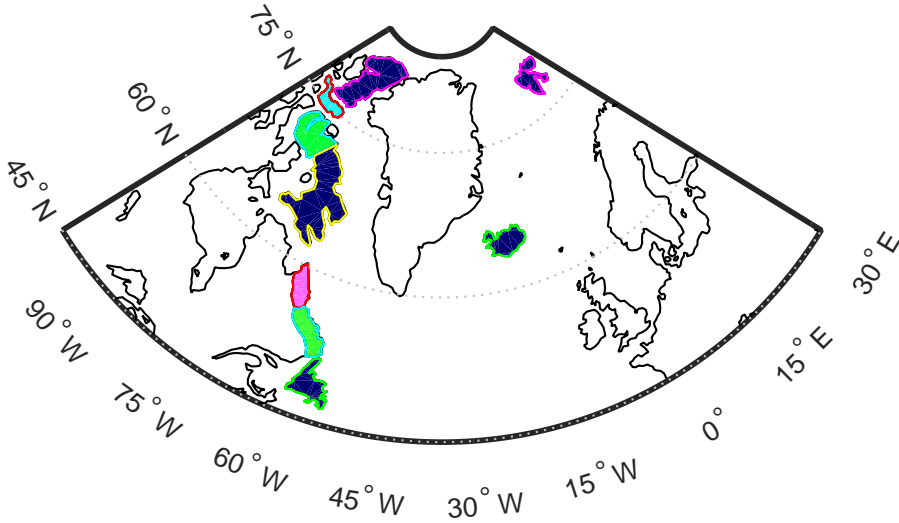
Figure 4.2: Mascons outside Greenland used in this study.

eigenvalues close to zero. Therefore, some kind of regularization is needed before this matrix is inverted. Here, we use an eigendecomposition to compute an approximate inverse, i.e.,

$$\mathbf{C_d} = \mathbf{Q}\Lambda\mathbf{Q}^T, \tag{4.13}$$

where $\mathbf{Q}$ is a unitary matrix which contains the eigenvectors of $\mathbf{C_d}$ and Λ is the square diagonal matrix of eigenvalues of $\mathbf{C_d}$. In Appendix A, we show that the matrices $\mathbf{Q}$ and Λ can be computed without an explicit computation of the matrix $\mathbf{C_d}$, which helps to minimize the loss of significant digits.

Formally, the inversion of the matrix $\mathbf{C_d}$ can be written as

$$\mathbf{C_d}^{-1} = (\mathbf{Q}\Lambda\mathbf{Q}^T)^{-1} = \mathbf{Q}\Lambda^{-1}\mathbf{Q}^T. \tag{4.14}$$

However, many eigenvalues of the matrix $\mathbf{C}_d$ are small, reflecting the ill-conditioning of this matrix. Therefore, an approximate inverse of this matrix is computed as follows. The matrix Λ is truncated in such a way that only the eigenvalues exceeding a pre-defined threshold are retained:

$$\Lambda_\mathbf{t} = \mathbf{J}\Lambda\mathbf{J}^T, \tag{4.15}$$

where $\mathbf{J} = [\mathbf{I} \quad \mathbf{0}]$ is the truncation operator with $\mathbf{I}$ being an unit matrix and $\Lambda_\mathbf{t}$ is the resulting diagonal matrix, containing a truncated set of eigenvalues. By retaining only sufficiently large eigenvalues, we stabilize the computation of the inverse of the matrix

Λ_t. An approximate inverse $\tilde{\Lambda}^{-1}$ of the original matrix Λ is obtained by replacing the missing elements with zeros:

$$\tilde{\Lambda}^{-1} = \mathbf{J}^T \Lambda_t^{-1} \mathbf{J}. \tag{4.16}$$

After that, we define the approximate inverse $\tilde{\mathbf{C}}_d^{-1}$ of the matrix $\mathbf{C}_d$ as

$$\tilde{\mathbf{C}}_d^{-1} = \mathbf{Q}\tilde{\Lambda}^{-1}\mathbf{Q}^T = \mathbf{Q}\mathbf{J}^T\tilde{\Lambda}_t^{-1}\mathbf{J}\mathbf{Q}^T = \mathbf{Q_t}\tilde{\Lambda}_t^{-1}\mathbf{Q_t}^T, \tag{4.17}$$

where

$$\mathbf{Q_t} = \mathbf{Q}\mathbf{J}^T \tag{4.18}$$

is the truncated matrix $\mathbf{Q}$ containing only the eigenvectors related to the retained eigenvalues. Then, according to Eq. (4.12), the weighted least-squares solution $\hat{\mathbf{x}}$ is

$$\begin{aligned}
\hat{\mathbf{x}} &= (\mathbf{A}^T\tilde{\mathbf{C}}_d^{-1}\mathbf{A})^{-1}\mathbf{A}^T\tilde{\mathbf{C}}_d^{-1}\mathbf{d} \\
&= (\mathbf{A}^T\mathbf{Q_t}\tilde{\Lambda}_t^{-1}\mathbf{Q_t^T}\mathbf{A})^{-1}\mathbf{A}^T\mathbf{Q_t}\tilde{\Lambda}_t^{-1}\mathbf{Q_t^T}\mathbf{d} \\
&= (\mathbf{B}^T\tilde{\Lambda}_t^{-1}\mathbf{B})^{-1}\mathbf{B}^T\tilde{\Lambda}_t^{-1}\mathbf{Q_t^T}\mathbf{d},
\end{aligned} \tag{4.19}$$

where

$$\mathbf{B} = \mathbf{Q_t^T}\mathbf{A}. \tag{4.20}$$

This solution is still unbiased, but the dispersion is not minimum.

4.3. Numerical experiments

We do a number of numerical experiments to investigate the performance of the improved mascon approach and to fine-tune some data processing parameters. In Section 4.3.1, we present the basic set-up of the numerical experiments. Section 4.3.2 is devoted to a presentation and discussion of the results. The importance of the spectral consistency is discussed in Section 4.3.3.

4.3.1. Experimental setup

The basic set-up used in all numerical experiments includes the definition of i) the "true" signal and ii) the error sources.

"True" signal

We define the "true" signal as the yearly mass change, which is determined on the basis of trends extracted from ICESat altimetry data (see Table 4.1)(*Felikson et al.*, 2016). As shown in Fig 4.3, these trends represent the mean rate of mass change over the period 2003–2009 per 20 × 20 km patch covering entire Greenland, converted from the surface elevation change rate by applying a density of 917 kg/m^3 (*Wahr et al.*, 2000). This signal is directly used to compute the mass anomaly per mascon as "truth". Using the proposed mascon approach, we generate gravity disturbances at satellite altitude from the ICESat altimetry data. Thereafter, we lowpass-filter them to limit the spectrum to spherical harmonic degrees from 1 to 120. Finally, we estimate the mascon mass anomalies

and compare them with the "true" mass anomalies to evaluate the performance of the methodology.
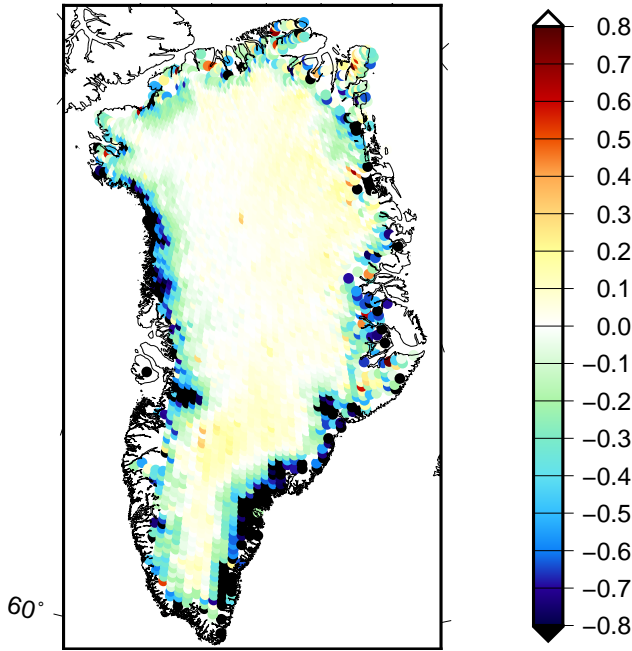
Figure 4.3: The "true" signal defined as the yearly mass change over the GrIS, in terms of EWH in units of metres.

Table 4.1: A summary of the data used in this study.

Data	Role	Temporal resolution	Spatial resolution	Pre-Processing
ICESat elevation change rate	Simulating the true signal	2003-2009	20 km blocks	-
GRACE SHCs from DMT	Simulating signal leakage	Month	Degree 120	-
GRACE SHCs from CSR RL02	Real data	Month	Degree 96	-
Surface mass balance from RACMO2.3	Validating estimates	Daily	11 km blocks	Resampled to monthly mean SMB for each drainage system and entire Greenland

There is much freedom in the definition of the "true" signal in the presence of secular trends. The "true" signal may reflect total mass change over an arbitrary time interval, ranging from one month to many years. The choice of the time interval determines the contribution of error sources like signal leakage and parameterization errors to the overall error budget. If the time interval is short (e.g., one month), signal leakage and

32

4. Statistically optimal estimation of Greenland mass variations from GRACE monthly solutions using an improved mascon approach

parameterization errors may be small compared to the data noise. However, the relative contribution of these error sources to the overall error budget increases with increasing time interval. In this study, we define the "true" signal as the *yearly* mass change, which represents a kind of intermediate choice between the two extremes of a monthly signal and a multi-year signal. Our time interval is somewhat shorter than that considered in the study by *Bonin and Chambers* (2013), which was equal to 4 years. In any case, the amplitude of the true signal in real GRACE data processing may differ depending on the signal of interest, which may range from short-term mass variations to long-term trends.

Error sources

The data generated in the previous section are superimposed by errors. In this study, we consider 4 error sources, i.e., signal leakage, AOD noise, random noise in GRACE-based SHCs, and parameterization error. The latter is also sometimes referred to as the "model error" (e.g., (*Xu*, 2010; *Stedinger and Tasker*, 1986)).

Signal leakage. In this study, signal leakage refers to the impact of mass variations from outside Greenland on the estimated mascons. To simulate signal leakage, we introduce mass variations in Alaska, northern Canada, northern Russia, and Fennoscandia, see Fig 4.4. The "true" signal over these areas is also defined as the yearly mass variation. It is generated using the available optimally filtered trend over 2003-2008 based on the Delft Mass Transport model (DMT) (*Siemes et al.*, 2013).
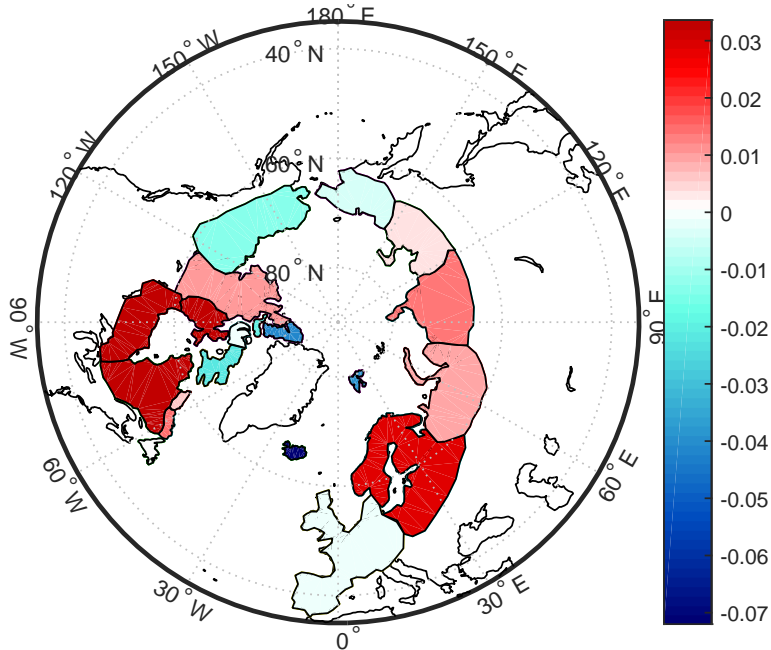

Figure 4.4: Mascons used to simulate signal leakage. The value of each mascon is the full signal generated using the trend over the period 2003–2008 derived from the DMT model, in terms of EWH in units of metres.

AOD noise. AOD noise refers to errors in the background models, which are used to reduce non-tidal mass transport in the atmosphere and ocean. AOD error is considered to be one of the largest error sources in the produced monthly GRACE solutions. Here, we also take 10% of the difference of two AOD models (see Fig. 4.5) separated by one year as the AOD noise, in line with the definition of the true signal (yearly mass accumulation). To that end, we choose AOD models in August of 2005 and 2006, because this period is roughly in the middle of the true signal (ICESat trend over 2003-2009). Based on our numerical study, we find that the AOD noise plays a minor role. Therefore there would be negligible impact if a different time interval were chosen. Defining the AOD error as 10% of the AOD model signal is believed to be a reasonable choice, in view of previous studies (*Thompson et al.*, 2004; *Ditmar et al.*, 2012).
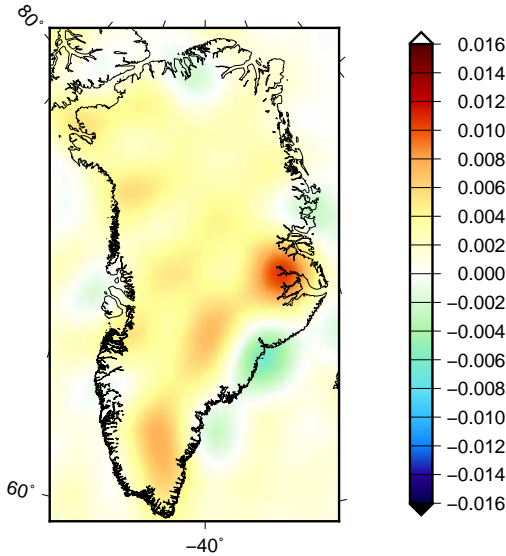
4

Figure 4.5: The AOD error (EWH in units of metres), which is taken as 10% of the difference between August 2005 and August 2006.

Random noise. We assume that the yearly mass change is the result of the difference between two monthly solutions separated by a time interval of one year. Furthermore, we assume that there is no noise correlation between monthly solutions. This implies that the random noise in the generated yearly mass change can be set equal to the noise in a monthly solution multiplied with a factor of $\sqrt{2}$. First, we generate a vector $\mathbf{n}$ of zero-mean white Gaussian noise with unit variance; the length of $\mathbf{n}$ is equal to the number of SHCs. Then, a realization of correlated noise with the covariance structure of the matrix C_{δ_p} is obtained as

$$\mathbf{n_c} = \mathbf{Ln}, \qquad (4.21)$$

34

4. Statistically optimal estimation of Greenland mass variations from GRACE
monthly solutions using an improved mascon approach

where **L** is the lower triangular Cholesky factor of the noise covariance matrix $\mathbf{C}_{\delta_{\mathbf{p}}}$ of
GRACE monthly SHCs:

$$\mathbf{C}_{\delta_{\mathbf{p}}} = \mathbf{L}\mathbf{L}^{T}. \tag{4.22}$$

In this study, the noise covariance matrix is complete to degree 120. It describes the
noise in GRACE SHCs in August 2006 and was produced together with the DMT model.
Note that the noise in the degree-one coefficients is not included. One hundred random
noise realizations are simulated in this way in order to make the results of the numerical
study more representative. Figure 4.6 shows one of these noise realizations in terms of
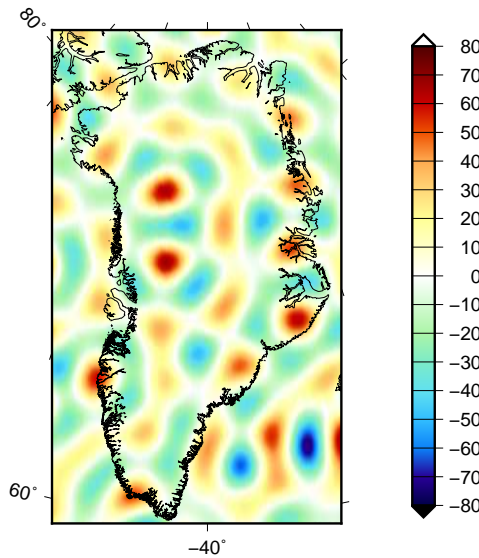EWHs (Equivalent Water Height).

Figure 4.6: A realization of simulated random errors (EWH in units of metres). The simulations are based on
the DMT noise covariance matrix of spherical harmonic coefficients for August 2006. This matrix is complete
to degree 120.

Parameterization errors. Parameterization errors are caused by the fact that the
adopted parameterization assumes a uniform surface density distribution within each
mascon, whereas the actual distribution within a mascon may spatially vary. Here,
parameterization errors are automatically introduced, as the "true" signals are generated
with ICESat altimetry data with a spatial resolution of 20 km, which is much finer than
the mean size of a mascon.

4.3.2. Choice of the optimal data processing strategy

There are a number of choices to be made when using the improved mascon approach:

- the size of the buffer zone around Greenland;

- the number of additional data points in the oceans outside the data area;

- the number of mascons covering entire Greenland;

- the choice of the least-squares estimator (i.e., ordinary least-squares versus weighted least-squares);

- the number of eigenvalues to be retained when computing an approximate inverse of the noise variance-covariance matrix $\mathbf{C_d}$.

In a series of numerical experiments, we have investigated various choices. For each choice, 100 solutions have been computed each using a different random noise realization. Other error sources were kept the same in all experiments. Each solution has been converted into mass anomalies per mascon (in Gt), and then summed up over all "Greenland" mascons to yield the total mass anomalies over entire Greenland. The total mass anomalies are then compared with the "true" ones; the RMS difference between estimated and true total mass anomalies is used as a measure of the quality of the solution.

In this way, we found the optimal choice of the various parameters mentioned before, which is shown in Table 4.2. In the next sections, we show how the inversion results deteriorate if a sub-optimal choice is made. In each test, only one parameter is changed. Regarding data weighting, we always compute two solutions; a weighted least-squares solution (weight matrix is the inverse of the full noise covariance matrix), and an ordinary least-squares solution (weight matrix is the unit matrix).

Table 4.2: Optimal set of parameters for the estimation of total mass variations of entire Greenland.

Options	Optimal choice
Width of the buffer zone around Greenland	800 km
Using additional data points over the global oceans	Yes
Number of mascons within Greenland	23
Optimal data weighting applied	Yes
Number of eigenvalues retained in the approximate inversion of $\mathbf{C_d}$	600
Spectral consistency maintained	Yes

Width of the buffer zone around Greenland

It is well-known that the data area has to extend beyond the area of interest (*Baur*, 2013). In this study, the extension is referred to as the buffer zone. To investigate the impact of the choice of the buffer zone on the estimated mass anomalies over entire Greenland, we consider buffer zones varying from 100 km to 1,400 km (cf. Fig 4.7). For each choice of the buffer zone a weighted least-squares solution and the ordinary least-squares solution are computed. The other parameters are set equal to the values shown in Table 4.2. The resulting RMS error of the recovered Greenland mass anomalies is shown in Fig 4.8. Using a weighted least-squares estimator, the RMS error is minimum for a 800 km buffer zone, though other choices only increase the RMS error with a few Gt. From this we conclude that when using a proper data weighting, the solution is quite robust against

the choice of the buffer zone. The situation is different when an ordinary least-squares estimator is used. The smallest RMS errors are obtained for buffer zones larger than 600 km with little variations. For smaller buffer zones, however, the RMS errors increase quickly and attain values which are a few tens of Gts higher then the minimum. Overall, the RMS error of a weighted least-squares solution is always smaller than the RMS error of an ordinary least-squares solution.
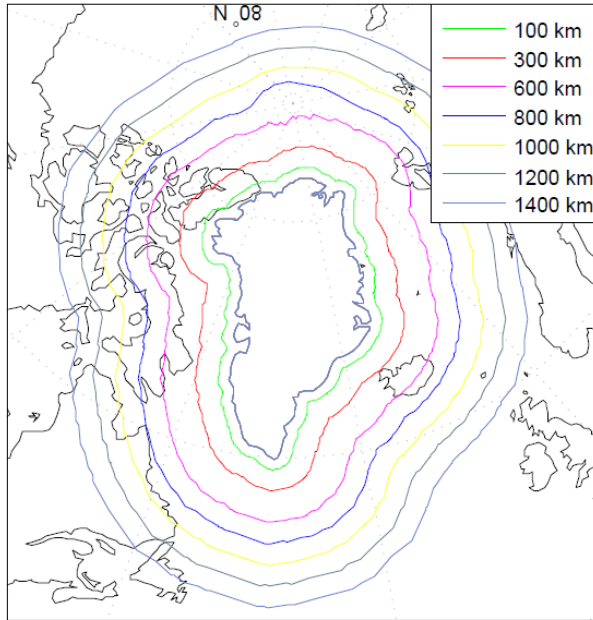

Figure 4.7: Buffer zones around Greenland considered in this study.

Using data points distributed over the oceans globally

GRACE-based SHCs at very low degrees (particularly, at degree 2) are relatively inaccurate. In principle, the implemented data weighting should suppress noise which originates from these low-degree coefficients (*Chen et al.*, 2005). However, in regional studies as considered here, the contribution of different low-degree SHCs cannot be separated. Therefore, any attempt to suppress noise in the very low-degree SHCs may introduce a bias in the estimated mass anomalies over entire Greenland. For instance, eliminating the C_{20} may reduce the estimated trend over 2003-2013 of GrIS mass variation by ~18 Gts. To avoid such a bias, we add additional data points. To avoid that they capture signal below them, they are confined to the oceans assuming that mass variations over the oceans are negligible. Figure 4.9 shows the geographic location of these additional data points.

The additional data points are located on a Fibonacci grid with a mean distance of about 2,000 km. Solutions are computed with and without the additional data points. A
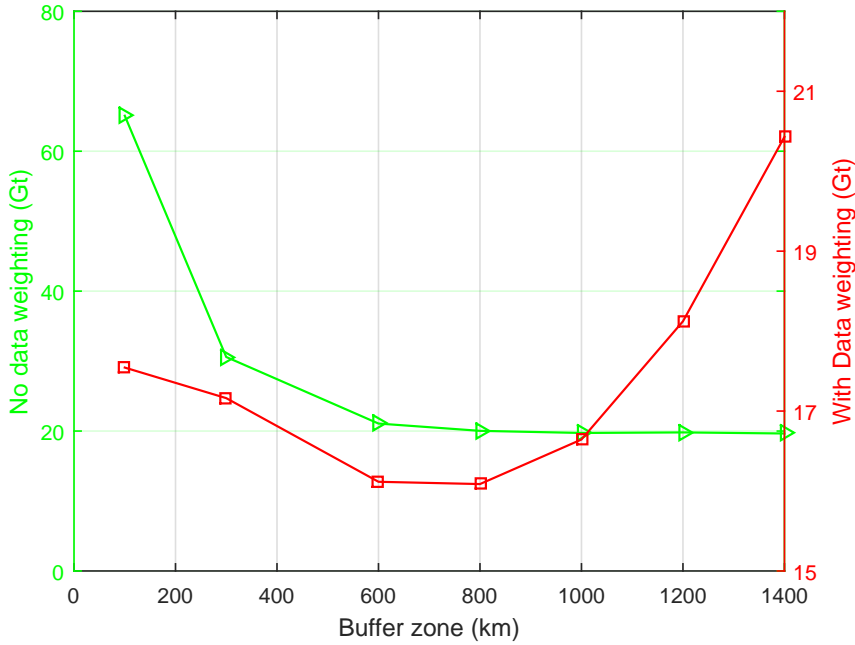
Figure 4.8: The RMS error of estimated mass anomalies as function of the buffer zone size. Red: with data weighting, green: without data weighting. Different vertical scales are used when plotting the red and green curves.

comparison of these solutions reveal that the added value of using additional data points is 0.02% when using ordinary least-squares and 0.5% when using weighted least-squares. Though the improvement is minor, we recommend to add additional data points in regional studies. The numerical complexity does not change much as the total number of extra points is very limited.

Optimal number of mascons over Greenland

In this test, we split the territory of Greenland into mascons of different sizes: from approximately 300 × 300 km to approximately 150 × 150 km, which corresponds to the number of mascons ranging from 23 to 95 (see Fig 4.1). In addition, we consider also the division of Greenland into 6 or 12 mascons, as proposed in (*Luthcke et al.*, 2006a) (Fig 4.10). The RMS differences between the recovered and true mass anomaly estimations are shown, as a function of the number of mascons over entire Greenland, in Fig 4.11. We notice a significant reduction of the RMS error when a weighted least-squares estimator is used; between 19% and 65%, depending on the size of the mascons.

From the green curve in Fig. 4.11, obtained without optimal data weighting, we find that the RMS error when using 6 mascons is larger than the RMS error when using 23 mascons. Note that the numerical study showed in Fig. 4.11 considered all noise

38

**4. Statistically optimal estimation of Greenland mass variations from GRACE
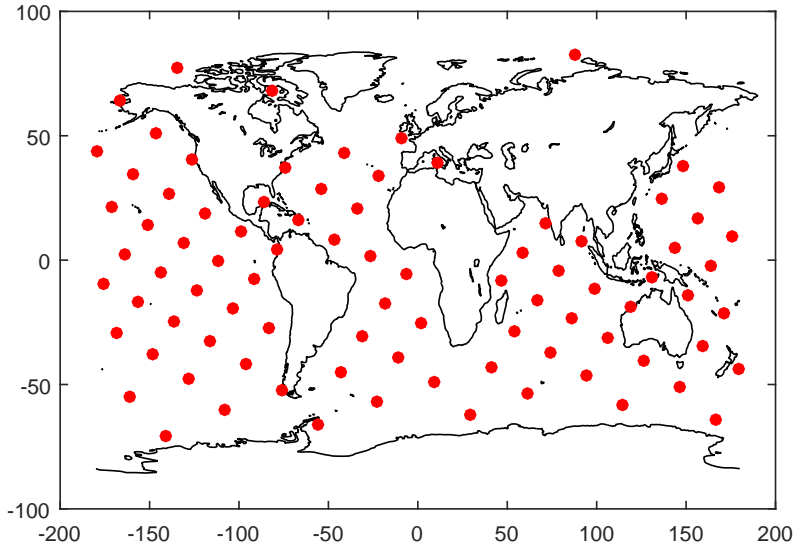monthly solutions using an improved mascon approach**

Figure 4.9: Location of additional data points over the oceans. The mean distance is about 2,000 km.

types, including random noise, representation error, etc. It is also worth noticing that
when using weighted least-squares, the quality of results based on 6 drainage systems is
slightly higher than based on 23 mascons (see the red curve in Fig. 4.11). This is caused
by the fact that the random noise in the case of 6 mascons is reduced (i.e., from 15 to 9
Gt), as compared to 23 mascons. The numbers of 15 and 9 Gt are the result of additional
numerical studies where random noise was the only error source (not shown here). As
the difference of the RMS values in the cases of 6 and 23 mascons (see the red curve in
Fig. 4.11) is rather small and 23 mascons provide a much better spatial resolution than 6
mascons, we recommend using 23 mascons.

The estimated mass anomalies for 23 mascons are shown in Fig. 4.12a; They are
estimated from the data that were contaminated by the errors presented in Figs 4.4-4.6.
We find that in general the recovered mass anomalies show some agreement with the
true signal. For instance, the mass losses take place in the coastal area, and are mainly
located in the northwest and southeast of Greenland. However, we could also find that
the recovered mass per mascon does not exactly represent the spatial pattern of the
signal. This finding is consistent with *Baur* (2013) and *Bonin and Chambers* (2013). For
instance, the recovered spatial pattern in the inner part of Greenland noticeably deviates
from the true signal. The recovered solution is much worse when using too many (i.e.,
54) mascons as shown in Fig. 4.13. Due to a small size of mascons (about 150 × 150 km),
the recovered mean mass anomalies are quite unstable, with many positive and negative
estimates next to each other.
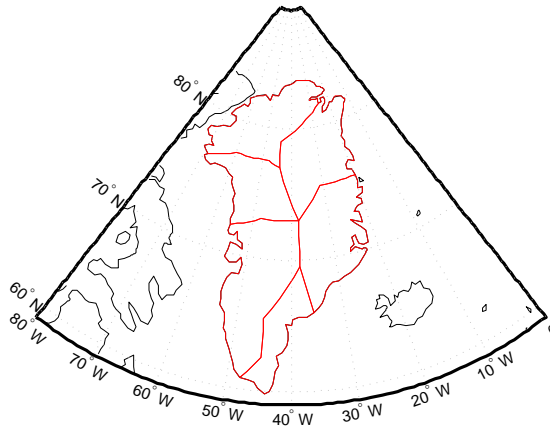
(a) 6 drainage systems

4
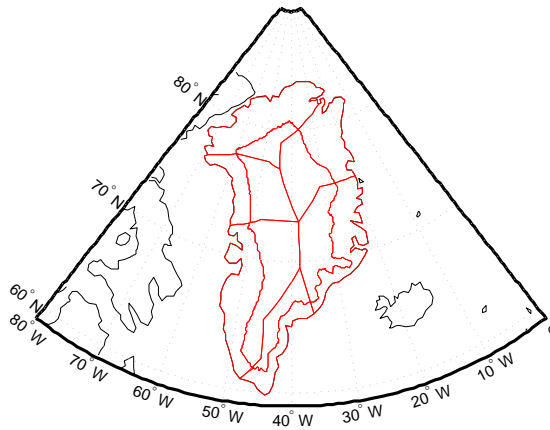
(b) 12 mascons

Figure 4.10: Partitioning of Greenland into 6 and 12 mascons, respectively, in line with *Luthcke et al.* (2006a).

Number of eigenvalues retained in the approximate inversion of the noise covariance matrix

The high condition number of the noise covariance matrix does not allow a stable computation of the weight matrix, and some regularization is necessary. In this study, we use a truncated eigenvalue decomposition to improve the condition number prior to inversion (cf Section 4.2.4). In order to estimate the optimal number of eigenvalues to be retained, we consider values between 200 and 1,600. The dimension of the noise covariance matrix is $6,953 \times 6,953$ in our case.

The RMS error of the estimated mass anomalies over the Greenland is relatively large

40

4. Statistically optimal estimation of Greenland mass variations from GRACE monthly solutions using an improved mascon approach
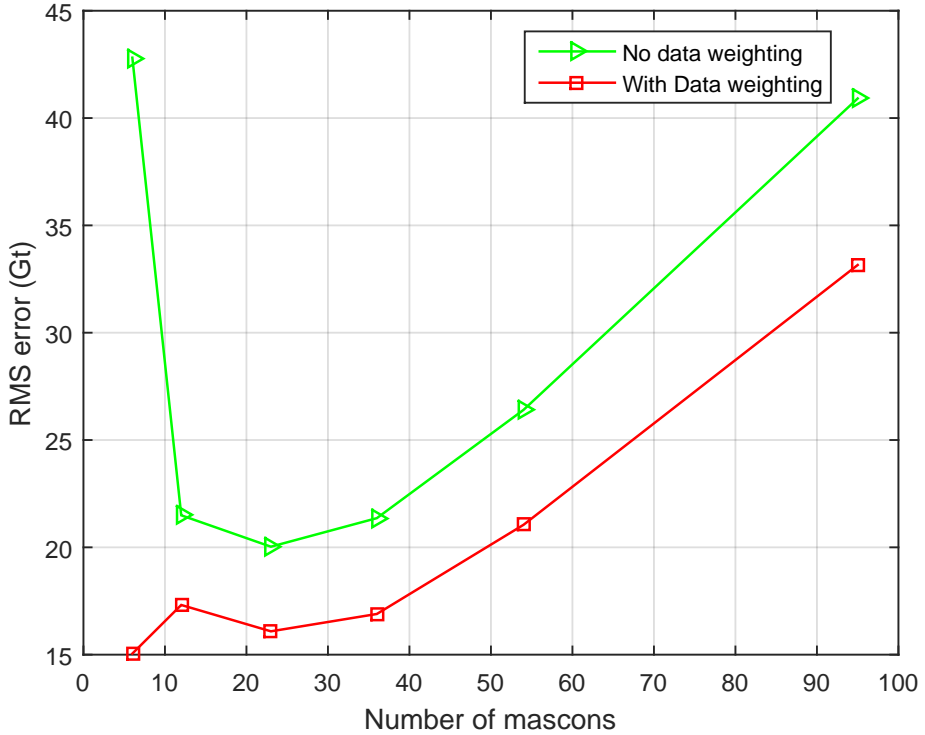
Figure 4.11: RMS errors in estimated mass anomalies over the Greenland as a function of the number of mascons.

when only 200 eigenvalues are retained, but decreases by 49%, as the number of retained eigenvalues increases to 600 (see the red curve in Fig 4.14a). A further increase also increases the RMS error. Therefore, we retain only the first 600 eigenvalues, i.e., about 10%. The condition number of the noise covariance matrix obtained in this way is $1.2 \cdot 10^7$. Based on the Fig. 4.14b, which shows the same RMS error as a function of the condition number, we conclude that in general it makes sense to keep the condition number below a value of about 10^7.

4.3.3. Spectral consistency

As explained in Section 4.2, the parameterization of the signal has to be spectrally consistent with the data. In this section, we demonstrate the importance of that requirement, as this requirement has not been fulfilled in previous studies. A series of tests will be done. For each test, two solutions are computed. One, which is already considered in the previous section, uses the lowpass-filtered design matrix **A**, the other
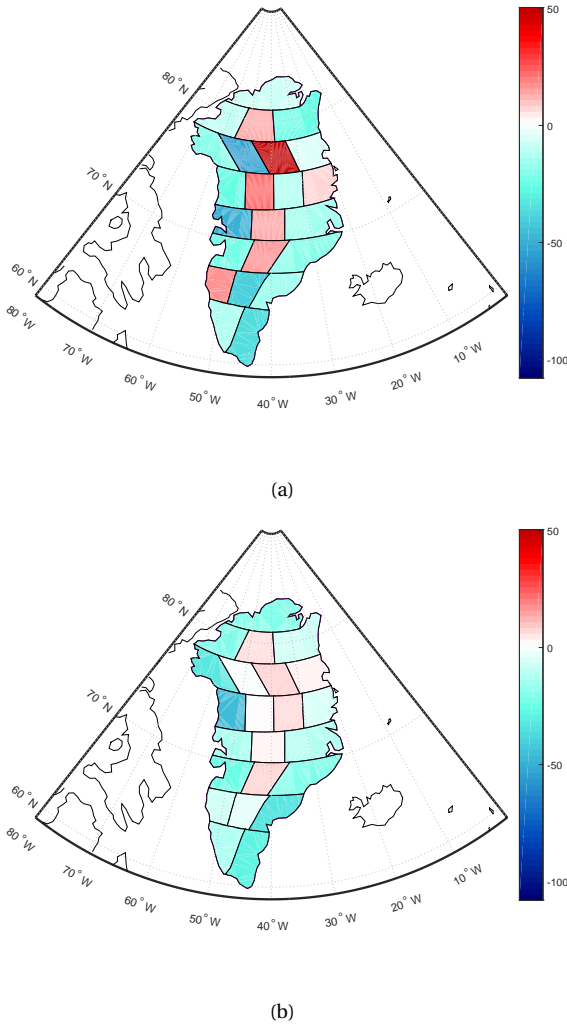
(a)

(b)

Figure 4.12: (a): The spatial pattern of recovered mass anomaly per mascon. They are estimated from the data that were contaminated by the errors presented in Figs 4.4-4.6 (Gt). (b): For a better visual comparison, the true signal defined in Fig. 4.3 is spatially resampled to 23 mascons and shown in the unit of Gt.

one the unfiltered design matrix, $\mathbf{A}'$ (cf. Eq. (4.9)). In all tests, the "true" data are generated using the design matrix $\mathbf{A}$. The number of eigenvalues which are retained in the data weighting varies between 200 and 1,600.

Figure 4.14a, shows the RMS error of the estimated total mass anomalies as a function of the retained eigenvalues. There are hardly any differences between the solutions using design matrix $\mathbf{A}'$ compared to $\mathbf{A}$ if no more than 600 eigenvalues are retained. Above 600 eigenvalues, the RMS error increases quickly if the design matrix $\mathbf{A}'$ is used and attains

42

4. **Statistically optimal estimation of Greenland mass variations from GRACE monthly solutions using an improved mascon approach**
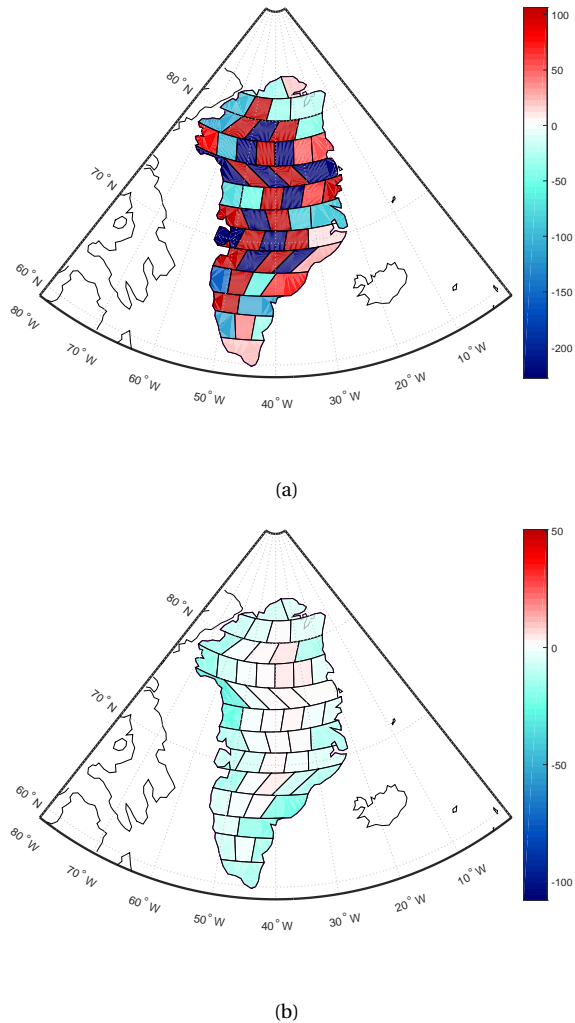
(a)

(b)

Figure 4.13: The same as Fig. 4.12, but for 54 mascons.

values close to the signal. We explain this high RMS error with the fact that the estimated mass anomalies go to zero. When using the spectrally consistent design matrix **A**, the RMS error is almost the same (around 20 Gts) if at least 400 eigenvalues are retained. From this experiment we conclude that spectral consistency is important to obtain high-quality mass anomalies.

In addition, we do a number of experiments to demonstrate the importance of using realistic signal spectra in GRACE numerical studies in general. In those tests, the unfiltered design matrix **A'** is used not only to invert gravity disturbances, but also to simulate them on the basis of yearly mass changes (Section 4.3.1). In that sense, the

mascon functional model in these tests is consistent with the input data. At the same time, the simulated data are not realistic in the sense that the generated signal is not bandlimited unlike signals, which are represented by a truncated spherical harmonic series. Furthermore, the only error source considered in these tests are random errors. Data weighting is used when estimating the mass anomalies.

The tests are performed for different numbers of retained eigenvalues in the spectral representation of the matrix $\mathbf{C_d}$. As shown in Fig 4.15, an unrealistic (not bandlimited) signal spectrum provides error estimates of the mass anomalies, which are much too small. If the number of retained eigenvalues exceeds 1400, the estimated formal RMS uncertainties of the mass anomalies is 10^{-6} Gt. We explain this by a spectral mismatch between signal and noise. Whereas in these experiments the signal bandwidth is not bandlimited, the generated data noise is bandlimited to a maximum spherical harmonic degree 120. Thus, signal above degree 120 is considered as being noise-free. Then, the exploited data inversion procedure, which suppresses data noise in the statistically-optimal way, manages to exploit that high-frequency error-free signal in the recovery of mass anomalies. From these experiments, we conclude that when ignoring a proper reproduction of the signal content in numerical tests, the obtained results may be over-optimistic, particularly when a weighted least-squares estimator is used.

This experiment also explains the poor performance of the statistically-optimal data inversion in the presence of spectral inconsistencies, which have been reported in the previous section. In that case, the applied data weighting assigns unrealistically high weights to high-frequency components of the signal. These signal components, however, have been removed when lowpass-filtering the design matrix. Then, the estimated mass anomalies tend to zero when more and more eigenvalues of the matrix $\mathbf{C_d}$ are retained.

4.4. Real GRACE data analysis

The performance of the proposed approach is analyzed using real GRACE data. Here we use Release-05 GRACE monthly gravity field solutions from CSR from January 2003 – December 2013. Missing months are not interpolated, but just left out. Each monthly solution is provided as a set of SHCs complete to degree 96 including a full noise covariance matrix. We replace the C_{20} coefficient of all monthly solutions with estimates based on satellite laser ranging (*Cheng et al.*, 2013). Degree-1 coefficients are taken from *Swenson et al.* (2008) including noise variances. The Glacial Isostatic Adjustment (GIA) signal in GRACE data is removed using the model compiled by *A et al.* (2013).

The data are used to compute a time-series of Greenland mass anomalies. To that end, we follow the recommended data processing set-up, which is summarized in Table 4.2. We both compute weighted least-squares solutions and ordinary least-squares solutions.

The results are analyzed in three different ways. In Section 4.4.1, we quantify the noise

in the time-series of estimated Greenland mass anomalies using the method proposed by *Ditmar et al.* (2016). It is briefly described in Section 4.4.1. In Section 4.4.2, we compare the GRACE-based time-series (after correction for ice discharge) with time-series of SMB synthesized from the RACMO 2.3 model. We evaluate mass anomalies not only for entire Greenland, but also for individual drainage systems. In line with *van den Broeke et al.* (2009), we merge the 23 patches into five drainage systems: North (N), Northwest (NW), Southwest (SW), Southeast (SE) and Northeast (NE), cf. Fig 4.16. In Section 4.4.3, a comparison between the estimates in this study and other mascons solutions is presented.

4.4.1. Estimating mass anomaly uncertainties

To quantify noise in a mass anomaly time-series, we make use of the approach by *Ditmar et al.* (2016). That approach is based on the assumptions that (i) true signal in the data time-series is close (but not necessarily equal) to a combination of an annual periodic signal and a linear trend; (ii) noise in the data time-series is uncorrelated and (optionally) non-stationary; and (iii) time-series of noise variances is known up to a constant scaling factor. Then, the original data time-series is approximated by a regularized one on the basis of a properly designed regularization functional. Specifically, the regularization functional is defined such that periodic annual signals and a linear trend in the data are not penalized. The optimal regularization parameter is computed with the Variance Component Estimation (VCE) technique (*Koch and Kusche*, 2002). This operation includes the proper scaling of the provided noise variances. Then, the time-series of scaled noise variances is the measure of actual random noise in the considered data. If noise in the data is assumed to be white, the proposed technique allows its standard deviation to be estimated. In this study, we use this method to quantify the uncertainties in mass anomaly estimates both for entire Greenland and for the five drainage systems mentioned before.

Table 4.3 summarizes the main results. They confirm that, compared to an ordinary least-squares solution, optimal data weighting reduces random noise in mass anomaly estimates substantially. The largest reduction, 69%, is observed for the SW drainage system. This is likely due to a relatively large contribution of random noise to the estimated mascon of this drainage system, so that the statistically-optimal data weighting becomes particularly efficient. An increased level of random noise over the SW drainage system can be explained by its relatively small size. The smallest reduction of random noise, which is observed in the NE drainage system, is still substantial, about 35%. For entire Greenland, the random noise is reduced by a factor of two.

4.4.2. Validation against modelled SMB time-series

The estimated mass anomalies are compared with modelled SMB estimates over the period 2003–2013 computed using the Regional Atmospheric Climate Model (RACMO) version 2.3 (*Noël et al.*, 2015). The spatial resolution of the RACMO 2.3 model is 11 × 11 km (see Table 4.1). We integrate the daily SMB estimates over time to produce daily mass

Table 4.3: VCE-based noise standard deviations (in Gt) of estimated mass anomalies for i) entire Greenland, and ii) five individual drainage systems.

Data weighting	N	NW	SW	SE	NE	GrIS
No	14	49	30	39	34	33
Yes	9	16	9	17	17	16
Reduction	35%	67%	69%	56%	52%	50%

Table 4.4: Ice discharge-corrected RMS differences (in Gts) between GRACE-based mass anomaly estimates and SMB-based mass anomalies for i) entire Greenland and ii) five individual drainage systems.

Data weighting	N	NW	SW	SE	NE	GrIS
No	16	48	34	54	37	76
Yes	12	27	18	41	27	63
Reduction	28%	44%	47%	24%	27%	17%

4

anomalies, and then compute on their basis monthly mean values, to be consistent with the temporal resolution of GRACE. Finally, the computed mass anomalies are spatially integrated over individual drainage systems and over entire Greenland, respectively.

The mass anomalies derived from GRACE account for both SMB and ice discharge. According to *van den Broeke et al.* (2009), ice discharge manifests itself mostly as a long-term trend, whereas the seasonal mass variations are largely attributed to surface processes. In view of that, we de-trend both SMB- and GRACE-based time-series prior to their comparison. To that end, we approximate each of them with the analytic function $f(t)$:

$$\begin{aligned} f(t) = {}& A + B(t - t_0) + C\sin\omega(t - t_0) + D\cos\omega(t - t_0) + \\ & E\sin 2\omega(t - t_0) + F\cos 2\omega(t - t_0), \end{aligned} \tag{4.23}$$

where A to F are constant coefficients, which are estimated using ordinary least-squares, t_0 is the reference epoch defined as the middle of considered time interval, and $\omega = \frac{2\pi}{T}$ with $T = 1$ year. The de-trending comprises the first two terms of $f(t)$. After de-trending, the residual GRACE-based and SMB-based time-series are compared. In the comparison, GRACE-based mass anomalies produced both with and without data weighting are considered. The de-trended GRACE-based and SMB-based time-series are shown in Fig 4.17 with and without using data weighting. Remarkable is the erratic behaviour of GRACE-based time-series per drainage system when no data weighting is used. This erratic behavior is averaged out when computing mass anomaly times-series for entire Greenland.

Fig 4.18 shows the time-series of the differences between GRACE-based and SMB-based time-series of mass anomalies. Statistics of the differences are shown in Table 4.4. When data weighting is used, the differences are much smaller compared to solutions without data weighting. The most significant improvement is attained in the SW drainage system, which is consistent with the results obtained with the VCE

46

4. Statistically optimal estimation of Greenland mass variations from GRACE monthly solutions using an improved mascon approach

Table 4.5: Greenland mass anomalies trends over the period 2003–2013 (in Gt/yr) estimated from different solutions and experimental setups.

Different estimates	Trend
With data weighting (this study)	-286
No data weighting (this study)	-276
JPL mascon	-289
CSR mascon	-262
GSFC mascon	-283
Wouters et al. (2008)	-264
Velicogna et al. (2014)	-280
Schrama et al. (2014)	-278

technique (cf. Section 4.4.1). At the same time, the improvement observed for entire Greenland is smaller, about 17%, than those of individual drainage systems (24-47%). This is likely due to the fact that when summing up mass anomalies per mascon to get the mass anomalies of entire Greenland, the random noise is reduced by averaging out. Therefore a relatively low level of random noise can be achieved for the estimates of entire Greenland, compared with the estimates per mascon. However this will not affect the determination of other optimal parameters in Table 4.2. Because our operation (i.e., summing up mass anomalies per mascon to get the mass anomalies of entire Greenland) is applied to the final estimates. As a result, the remaining difference in Fig. 4.18f should rather be explained by residual physical signals than by noise. Such signals may reflect non-linear mass variations not related to SMB, such as inter-annual variability in ice discharge or meltwater retention. A physical interpretation of these signals is outside the scope of this study.

4.4.3. Comparison with Greenland mass anomalies from other studies

The mass anomaly estimates are further compared with those based on existing global and regional mascon solutions, as well as with results from the literature. The available global mascon solutions discussed in this study are the products released by JPL (*Watkins et al.*, 2015), GSFC (*Luthcke et al.*, 2013) and CSR (*Save et al.*, 2016). Note that these mascon solutions are estimated from GRACE KBR data, while the method developed in this study uses GRACE SHCs. We also include the regional mascon solution by *Wouters et al.* (2008), which also takes GRACE SHCs as input. As shown in Fig. 4.19, different mass anomaly time-series of entire Greenland agree with each other very well. The same applies to the linear trend estimates, which are shown in Table 4.5.

As before, we use VCE-based estimation of random noise standard deviations and a validation against modelled SMB estimates to assess the quality of the various mascon solutions. The smallest noise standard deviation (16 Gt) is observed for the solution produced in this study with the optimal data weighting (Table 4.6). A comparable noise standard deviation (19 Gt) is estimated for the JPL solution, whereas standard deviations for other solutions are much larger. When validating against independent SMB output, the solution produced in this study with the optimal data weighting shows, again, the

best performance (see Table 4.7). From Tables 4.6 and 4.7, it follows that relatively low VCE-based standard deviations in the JPL solutions does not indicate a better quality. This might be caused by the fact that spatio-temporal constraints applied in the production of those solutions could reduce random noise, but at a price of introducing a bias in the estimates. The bias becomes visible when validating with independent data such as SMB model estimates. This justifies our decision not to apply any spatial or temporal constraints in producing our solutions in order to minimise biases.

Table 4.6: VCE-based noise standard deviations (in Gts) of estimated mass anomalies for entire Greenland from different mascon solutions. "BW" refers to the solution of *Wouters et al.* (2008).

With data weighting (this study)	Without data weighting (this study)	JPL mascon	CSR mascon	GSFC mascon	BW
16	33	19	29	45	36

Table 4.7: Ice discharge-corrected RMS differences (in Gts) between GRACE-based mass anomaly estimates from different mascon solutions, and SMB-based mass anomalies for entire Greenland. "BW" refers to the solution of *Wouters et al.* (2008).

| With data weighting (this study)	Without data weighting (this study)	JPL mascon	CSR mascon	GSFC mascon	BW
63	76	73	70	76	79

4.5. Summary and conclusions

In this study, we proposed an improved mascon approach compared to the previous studies of *Forsberg and Reeh* (2007) and *Baur and Sneeuw* (2011). Based on numerical experiments, we optimise a number of parameters, which are shown in Table 4.2. The proposed methodology allows the estimation of mass anomalies over Greenland in a statistically-optimal way, by propagating the full noise covariance matrices of SHCs into full noise covariance matrices of gravity disturbances at altitude, which are then used as data in the mass anomaly estimation scheme. We show that the data weighting improves the accuracy of the estimated mass anomalies substantially. The high condition number of the noise covariance matrix is addressed successfully using a truncated eigenvalue decomposition, which retains about 10% of the eigenvalues corresponding to a condition number of about 10^7. We also demonstrated that the optimal size of a mascon is about 300×300 km, which implies about 23 mascons for Greenland. This finding is consistent with the spatial resolution of GRACE reported in the literature (*Longuevergne et al.*, 2010; *Ramillien et al.*, 2004; *Beighley et al.*, 2011). Furthermore, we have proven that spectral consistency of the mass anomaly model and the data is very important to obtain accurate estimates of the mass anomalies. If data weighting is applied, a spectral inconsistency makes the recovery of mass anomalies non-robust and provides severely biased estimates. This is more pronounced if more eigenvalues of the noise covariance matrix are retained. Then, the high-frequency components of the model are over-weighted, resulting in gravity anomalies close to zero, because high-frequency signal is absent in the data. The maximum degree in the

48

4. Statistically optimal estimation of Greenland mass variations from GRACE monthly solutions using an improved mascon approach

low-pass filter applied to maintain a spectral consistency must be consistent with the GRACE solutions utilized to generate the pseudo-observations. More specifically, in the simulation, we choose the maximum degree to be 120, in line with the DMT solutions. However, in the real data processing, the CSR solutions are utilized. Then, the maximum degree is 96, in line with the CSR solutions.

It is worth to mention that the set of parameters shown in Table 4.2 is optimal if the main goal is to estimate mass anomalies of the GrIS over a one-year interval. However, if the main focus is on monthly mass anomalies or on a long-term trend, another setup would have to be preferred, e.g., using the trend from ICESat trend and a SMB model to generate the true signal. We found that then the impact of errors on the results is different from the scenario considered in this paper. For instance, if the target is to obtain an accurate long-term trend, the impact of random noise (north-south stripes) is negligible whereas the parameterization error is the dominant error source. Moreover, then, the optimal number of mascons is below 23. On the other hand, if the main interest is on seasonal mass variations, random noise is the dominant error source, and the optimal number of mascons is larger than 23. These results will be discussed in detail in Chapter 6. For instance, the analysis of a long-term trend is based on a many monthly GRACE solutions. Consequently, random noise in the obtained estimates is likely substantially reduced, as compared to our numerical study. In that case, the optimal mascon size may be smaller than 300 × 300 km, which was found to be the best one in our analysis.

We also applied the proposed data processing scheme to real GRACE data and computed mass anomaly time-series for 5 drainage systems and entire Greenland. Using VCE, we found that when a proper data weighting is used, the accuracy of the estimated mass anomalies increases by a factor of 1.5 to 3.0, depending on the drainage system. A comparison of the GRACE-based mass anomalies with modelled SMB mass anomalies revealed that a proper data weighting provides a better fit of GRACE-based and SMB-based mass anomalies, with improvements between 24% and 47% depending on the drainage system. We consider this as indication that a proper data weighting provides much more accurate estimates of mass anomalies. The improvement is, however, marginal for entire Greenland. This is likely due to a relatively minor role of random noise when estimating mass anomalies over very large areas.
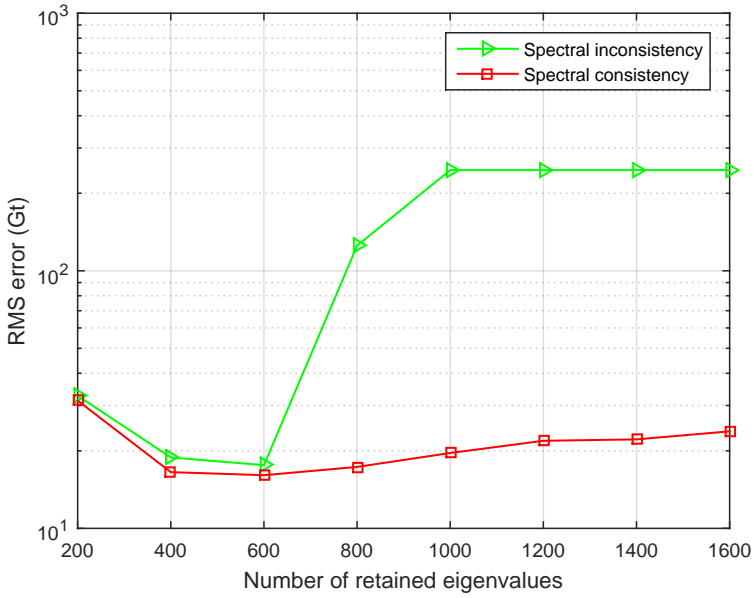
(a)
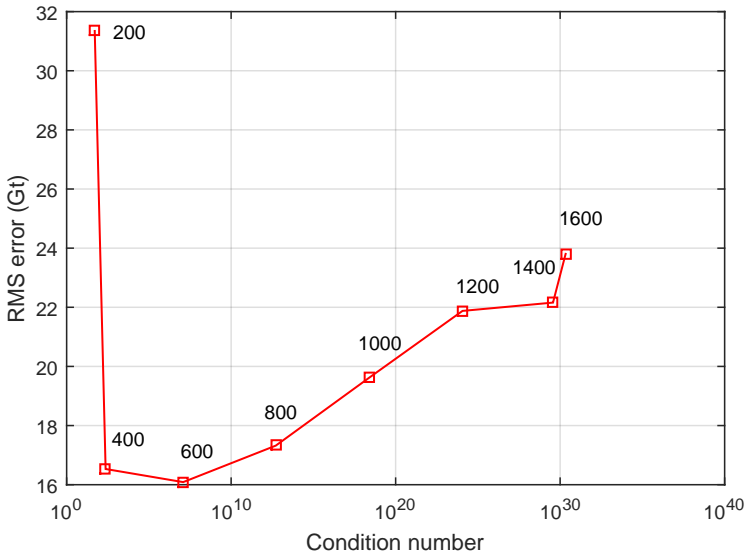
(b)

Figure 4.14: RMS errors in estimated mass anomalies as function of (a) the number of retained eigenvalues and (b) the condition number after truncation.
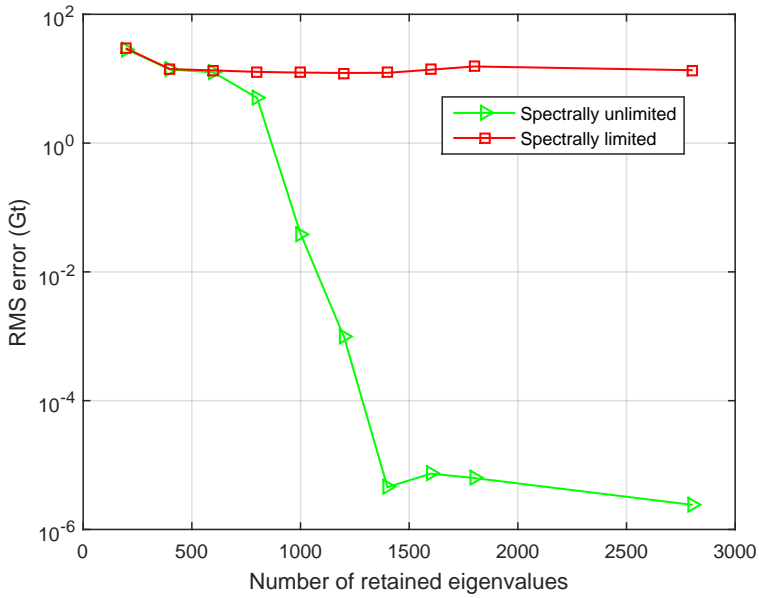
Figure 4.15: RMS errors of estimated mass anomalies over entire Greenland as function of the number of retained eigenvalues. Data weighting is applied.
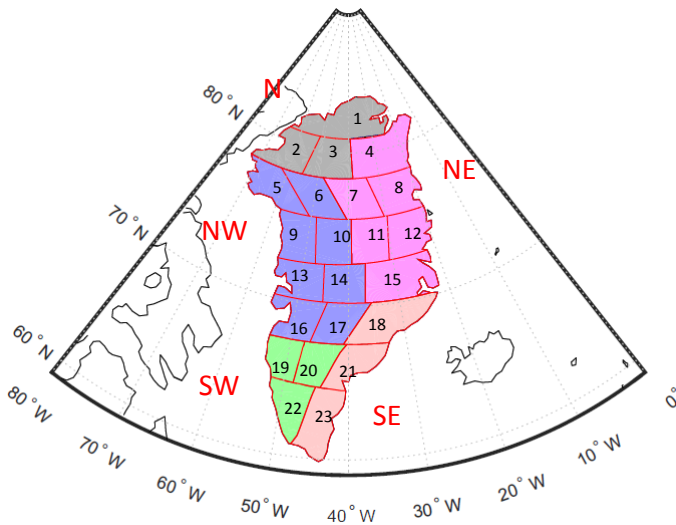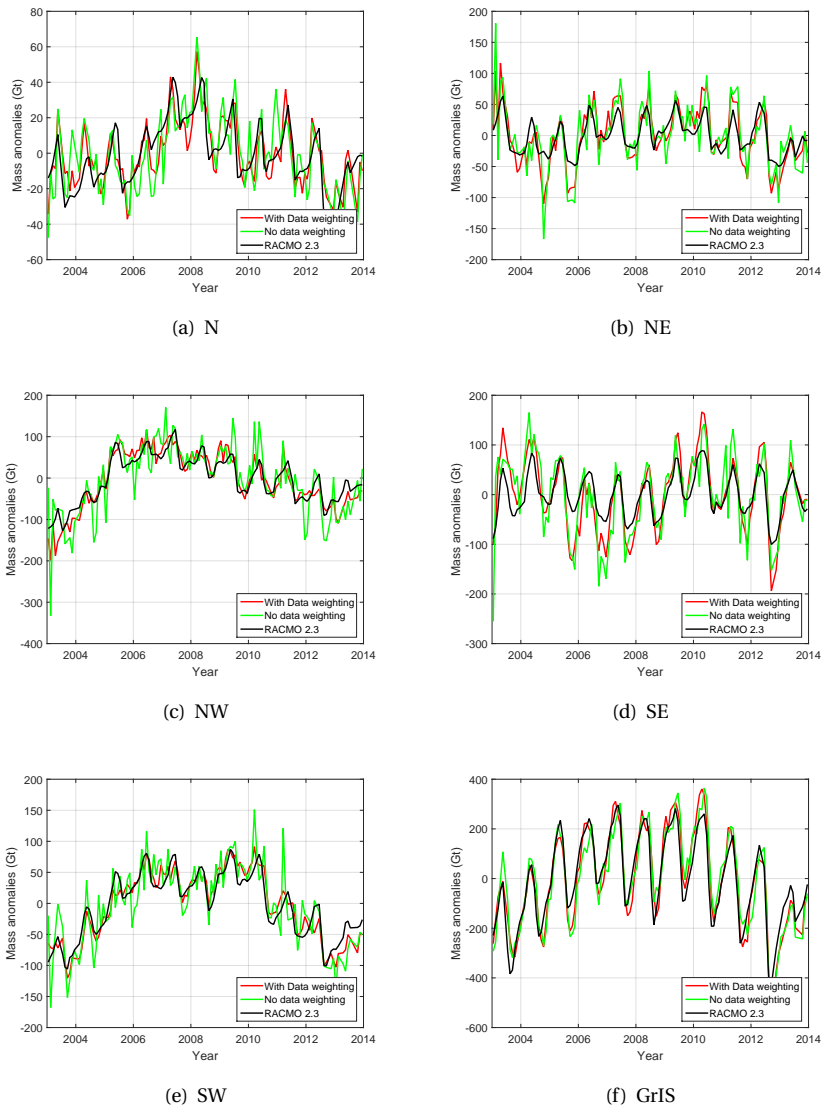

Figure 4.16: Partitioning of Greenland into 23 mascons and the definition of the five individual drainage systems.

Figure 4.17: De-trended mass anomaly time-series based on modelled SMB and GRACE data, respectively, for individual drainage systems and entire Greenland. GRACE-based time-series were computed with (red) and without (green) data weighting.
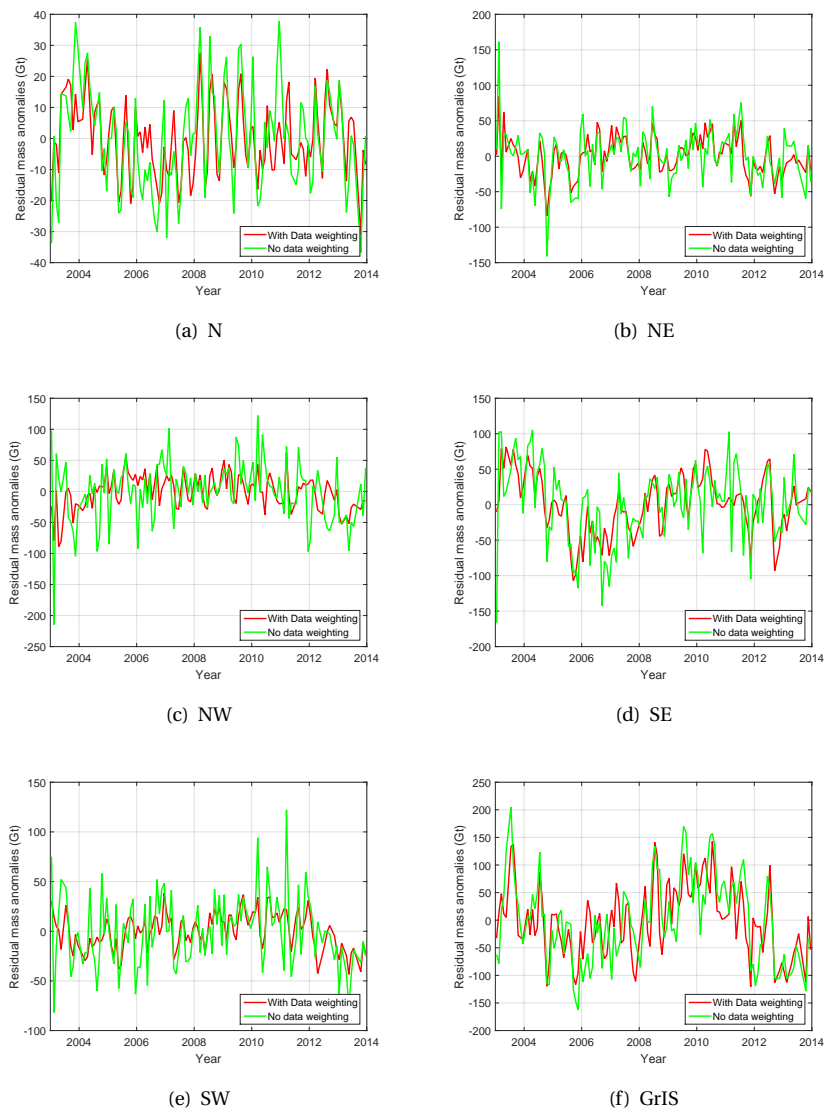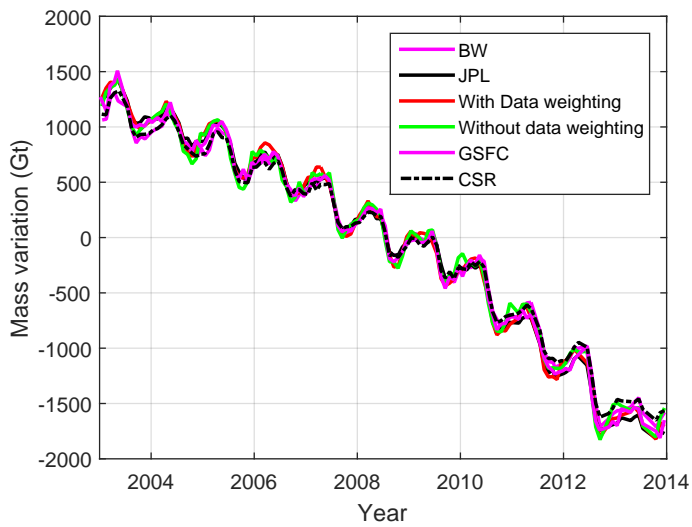
(a) N

(b) NE

(c) NW

(d) SE

(e) SW

(f) GrIS

Figure 4.18: Differences of SMB-based and GRACE-based de-trended mass anomaly time-series for individual drainage systems and entire Greenland. GRACE-based time-series were computed with (red) and without (green) data weighting.

Figure 4.19: The mass anomaly time-series produced by *Wouters et al.* (2008) (marked as "BW"), JPL, with data weighting (this study), without data weighting (this study), GSFC and CSR.

5

Seasonal mass variations show timing and magnitude of meltwater storage in the Greenland ice sheet

5.1. Introduction

In this Chapter, we analyze the meltwater accumulation and runoff in Greenland using data from GRACE, SMB, and ice discharge. GRACE is a powerful tool to moniter mass variations over Greenland (including peripheral glaciers and tundra), on monthly to multi-year time scales. Those variations result from the combination of three effects: (i) mass accumulation due to surface mass balance (SMB), (ii) mass loss due to ice discharge to the ocean, and (iii) sub-glacial meltwater accumulation and run-off.

Recent GrIS mass loss has been quantified in several studies (e.g., *Shepherd et al.*, 2012; *Schrama et al.*, 2014; *Velicogna et al.*, 2014). Furthermore, several authors have estimated the contribution to this mass loss of SMB and ice discharge individually (*van den Broeke et al.*, 2009; *Enderlin et al.*, 2014; *Velicogna et al.*, 2014; *van den Broeke et al.*, 2016). To quantify the contribution of SMB, regional climate models (RCMs) are typically used, such as the Regional Atmospheric Climate Model v. 2 (RACMO2) (*Ettema et al.*, 2009b), MAR (*Fettweis et al.*, 2005) and Hirham (*Christensen et al.*, 1996). The contribution of annual ice discharge rates is estimated by combining ice flow velocity data and ice thickness data at flux gates (*Thomas et al.*, 2000). Importantly, ice velocities have, on average, increased during the last two decades (*Moon et al.*, 2012), so that they have to be monitored on a regular basis. The motivation to investigate the multi-year mass variation trend and acceleration budgets in this Chapter is two-fold. First, we compare the estimates of long-term mass variations with the values provided in literature over the same time interval, to validate the novel approach proposed in Chapter 4. Second, we attempt to examine the accuracy of long-term mass variations modelled by SMB, using GRACE data and ice discharge observation.

The analysis of GrIS mass variations at the intra-annual time scale is still in its infancy. This is largely because (i) the accuracy and resolution of GRACE monthly solutions is relatively poor, as compared to long-term trend estimates, and (ii) ice velocity data at this time scale are scarce (typically, only a few estimates per year, often spanning only a few years). A first attempt to combine GRACE data and SMB modelling in order to evaluate an ice dynamics model of the GrIS at the monthly time scale was made by *Schlegel et al.*

(2016). The only study of multi-regional intra-annual variations of GrIS outlet glacier velocities was conducted by *Moon et al.* (2014), who analyzed 55 marine-terminating glaciers in northwest and southeast Greenland over the period 2009–2013.

The GrIS mass balance is also characterized by supra-, en- and subglacial meltwater retention. An example is the abundance of supra-glacial lakes primarily in west Greenland, which store water during the melt season (*Selmes et al.*, 2011). Sub-glacial hydrology is an area of active research (see e.g., *Chandler et al.*, 2013; *Slater et al.*, 2015). Until now, however, time-varying meltwater retention has been mostly investigated at a local scale. For instance, *Rennermalm et al.* (2013a) quantified meltwater retention in a small watershed (36-65 km^2) near Kangerlussuaq. They suggested that ~54% of liquid water is retained during one to six months in this watershed. An exception is the study by *Van Angelen et al.* (2014). From fitting de-trended GRACE observations and SMB model output, they found that the mean period of meltwater retention at the whole-ice-sheet scale is ~18 days.

In this Chapter, we systematically analyze the individual contributions to total inter- and intra-annual mass variations over Greenland at both regional and whole-ice-sheet scales. This includes isolating the signal associated with the seasonal accumulation and run-off of meltwater. For this purpose, we combine observations of total mass variations from GRACE with observations of ice discharge to the ocean (*Enderlin et al.*, 2014; *Moon et al.*, 2014) and modelled SMB estimates from RACMO2.3 (*Noël et al.*, 2015). Since the spatial resolution of GRACE data is limited, the obtained estimates cover both the GrIS and the areas outside the GrIS, including the tundra and the peripheral glaciers disconnected from the GrIS.

The structure of this Chapter is as follows. Section 5.2 describes the adopted parameterization. The data used in this Chapter are introduced in Section 5.3. In Section 5.4, we present and discuss our results. Finally, we present our conclusions in Section 5.5.

5.2. Adopted parameterization

To study GrIS mass variations at the regional scale, we make use of a variant of the mascon approach presented in Chapter 4. We update the recommended parameterization of 23 mascons, by subdividing the territory of Greenland into 28 mascons. This is because of the fact that the mass losses of the GrIS are concentrated in the narrow coastal zone near the margin of the ice sheet. To take this information into account, we introduce additional mascons of 100-km width along the ice mask border. The resulting parameterization is shown in Fig. 5.1.

In addition, and similar to Chapter 4, we include nine patches around Greenland to attenuate leakage of signals from outside Greenland. The data processing scheme recommended in Chapter 4 is used in the computations presented below, unless stated otherwise.

Finally, we aggregate the 28 mascons inside Greenland into five drainage systems (cf Fig. 5.1), similarly to *Luthcke et al.* (2006a) and *van den Broeke et al.* (2009). We refer to these drainage as: (a) North (N); (b) Northwest (NW); (c) Southeast (SE); (d) Southwest (SW); and (e) Northeast (NE) (Fig. 5.1). We slightly shifted the border between the NW and SW drainage systems southwards compared to *Luthcke et al.* (2006a) and *van den Broeke et al.* (2009), to ensure that the SW drainage system is mostly limited to land-terminating outlet glaciers. In addition, whole-ice-sheet anomalies are obtained by a summation over all 28 Greenland mascons.
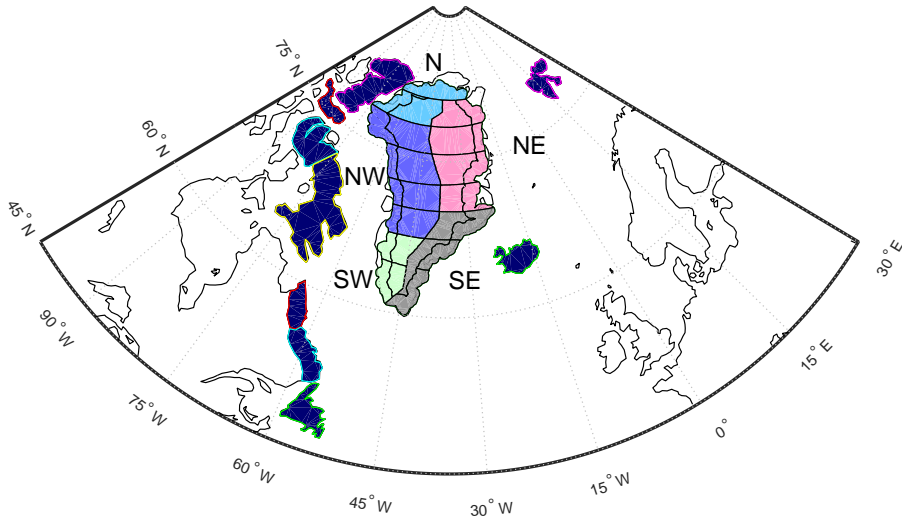
Figure 5.1: The 28-patch parameterization of Greenland used in this study for GRACE data processing. For the purpose of further analysis, these patches are merged into five drainage systems (N, NE, SE, SW, and NW) defined approximately as in *van den Broeke et al.* (2009). 55 glaciers utilized to compute seasonal ice discharge are marked as red pentagrams.

5.3. Data

In addition to GRACE monthly solutions, we also use SMB output from RACMO2.3 (*Noël et al.*, 2015). It is worth to mention that previous work on the sources of current GrIS mass loss used relative SMB and ice discharge anomalies with respect to an equilibrium state (1961-1990) (e.g., *van den Broeke et al.*, 2009; *Velicogna et al.*, 2014). Effectively, this means that the time-series of mass anomalies were de-trended to ensure that they are close to zero during the reference equilibrium period. Here, we use time-series of absolute total SMB, and ice discharge mass anomalies, i.e., without referring to a hypothesized equilibrium state. In this way, we are able to extract more information from the data. For instance, absolute mass anomalies related to ice discharge cannot increase over time, which is a valuable constraint that facilitates the correct interpretation of the results. In addition, since GRACE senses mass anomalies

not only within the GrIS, but also at ice caps and tundra areas, we use SMB estimates that included non-GrIS areas of Greenland, too.

For more basic information about the GRACE data and RACMO 2.3 output, we refer to Chapter 4. Moreover, we also use ice discharge observations both at multi-year and intra-annual scales. A brief explanation of how they were obtained is given below.

5.3.1. Ice discharge at multi-year scale

The long-term ice discharge of the GrIS over 2003-2012, which was derived for the flux gates within 5 km to the termini (*Enderlin et al.*, 2014), is utilized to investigate the GrIS mass variations at the multi-year scale. There are 178 outlet glaciers considered in this study. For more details about this data set, we refer to *Enderlin et al.* (2014).
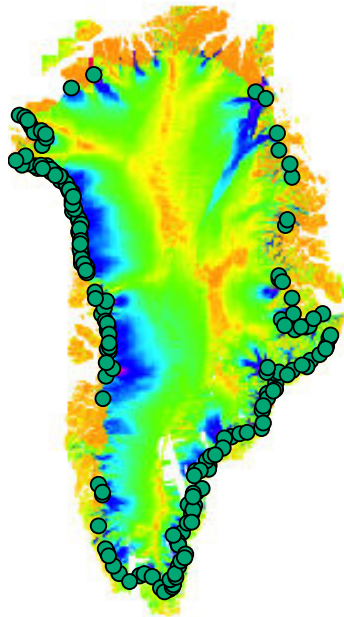

Figure 5.2: Outlet glaciers (178 in total) considered by *Enderlin et al.* (2014) to infer the long-term ice discharge of GrIS. The base-map is shown as the velocities over 2007-2010 by *Moon et al.* (2014).

5.3.2. Ice discharge at intra-annual scale

To investigate ice discharge at intra-annual scale, we consider 55 glaciers (cf Fig. 5.3) in northwest and southeast parts of Greenland, which are believed to be the two largest

contributors to ice discharge in Greenland. The data cover the time interval 2009-2013. We use ice flow velocities derived from TerraSAR-X image measurements (*Moon et al.*, 2014) and ice thicknesses from the IceBridge BedMachine Greenland version 2 data (*Morlighem et al.*, 2015) (cf Fig. 5.4). Ice discharge (D) for a given glacier is defined as the ice mass flux across the flux gate (f) close to the glacier terminus (within ~5 km):

$$D = \rho \int_f h(\boldsymbol{v} \cdot \mathbf{n}) \mathrm{df}, \tag{5.1}$$

where h is the ice thickness; $\mathbf{n}$ is the unit vector directed outwards normally to the flux gate; $\boldsymbol{v}$ is the ice flow velocity; and ρ is the ice density. It is worth to mention that when selecting flux gates, one needs to pay attention to variations of the terminus position by checking the images of glaciers during the whole time interval, to make sure the flux gate is in the upstream of the terminus. Furthermore, a flux gate should cover the whole outlet glacier to the ice flow edges. To compute D, we discretize the flux gates into nearly 200-m long intervals. The distance of the last interval is adjusted to make sure that the ice flow edge is sampled. We then use the values ($h, \boldsymbol{v}$ and $\mathbf{n}$) defined for the center of each interval, assuming that they are constant over the entire interval. Then Eq. 5.1 becomes

$$D = \rho \sum_{i=1}^{N} d^i h^i (\boldsymbol{v^i} \cdot \mathbf{n}), \tag{5.2}$$

where N is the total number of intervals of the flux gate and d^i is the length of the i-th interval.

5.4. Results and Discussion

5.4.1. Multi-year mass trend and acceleration budgets

First, we examine multi-year mass trends and accelerations in terms of the total mass balance and the contributions thereto from SMB and ice discharge (cf. Fig. 5.5). We approximate each mass anomaly time-series (cf. Figs. 5.5-5.10) with the following analytic function:

$$f(t) = a_1 + a_2(t - t_0) + a_3 \frac{(t - t_0)^2}{2} + a_4 \sin \omega t + a_5 \cos \omega t + a_6 \sin 2\omega t + a_7 \cos 2\omega t, \tag{5.3}$$

where a_1, ..., a_7 are parameters to be estimated, t_0 is a reference epoch defined as the middle of the considered time interval (i.e., 2003-2013), and $\omega = 2\pi/T$ with $T = 1$ year. Our estimate of the total-mass linear trend, a_2, which is based on the primary GRACE data time-series, is -286 ± 21 Gt/yr for 2003-2013. This value is in agreement with those published earlier: -280 ± 58 Gt/yr for January 2003 until December 2013 (*Velicogna et al.*, 2014) and -278 ± 19 Gt/yr over the same period (*Schrama et al.*, 2014). Our estimates of trend uncertainties are composed of signal leakage (including both signals which leaked from outside Greenland and signals from inside Greenland leaked between the mascons), the error of the GIA model (we set it as 50% of the signal), the measurement
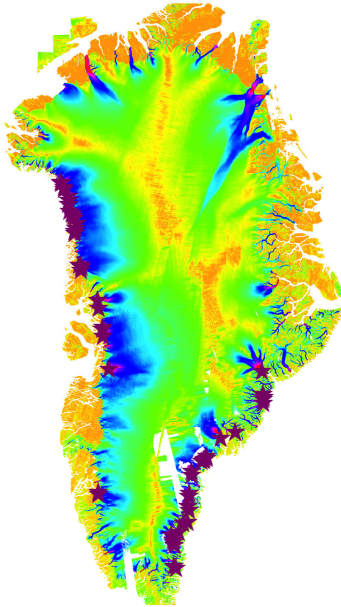
Figure 5.3: Similar to Fig. 5.2, but for the geographic distribution of 55 glaciers used to infer the ice discharge of GrIS at the intra-annual time scale.
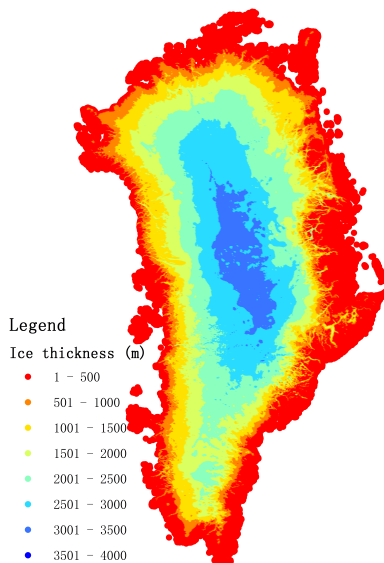

Figure 5.4: Ice thickness of Greenland from the IceBridge BedMachine Greenland version 2 data.

errors of GRACE propagated from full variance-covariance matrix of monthly solutions, and the uncertainty associated with a particular choice of the oceanic mascon layout (*Bonin and Chambers*, 2013) (cf. Table 5.1). Unlike *Velicogna and Wahr* (2013), we do not consider errors from atmospheric and ocean circulation corrections, due to their small contribution.
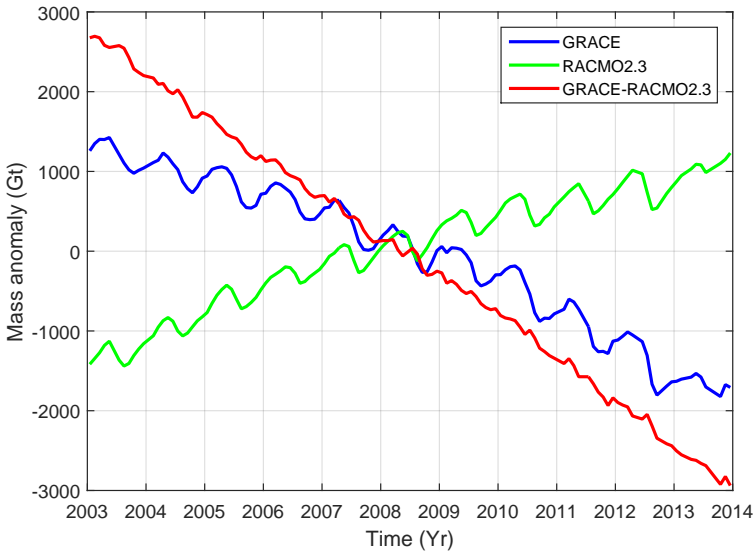
Figure 5.5: Time-series of mass anomalies over the period 2003-2013 for the entire GrIS: total mass anomalies from GRACE (blue), cumulative SMB anomalies from RACMO2.3 (green), and the difference between them, "Total-SMB" (red).

Table 5.1: Contribution of different error sources to the error in the total GrIS mass trend estimated from GRACE data (Gt/yr).

Contributor	Signal leakage	GIA correction	Ocean parameterization	GRACE data	Total error
Error	15	8	7	10	21

We examine also the SMB and ice discharge contributions to the total mass trend over the reduced time interval, 2003-2012, in order to be consistent with the ice discharge record, which ends in 2012 (Table 5.2). The multi-year average mass gain from SMB (RACMO2.3) over that period is 231 ± 122 Gt/yr. The standard error is computed by assuming a 9-% error in accumulation and a 15-% error in meltwater runoff signals modeled by RACMO2.3. The time-series of cumulative mass anomalies related to ice discharge and other processes not related to SMB is obtained as the difference between

the total mass variations and the cumulative SMB-related ones; this difference will be referred to as "Total-SMB" ("Total minus SMB", cf. red curve in Fig. 5.5). The associated rate of linear mass loss over 2003–2012 is 508 ± 124 Gt/yr, which perfectly matches the ice discharge estimate from *Enderlin et al.* (2014), 520 ± 31 Gt/yr.

Next, we present the results of a similar analysis for the individual DSs. The greatest total mass losses are observed by GRACE in DSs NW and SE (cf. Figs. 5.6-5.10 and Table 5.2). These two DSs account for 76% of the total mass loss over Greenland. The inter-annual behavior of these DSs is, however, different. SE loses mass with an approximately constant rate over the whole considered period. In contrast, NW is relatively stable in over the period 2003-2005, but starts loosing mass thereafter. The remaining three DSs lose mass at much smaller rates. Remarkably, two of these DSs (N and SW) show a similar behavior: they are relatively stable over the period 2003-2009, and start loosing mass in 2010. These findings are consistent with *Velicogna et al.* (2014). The SMB is negative in two DSs (N and SW) (cf. Table 5.2). However, with a large fraction of land-terminating glaciers, ice losses from ice discharge are an order of magnitude lower there than in the NW and SE DSs (cf. Figs. 5.6-5.10), resulting in only modest total mass loss in spite of the negative SMB.

The long-term trends of Total-SMB residuals in the DSs of NW, NE, and SW are consistent with the ice discharge estimates from *Enderlin et al.* (2014) within the error bar (Table 5.2). This suggests robustness of RACMO2.3 long-term SMB trends there, under the assumption that the meltwater storage signal is mainly seasonal. In the SE and N, however, we find relatively large discrepancies between our Total-SMB estimates and ice discharge observations from *Enderlin et al.* (2014). Under the conditions of realistic GRACE error estimates and minimal multi-year meltwater storage, all these inconsistencies indicate a precipitation overestimation in the SE and underestimation in the N in RACMO2.3. However, it is also important to keep in mind that discharge estimates are relatively inaccurate in SE because of various sources of large uncertainties: ice velocities (due to a decorrelation of SAR images in the presence of fast ice flows), ice thicknesses, and corrections for SMB signals at the locations between flux gates and grounding line.

Average accelerations of mass anomalies over the period 2003-2012 for entire Greenland are also estimated using Eq. 5.3 (parameter a_3). The SMB (-29.7±2.7 Gt/yr2) contributes with 95% to the total acceleration observed by GRACE (-31.1±8.1 Gt/yr^2) (Table 5.3). This is close to the estimates of *Velicogna et al.* (2014), who assessed the contribution of SMB to the total GrIS mass loss acceleration as 79%. The contribution of the residual term "Total-SMB" to the mass loss acceleration of entire Greenland is statistically insignificant. Analysis of individual drainage systems leads to similar conclusions (cf. Table 5.3).

5.4.2. Seasonal mass variations

We analyze the mean annual cycles of total (GRACE) and cumulative SMB (RACMO2.3) mass anomalies over the period 2003-2013 (Fig. 5.11). To derive them, we divide the
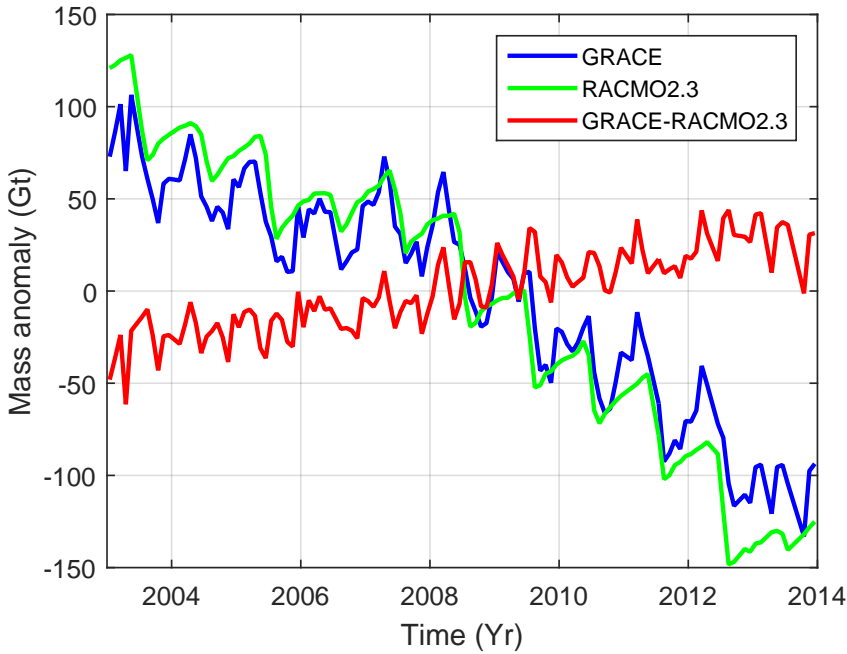
Figure 5.6: Same as Fig. 5.5, but for the N drainage system indicated in Fig. 5.1.

Table 5.2: Linear mass change rates over the period 2003-2012 for individual drainage systems; Total, SMB-related, and "Total-SMB" (GRACE minus RACMO2.3), as well as ice discharge (Gt/yr). The sign of "Total-SMB" estimates is changed to make them directly comparable with ice discharge estimates.

Contributor	N	NW	NE	SW	SE	GrIS
Area (10^{12}m^2)	0.26	0.69	0.60	0.21	0.40	2.16
Total (GRACE)	-16 ± 11	-107 ± 23	-20 ± 16	-40 ± 10	-105 ± 23	-277 ± 21
RACMO 2.3	-23 ± 11	84 ± 28	2 ± 20	-29 ± 27	197 ± 39	231 ± 122
-(Total-SMB)	-6 ± 16	190 ± 36	22 ± 26	1 ± 29	300 ± 45	508 ± 124
Ice discharge	21 ± 13	206 ± 14	41 ± 10	18 ± 7	234 ± 20	520 ± 31

Table 5.3: Acceleration of mass change over the period 2003-2012 for individual drainage systems: total, SMB-related, and "Total-SMB" (GRACE minus RACMO2.3), as well as ice discharge (Gt/yr^2). The sign of "Total-SMB" estimates is changed to make them directly comparable with ice discharge estimates.

Contributor	N	NW	NE	SW	SE	GrIS
Total (GRACE)	-2.9 ± 1.5	-15.6 ± 3.1	-1.1 ± 2.9	-10.9 ± 4.2	-0.8 ± 5.2	-31.1 ± 8.1
RACMO 2.3	-2.9 ± 0.4	-13.0 ± 1.1	-0.4 ± 0.2	-12.8 ± 0.9	-0.7 ± 0.4	-29.7 ± 2.7
-(Total-SMB)	0 ± 1.6	2.6 ± 3.3	0.7 ± 2.9	-1.9 ± 4.3	0.1 ± 5.2	1.4 ± 8.5
Ice discharge	0.5 ± 0.5	2.1 ± 0.7	0.2 ± 0.5	-0.1 ± 0.4	-0.1 ± 1.1	2.5 ± 1.5

entire period into eleven overlapping 13-month time intervals, each of which starts in December of the previous year and ends in December of the current year. Then, the
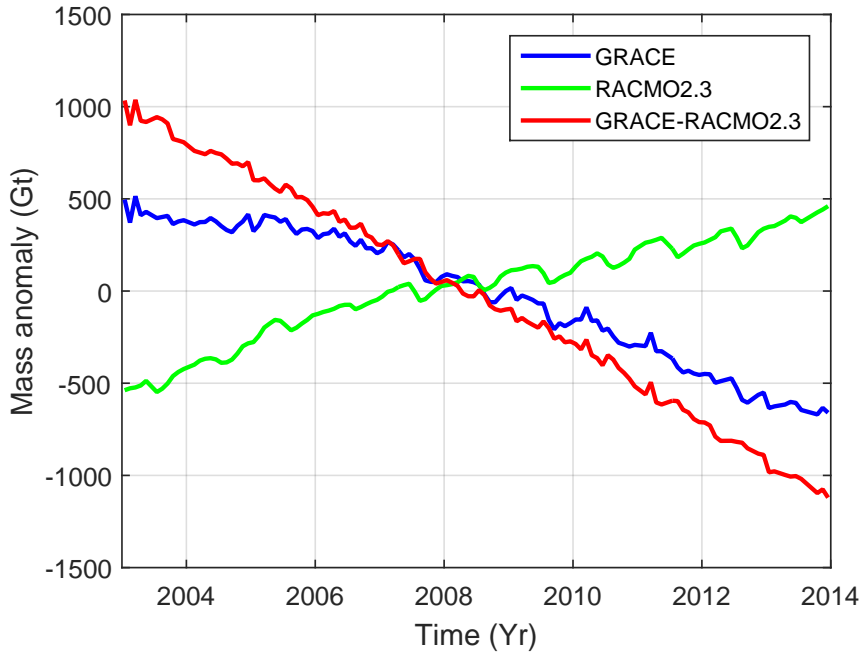
Figure 5.7: Same as Fig. 5.5, but for the NW drainage system.

mean mass anomaly for each calendar month is estimated by linear regression, together with one bias parameter per time interval, which accounts for a long-term variability. This scheme is less sensitive to gaps in data time-series than the plain averaging of mass anomalies per calendar month. The uncertainties of mean mass anomalies of GRACE are propagated from the error of each monthly GRACE estimates. The uncertainties of cumulative SMB mean mass anomalies are computed by assuming 9% and 15% errors in modeled mean mass anomalies due to precipitation and runoff, respectively. The uncertainties of Total-SMB mass anomalies are the root-sum-square of the two noises in GRACE and cumulative SMB estimates.

The whole-Greenland mean annual cycles of total and cumulative SMB mass anomalies present smooth month-to-month variations (Fig. 5.11). Importantly, the estimates of both types refer to the mean values for the months considered. The total mass from GRACE reaches its maximum in March and then steadily decreases until September. The most rapid mass loss is observed in July-August (~200 Gt). In contrast, the cumulative SMB decreases over a much shorter period - only from May to August.

We use the Total-SMB difference (brown line in Fig. 5.11) to evaluate the SMB modelling and to estimate non-SMB contributions to seasonal mass variations. Under the assumption of minor GRACE errors and SMB model biases, the Total-SMB represents the cumulative sum of ice discharge and meltwater storage. The Total-SMB shows three
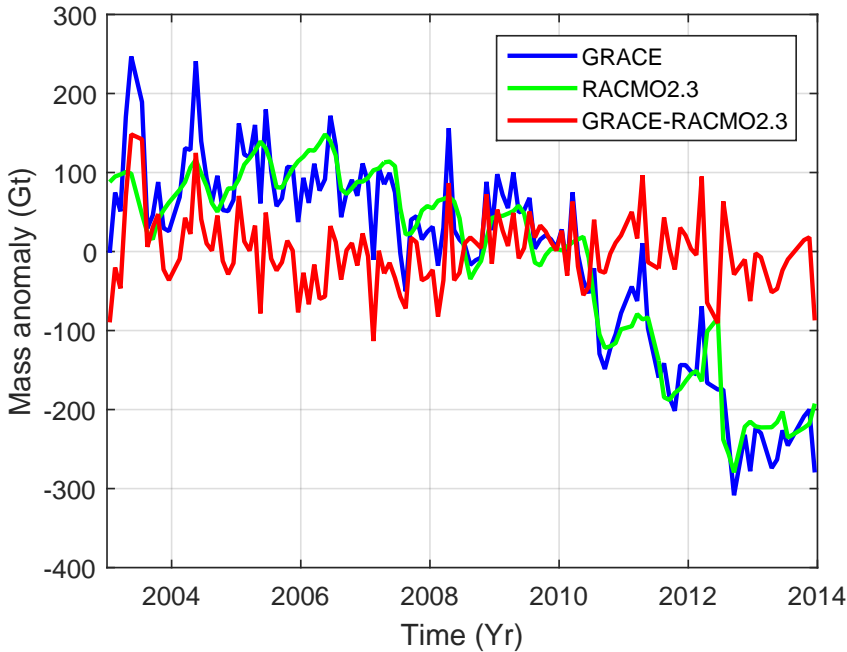
Figure 5.8: Same as Fig. 5.5, but for the SW drainage system.

periods of almost null variations (nearly flat segments in Fig. 5.11): February-March, May-July and November-December. If we assume that the main contributor to the Total-SMB is ice discharge, these nearly flat cumulative variations would indicate that ice discharge is negligible or negative, which is unphysical. From the obtained error bars and a comparison of Total-SMB from several different GRACE solutions (cf. Figs. B.1-B.5), we infer that the quasi-null Total-SMB variations during February-March and November-December are likely caused by noise in the estimates (see Appendix B). In the following, therefore, they will not be discussed. On the other hand, the summer flat feature of May-July persists, no matter how processing parameters are defined and which GRACE estimates are utilized. Therefore, we suggest that this feature is not triggered by noise in the estimates and must be attributed to a physical signal. Most probably, this signal is caused by meltwater retention.

According to RACMO2.3, meltwater is mostly produced between May and September, and peaks in July (cf. Fig. 5.12). Approximately 800 Gt of meltwater are produced on average in Greenland during the melt season, of which ~250 Gt are estimated to refreeze within the snowpack, and the rest is subject to run-off. However, RACMO2.3 does not take into account the time needed for meltwater to run off. During late spring and early summer, this time is particularly long due to an inefficiency of the sub-glacial channelized network (*Rennermalm et al.*, 2013b) and replenishing of firn aquifers (mainly in the SE and NW) (*Forster et al.*, 2014; *Miège et al.*, 2016).
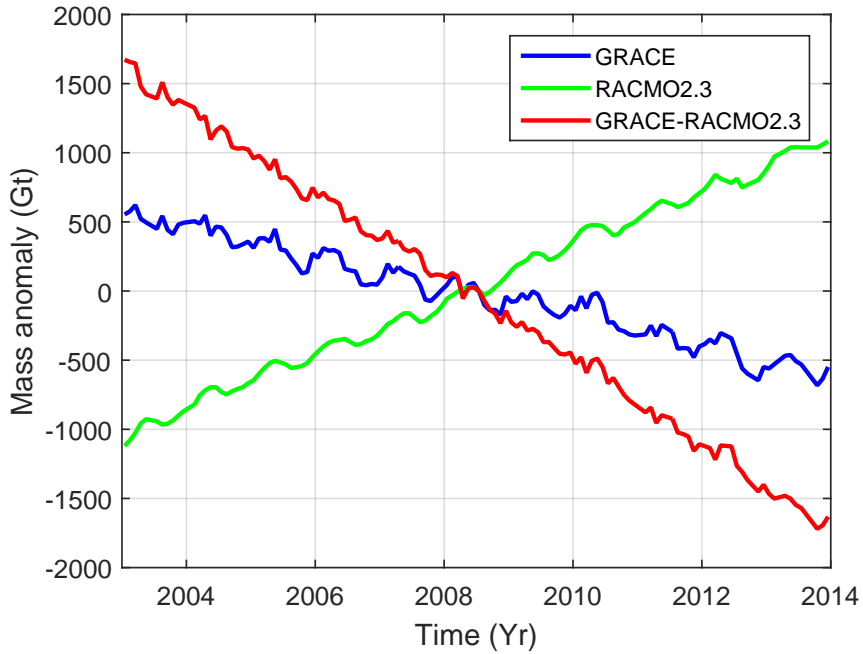
Figure 5.9: Same as Fig. 5.5, but for the SE drainage system.

In order to estimate the instantaneous amount of meltwater subject to runoff, we first fit the 11-year-mean Total-SMB residuals in two periods, before and after the flat feature (April-May and September-November), with a linear function. This function can be interpreted as an empirical estimation of the mean combined effect of ice discharge and the difference between the modelled meltwater refreezing and the actual one. Then, we force the mass budget at the beginning and the end of the melt season to be closed by subtracting the obtained linear function from the Total-SMB residuals (Fig. 5.13a). In this way, we find that meltwater is retained in Greenland between May and October, with a 100 ± 20 Gt maximum in July.

One may argue that seasonal variations of non-SMB mass anomalies (our "Total-SMB") may be caused not only by delayed meltwater runoff, but also by the variability of ice discharge. An effort to quantify the contribution of the latter is made here. To that end, we use an independent dataset of sub-annually resolved glacier discharge for 55 glaciers, which are mainly located in the NW and SE DSs. The sum of the obtained estimates over all 55 glaciers is shown in Fig. 5.14. One can see that at the whole-ice-sheet scale, the increase in ice discharge during the melt season is minor in all years (~10% or less). In the absence of complete coverage of the GrIS with observations of glacier velocities at the intra-annual time scale, we scale up the sum of ice discharge estimates by a factor of ~2 to reach an agreement with the discharge over the entire GrIS in terms of the long-term
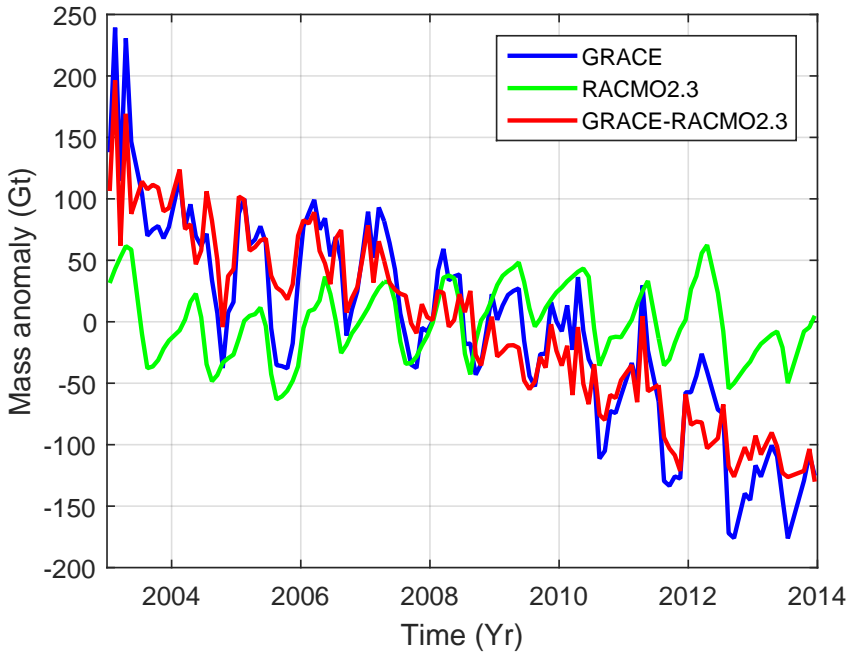
Figure 5.10: Same as Fig. 5.5, but for the NE drainage system.

5

linear trend (*Enderlin et al.*, 2014). Similar to Fig. 5.13a, we represent the ice discharge related mean mass anomaly per calendar month in terms of the deviation from the linear function fitting the values in April-May and September-November (cf. Fig. 5.15). One can see that the effect of ice discharge amounts to only a few Gt, i.e. its contribution to the total signal is negligible. This indicates that delayed runoff is the major contributor to the signal isolated in Fig. 5.13a.

Next, we examine individual drainage systems (cf. Figs. 5.16-5.20). As was the case for the whole Greenland, the Total-SMB flat features of February-March and November-December are not consistent across different GRACE processing methods, whereas the May-July feature is. This implies that seasonal meltwater retention also manifests itself at the scale of individual drainage systems. Regionally, the SE and NW show the largest meltwater accumulation per unit area (Fig. 5.13b). This is consistent with the fact that the rate of meltwater production is large in these sectors (see the bottom panel of Fig. 5.12), as is the retention potential owing to high accumulation rates (*Miège et al.*, 2016). In view of a later onset of the melt season, the NW and N regions store meltwater during a shorter period than the SE. In the NE region, the signal related to meltwater retention is less pronounced, which can be explained by the dry climate of this region, meaning that less pore space is available in the firn layer to store liquid water. As far as the SW region is concerned, we refrain from any conclusions due to a relatively high level of noise in the obtained estimates. It is likely caused by a relatively small area of the region. In terms of
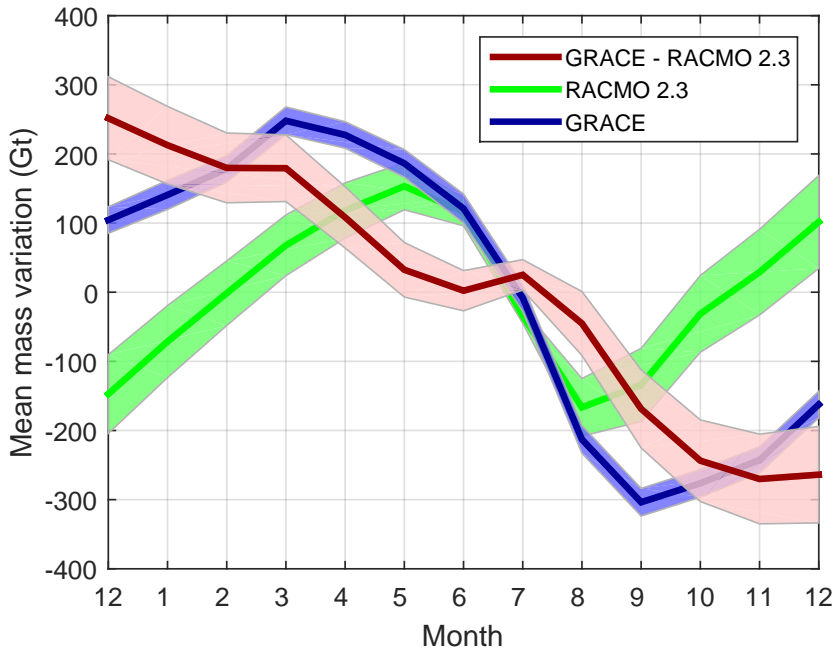
Figure 5.11: 2003-2012 Greenland mean annual cycle of cumulative total mass anomalies from GRACE (dark-blue), cumulative SMB anomalies (green) and the difference between them (red) for the period 2003-2012. The latter is used as proxy of the cumulative sum of seasonal ice discharge variations and meltwater retention, provided minor GRACE error and SMB model bias. The shaded strips show the 2-σ error bars. X-labels indicate month of the year (Month 1 denotes January, month 12 is December).

the total mass, the largest meltwater accumulation takes place in the NW and SE regions: the contribution of each region may reach in July-August about 40 Gt (see Fig. 5.21). As for the increase in ice discharge during the melt season, we find that it is relatively minor for both NW and SE DSs (less than 20% and 10%, respectively; see Figs. 5.22-5.23). As such, the contribution of ice discharge to the signal reported in Fig. 5.21 is minor for both NW and SE DSs: not more than 2.0 and 0.3 Gt, respectively (cf. Figs. 5.24-5.25). Interestingly, a much larger increase in ice discharge during the melt season is found for the single major contributor to ice discharge, the Jakobshavn glacier: up to 60% in 2012 (Fig. 5.26).

Finally, we note that the Total-SMB residuals can also be used to diagnose SMB model biases in the winter months. Due to negligible surface melt during this time of the year, unphysical increase of the cumulative Total-SMB would indicate insufficient snow accumulation. Our results suggest this for the N and NE regions (Figs. 5.16 and 5.20).
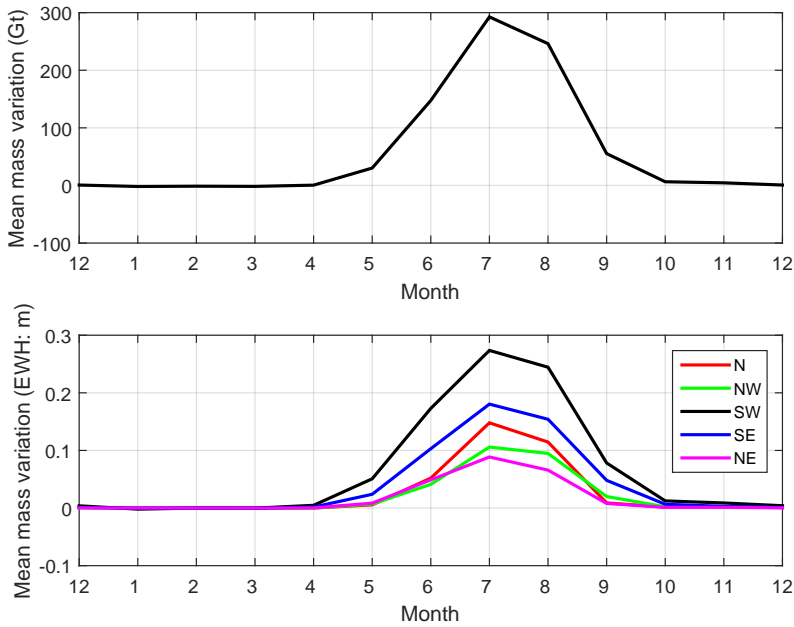
Figure 5.12: Mean monthly melt water production (Gt) for the whole Greenland (upper) and individual drainage systems (in meters of Equivalent Water Height, bottom) simulated by RACMO 2.3.

5.5. Summary

GRACE CRS RL05 monthly solutions processed with a variant of the mascon approach have been applied to systematically analyze the mass budget of the GrIS at various temporal and spatial scales. The obtained estimate of the mean rate of mass loss is 277 ± 21 Gt/yr over the period 2003-2012. The rate of SMB accumulation, as modelled by RACMO2.3, is 231 ± 122 Gt/yr. The difference between these trends is -508 ± 124 Gt/yr, which is consistent with 2003-2012 ice discharge observations by *Enderlin et al.* (2014): 520±31 Gt/yr. Moreover, we observe relatively large discrepancies between the estimates for the SE and N DSs. Those discrepancies imply that the adopted climate model likely overestimates precipitation in the SE DS and underestimate it in the N DS.

Our estimates of accelerations in SMB-related (-29.7±2.7 Gt/yr^2), ice discharge-related (2.5±1.5 Gt/yr^2), and total (-31.1±8.1 Gt/yr^2) mass anomalies are consistent: the residual does not exceed 1 Gt/yr^2, which is well within the error bar. This is consistent with *Velicogna et al.* (2014), who also found that most of the mass loss acceleration can be explained by the contribution of SMB. Furthermore, our results indicate that most of the total mass acceleration observed by GRACE is attributed to the SW and NW DSs, which is in agreement with *Sasgen et al.* (2010) and *Velicogna et al.* (2014).
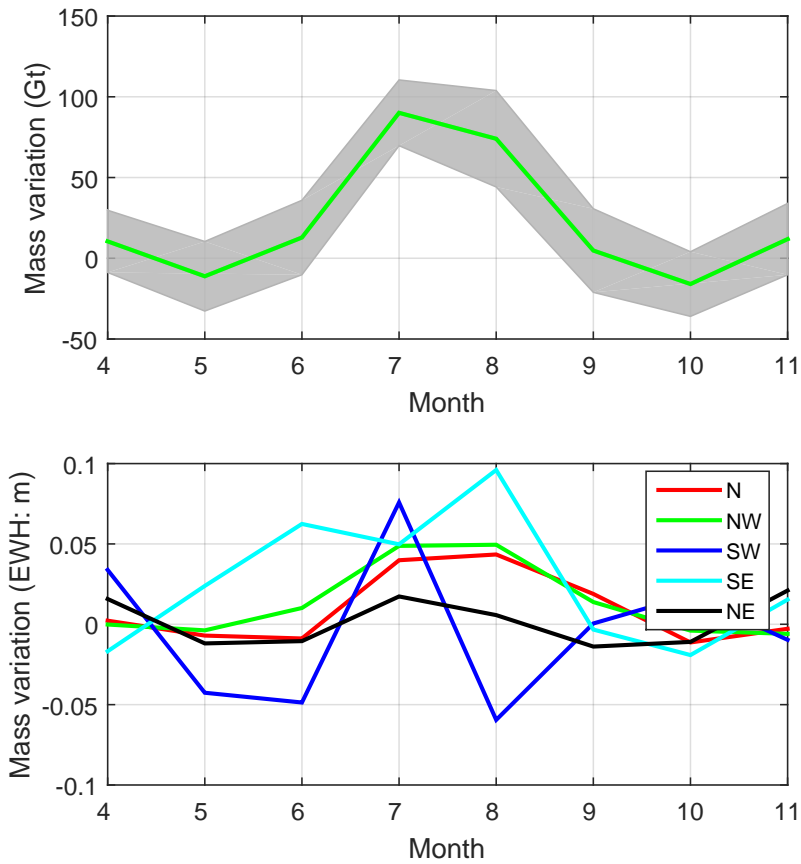
Figure 5.13: Estimates of seasonal meltwater storage, obtained as the monthly deviations from the April-May and September-November linear fit of "Total-SMB" (brown line in Fig. 5.11): for the whole GrIS (in Gt, top,) and for individual drainage systems (in meters of Equivalent Water Height, bottom). Labels along the horizontal axis represent months between April (4) and November (11). The shaded strip in the top plot shows the 2-σ error bar (the mean standard deviation is 23 Gt). The mean standard deviations of the estimates related to individual drainage systems are: 0.02 m (N), 0.02 m (NW), 0.06 m (SW), 0.03 m (SE), and 0.01 m (NE); they are not shown in the plot for the sake of its readability.

We found a remarkable seasonal cycle in the difference between non-detrended monthly total and SMB cumulative mass anomalies ("Total-SMB"), which likely reflects significant meltwater retention in the summer months. The peak in cumulative storage is 100 ± 20 Gt at the end of July, when monthly totals are used. To estimate the potential contribution of ice discharge to the observed signals, we exploited the estimates of ice discharge over 55 outlet glaciers obtained with the flux gate method. We showed that this contribution stays at the level of only a few Gt, i.e. plays a negligible role. We
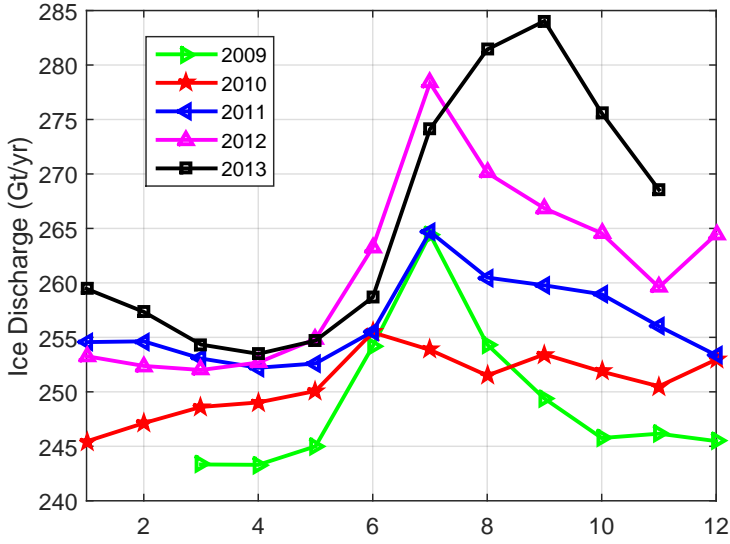
Figure 5.14: Monthly multi-regional ice discharge from 55 major marine-terminating glaciers of the NW and SE drainage systems. The unit is Gt/yr.
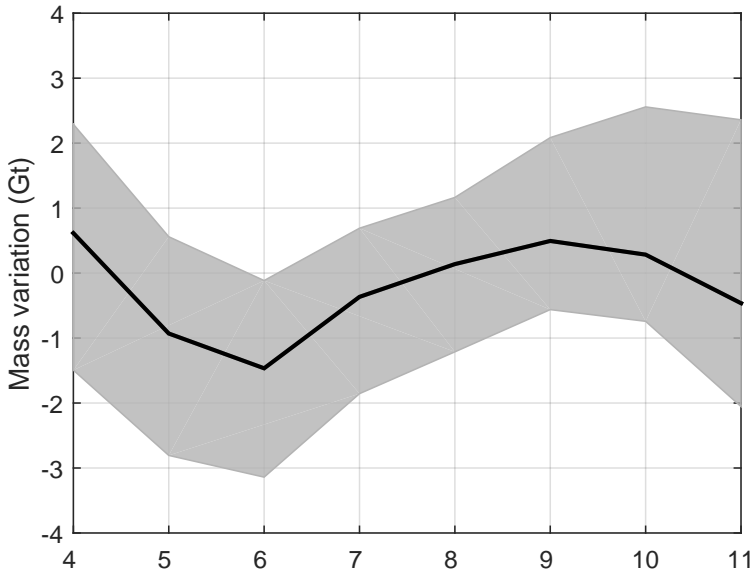
5

Figure 5.15: Similar to Fig. 5.13, but the cumulative mean ice discharge related mass anomalies over 2009-2013, based on seasonal estimates of ice discharge from 55 major marine-terminating glaciers and upscaled to represent entire Greenland.
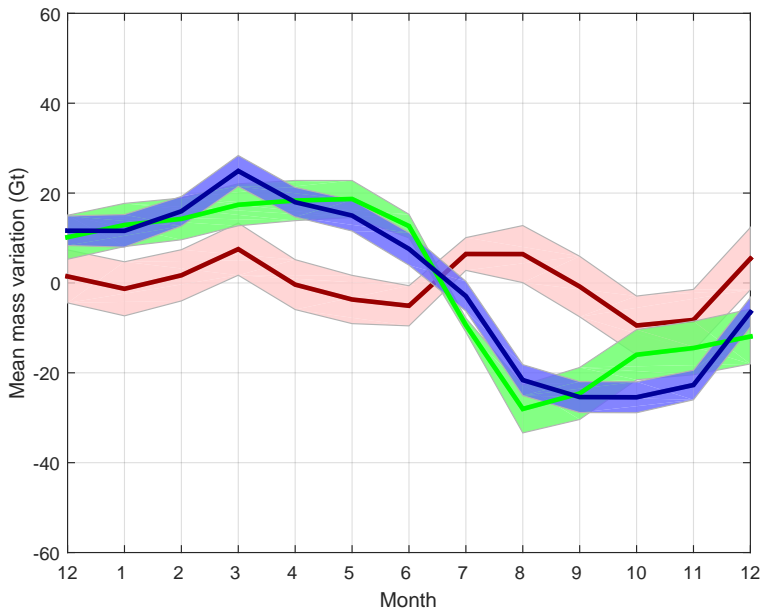
Figure 5.16: Monthly cumulative total (blue), surface (green) and residual "Total-SMB" (red) mass variations (see legend of Fig. 5.11), for drainage systems: N.

also analyzed this process per drainage system. We demonstrated that the processes of meltwater accumulation and runoff are particularly weak in the northeastern part of Greenland.

This study also suggests that the Total-SMB residuals are applicable to verify SMB estimates from climate models by applying the simple constraint that this residual cannot be negative in winter months, when it predominantly reflects ice discharge. In this way, we found that the adopted climate model likely underestimates the precipitation in the N and NE DSs in winter months. This precipitation deficiency in RACMO2.3 has been independently confirmed by a comparison with ice discharge in this region by *Mouginot et al.* (2015).

At the same time, a comparison of seasonal variations in the "Total-SMB" estimates derived from GRACE data in different ways revealed noticeable discrepancies, particularly in winter months. This indicates that further work is needed to ensure robustness of GRACE-based estimates.
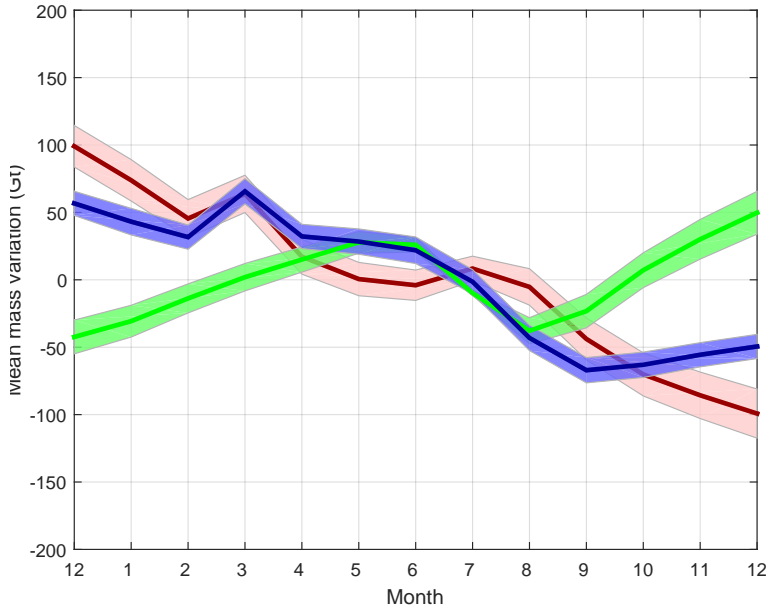
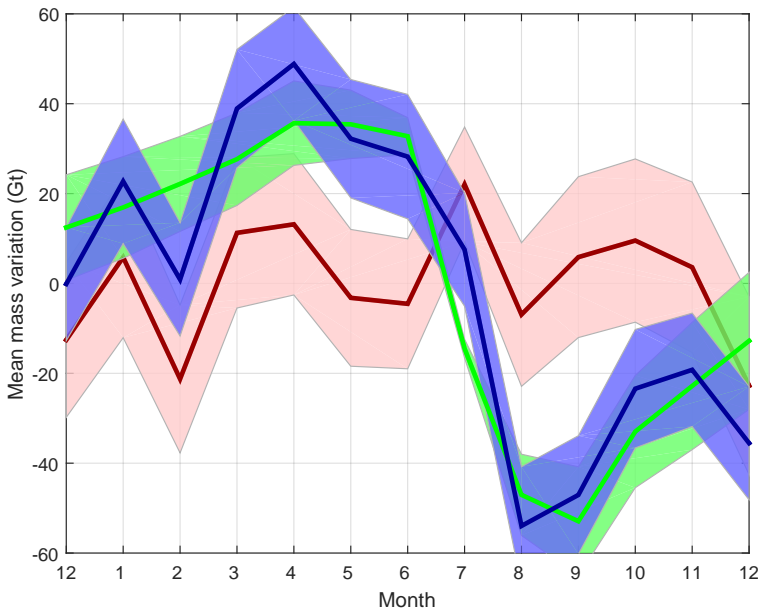Figure 5.17: The same as Fig. 5.16, but for drainage system: NW.

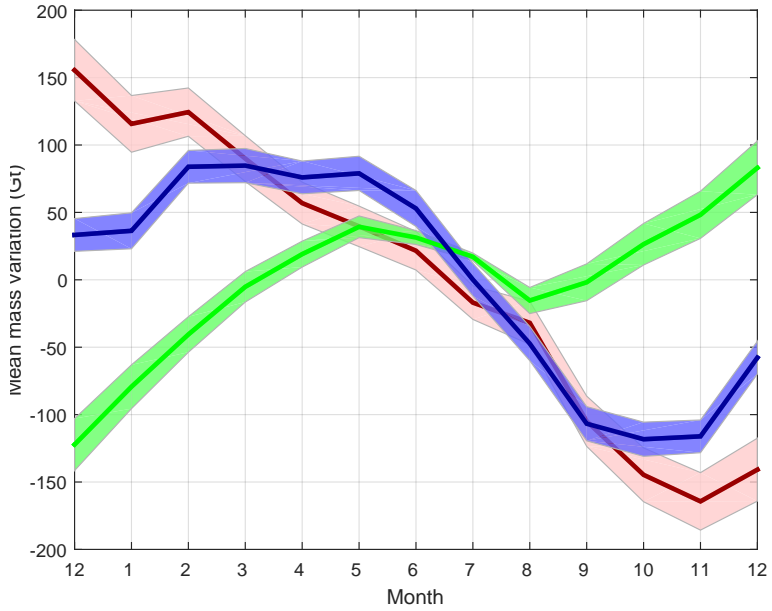Figure 5.18: The same as Fig. 5.16, but for drainage system: SW.

Figure 5.19: The same as Fig. 5.16, but for drainage system: SE.
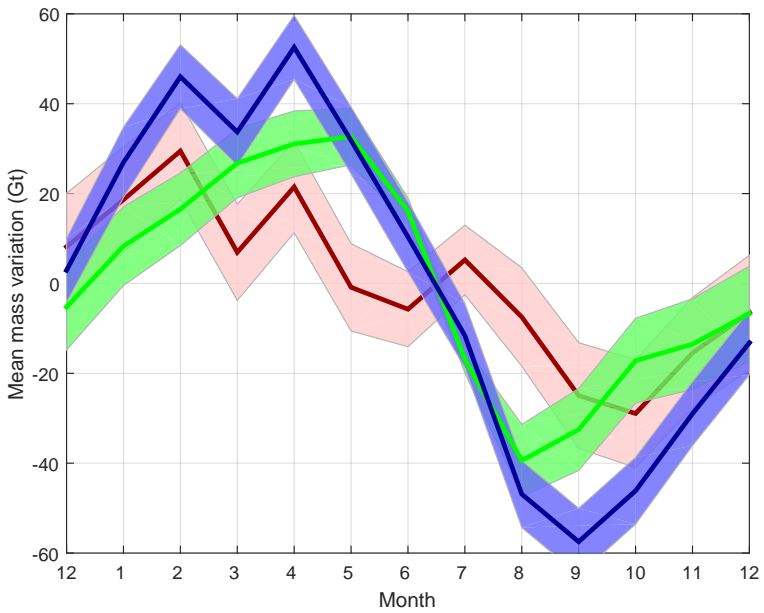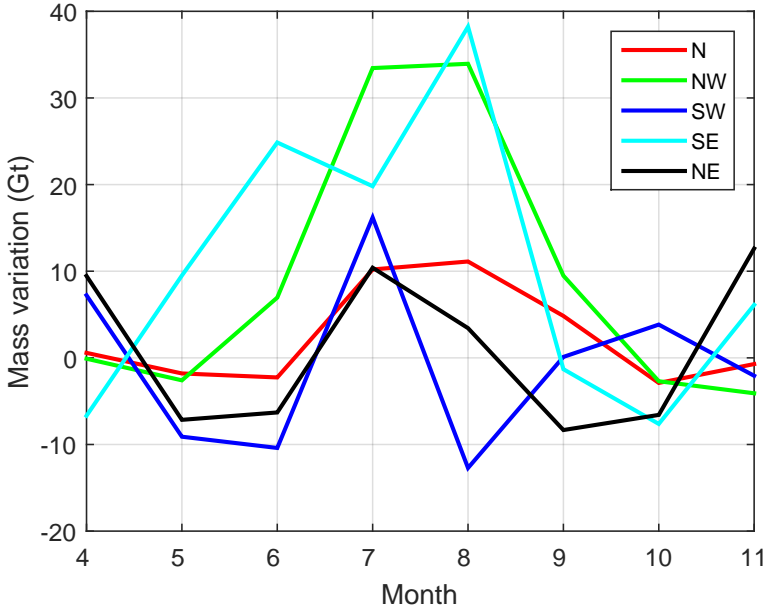

Figure 5.20: The same as Fig. 5.16, but for drainage system: NE.

Figure 5.21: The same as the bottom panel of Fig. 5.13, but in terms of mass variation (Gt).
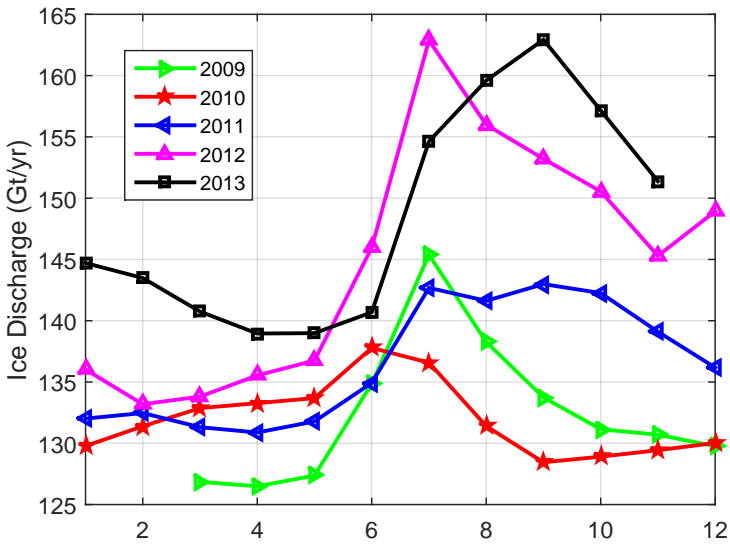

Figure 5.22: Similar to Fig. 5.14, but for the NW drainage system.

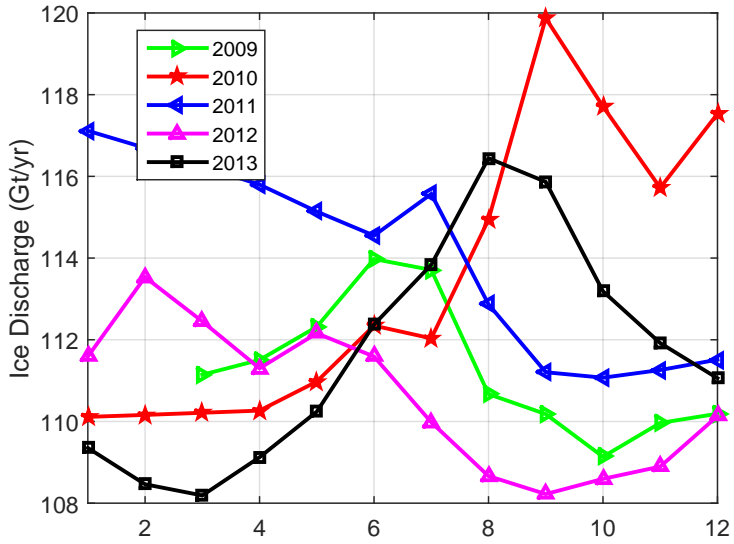Figure 5.23: Similar to Fig. 5.14, but for the SE drainage system.
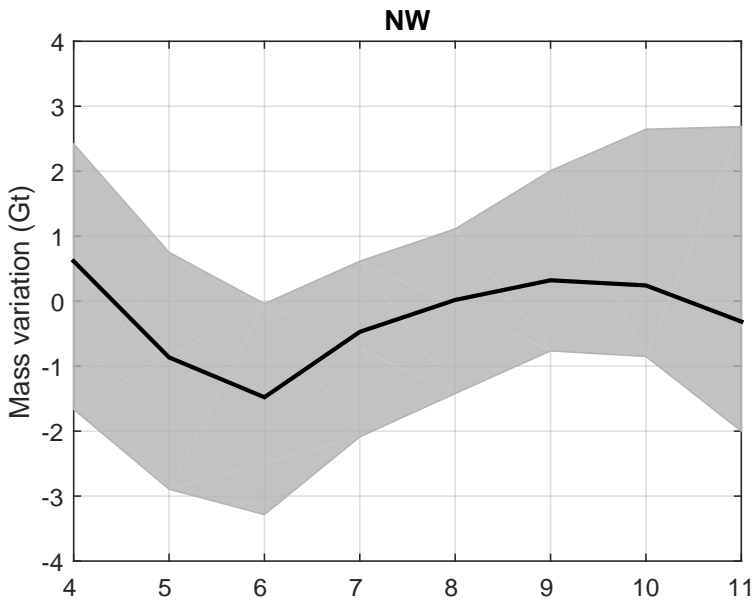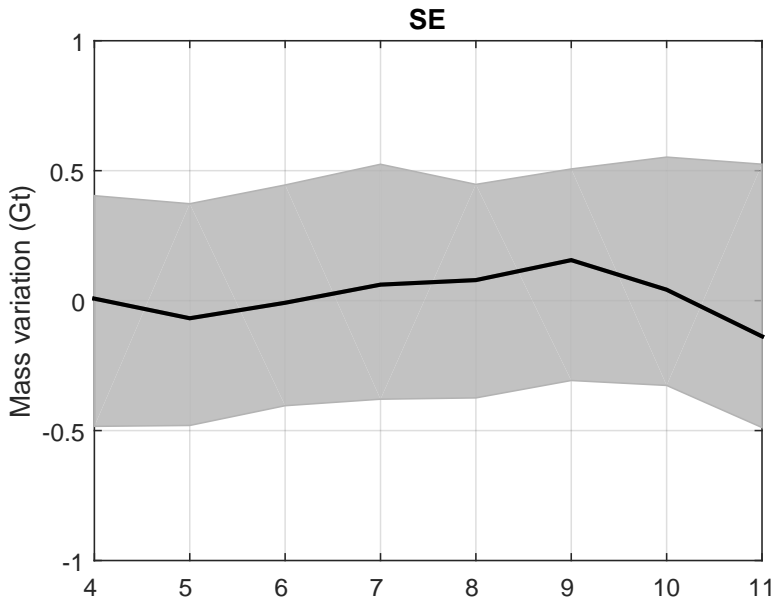

Figure 5.24: Similar to Fig. 5.15, but the glaciers in NW.

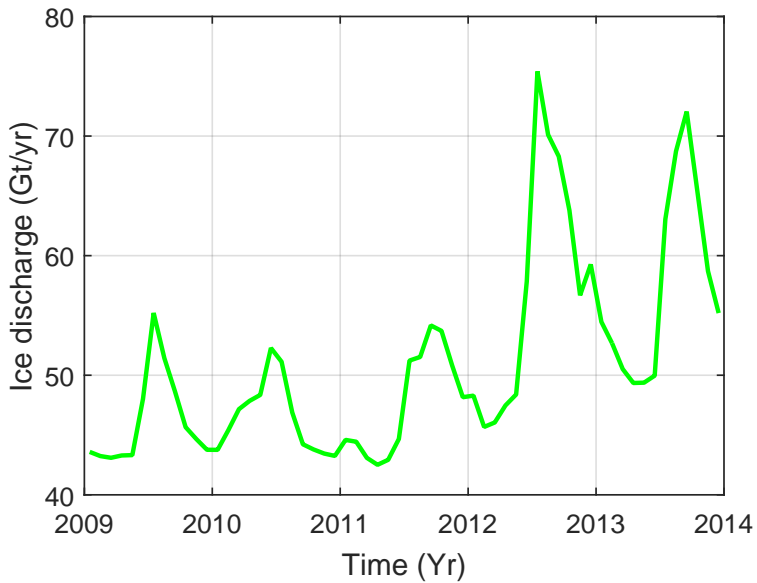Figure 5.25: Similar to Fig. 5.15, but for the glaciers in SE.

5

Figure 5.26: Monthly variations of ice discharge of Jakobshavn glacier over the period 2009-2013 (Gt/yr).

6

Optimal mascon geometry for estimating mass anomalies within Greenland from GRACE

6.1. Introduction

The mascon approach is very sensitive to the parameterization of the target area, i.e., to the choice of the number and the geometry of the mascons (*Bonin and Chambers*, 2013). Different parameterizations of the territory of Greenland have been used so far in literature. For instance, *Luthcke et al.* (2006a) identified 6 drainage systems and split each of them into two mascons, one for the area below the 2000 m elevation line and the other for the area above the 2000 m elevation line. This rather coarse parameterization is not able to fully exploit the spatial resolution of GRACE. Therefore, finer parameterizations using equal-angular or equal-area mascons or spherical caps have been proposed (*Rowlands et al.*, 2005; *Luthcke et al.*, 2013; *Schrama et al.*, 2014; *Baur and Sneeuw*, 2011; *Watkins et al.*, 2015). They are more flexible and can be adjusted in line with the spatial resolution of GRACE. However, it is still difficult to take into account a prior geophysical information, e.g., the boundaries of drainage systems and the geometry of the coastal line. The only exception in that respect is the point mass parameterization of *Baur and Sneeuw* (2011). In Chapter 4 of this study we suggested an alternative approach to subdivide Greenland into nearly equal-area mascons, which is free from the aforementioned limitations. This way of choosing the geometry and size of the mascons is also used here.

It is a common approach to choose the size of the mascons independently of the temporal scale under consideration. We believe that such an approach is sub-optimal. The primary goal of this Chapter is to investigate the optimal choice of the mascon size depending on the temporal scale under consideration. We consider three temporal scales: (i) long-term linear trends (multi-year temporal scale); (ii) mean mass anomalies per calendar month (intermediate temporal scale); and (iii) monthly mass anomalies (monthly temporal scale). Mean mass anomalies per calendar month are computed as the mean of mass anomalies of the same month over many years, after removing the long-term trend. When doing so, we do not introduce spatial constraints when estimating the unknown parameters using least-squares techniques as done in several previous studies (*Luthcke et al.*, 2006a; *Baur and Sneeuw*, 2011; *Schrama et al.*, 2014;

Bonin and Chambers, 2013). In this way, we want to avoid that the estimates are biased.

The rest of this Chapter is organized as follows. In Section 6.2 , we briefly introduce the different parameterizations used in this study. In Section 6.3, we do a numerical study using simulated signal and data. This allows a better understanding of the impact of the parameterization on the accuracy of the estimated mass variations for each temporal scale under consideration. In Section 6.4, we analyse real GRACE data. Finally, in Section 6.5, we provide a summary and the conclusions.

6.2. Adopted parameterization

The parameterizations considered in this study are designed using the method of Chapter 4. This comprises a subdivision of Greenland into almost equal-area mascons of a pre-scribed size. In this way, we split the territory of Greenland into 23 mascons ($\sim 90{,}000\,\mathrm{km}^2$), 36 mascons ($\sim 62{,}500\,\mathrm{km}^2$), and 54 mascons ($\sim 40{,}000\,\mathrm{km}^2$) (cf. Fig. 6.1). Finer parameterization are not considered, because they require a significant amount of regularization and biased solutions.

The three afore-mentioned parameterizations are complemented by three other parameterizations already used in the literature: the 6 mascons in *Luthcke et al.* (2006a), the 8 mascons in *Zwally et al.* (2012), and the 12 mascons in *Luthcke et al.* (2006a). The first two mascons are identical to major drainage systems. The different parameterizations are shown in Fig. 6.1.

6.3. Numerical study

To understand the impact of the parameterization on the accuracy of estimated mass variations at different temporal scales, and to understand how this error compares to other error sources, a series of numerical experiments are conducted with synthetic data. The experimental set-up and the results are presented in Section 6.3.1 and 6.3.2, respectively.

6.3.1. Experimental set-up

"True" signal

The "true" signal comprises a long-term trend and seasonal variations. The long-term trend is based on ICESat laser altimetry time series over the period 2003–2009. The resolution is 20 × 20-km (*Felikson et al.*, 2016). By assuming the density of the material responsible for elevation changes to be 917 kg/m^3 (*Wahr et al.*, 2000), the elevation change time series are converted into mass change time series in terms of equivalent water heights (EWH) (Fig. 6.2). From them, a linear trend is estimated. The linear trend over the tundra area is set equal to zero. To make the trend consistent with the GRACE-based trend (cf. Chapter 4) over the period 2003–2013, we compute a single scale factor
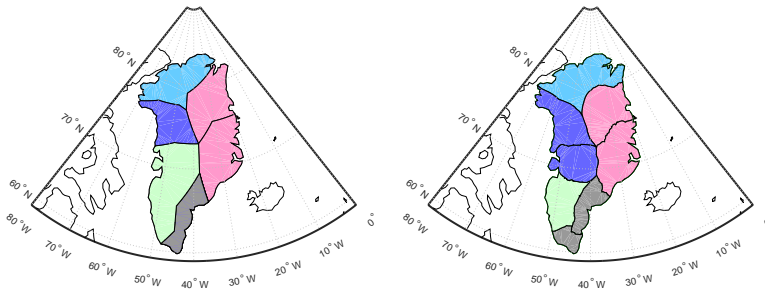
(a) 6 mascons

(b) 8 mascons
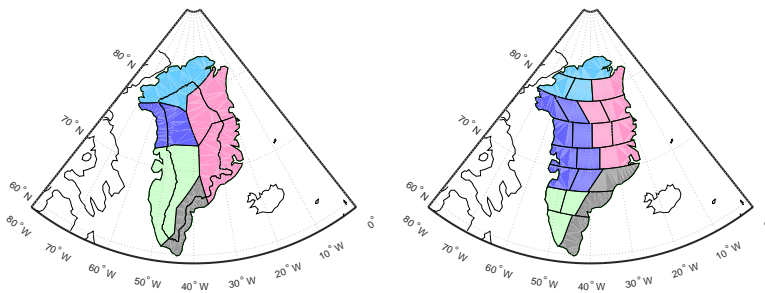
(c) 12 mascons

(d) 23 mascons

(e) 36 mascons

(f) 54 mascons

Figure 6.1: The 6 parameterizations of Greenland considered in this study. The colour-coded areas represent five drainage systems, essentially comprising a certain number of mascons: North (N) in light blue, Northeast (NE) in red, Southeast (SE) in gray, Southwest (SW) in green, and Northwest (NW) in blue.

Figure 6.2: GrIS mass change rate per 20 × 20-km patch from ICESat data over the period 2003–2009 (EWH: m/yr). The thick red curve is the ice mask, which indicates the boundary of the ice sheet.
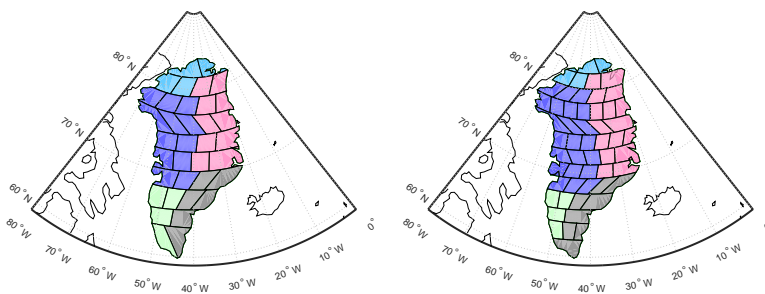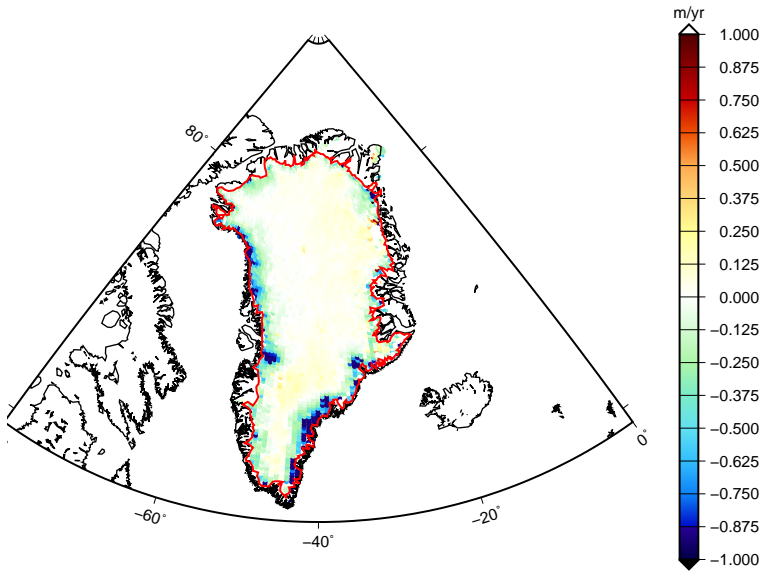
from the ratio of the GRACE-based trend over entire Greenland to the ICESat-based trend. The factor is 2.6. This factor is used to upscale the ICESat-based trends per 20 × 20 km block. This is similar to *Bonin and Chambers* (2013).

The seasonal variations are based on surface mass balance time series from the RACMO 2.3 model (*Noël et al.*, 2015). The spatial resolution is about 11 × 11 km. The output from RACMO 2.3 during the time interval 2003–2013 is integrated over time to produce daily mass anomalies. After this, we compute monthly mass anomalies, and averaged them to the 20 × 20-km patches from ICESat. Then, we de-trend the mass variations per patch (their annual amplitudes are shown in Fig. 6.3), and combine the de-trended signal with the trend from ICESat to form the "true" signal. Note that the "true" signal over the tundra area shows seasonal variations, but the long-term linear trend is zero.

Simulated noise

Different types of noise c.q. errors are added to the "true" signal: signal leakage, AOD noise, and random noise. Parameterization errors, sometimes referred to as "model errors" (*Xu*, 2010; *Stedinger and Tasker*, 1986), are automatically included due to the much higher spatial resolution of the "true" signal compared to the size of the mascons.

Signal leakage. The signal in surrounding land areas may leak into the estimates of mass anomalies within Greenland. To include leakage errors, we generate mass variations
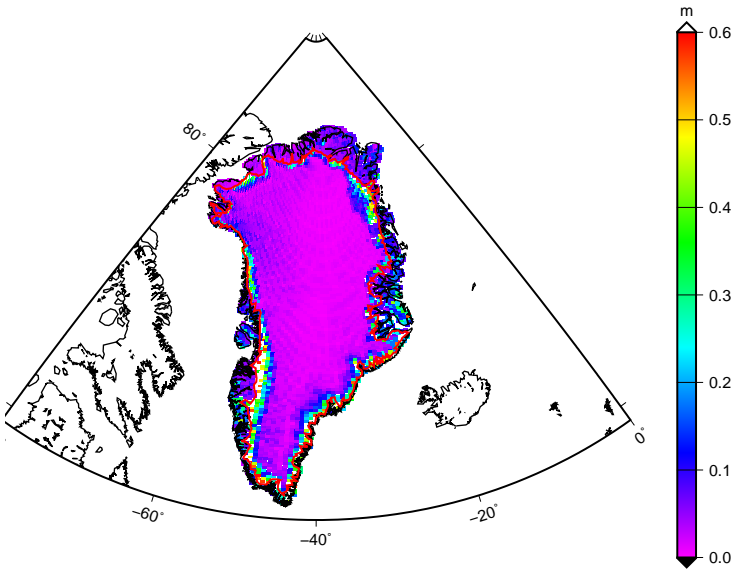
Figure 6.3: The amplitude of annual mass variations in meters of EWH over entire Greenland for the period 2003–2013 extracted from RACMO2.3.

6

in surrounding land areas using GRACE monthly land water mass grids from GRACE Tellus (*Swenson*, 2012). In line with the time interval of the "true" signal, we consider 123 monthly solutions over the period 2003–2013 (9 months are excluded from the data processing due to lack of data). The simulated trends and annual amplitudes extracted from monthly GRACE Tellus solutions over the mascons located outside Greenland are shown in Fig. 6.4-6.5.

AOD noise. Uncertainties in the background models which are used to produce monthly GRACE solutions may cause inaccuracies in the mass variation estimates. One of such background models is the Atmosphere and Ocean De-aliasing model release 05 (AOD) (*Dobslaw et al.*, 2013; *Ditmar et al.*, 2012). Here, we define AOD errors as 10% of the mean monthly signal, which is believed to be a reasonable level (*Thompson et al.*, 2004; *Ditmar et al.*, 2012).

Random noise. The random noise in monthly GRACE solutions, which mainly manifest itself as the so-call "north-south" stripes, is generated from the noise covariance matrices of monthly GRACE solutions provided by CSR. Ideally, this needs to be done per month using the corresponding noise covariance matrix. However, such an approach is very time consuming, especially when using a weighted least-squares estimator. Therefore, we choose the noise covariance matrix of June 2008, and generate for each month noise realizations based on this noise covariance matrix.

Parameterization errors. Since the actual mass anomaliy distribution may be inhomo-
geneous within a mascon, we need to add a parameterization error. This is automatically
done, since the "true" signal is defined over 20×20 km patches, i.e., the patch size is much
smaller than the size of the mascons. In the simulation runs without parameterization
error, we define the "true" signal per mascon as the average over all 20×20 km patches
located inside the mascon.
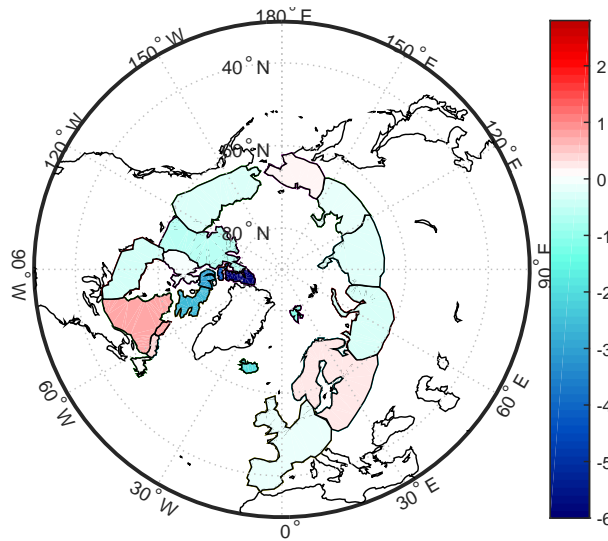
Figure 6.4: The rate of linear mass changes for mascons outside Greenland, which are introduced to simulate
signal leakage (EWH: cm/yr).

6.3.2. Results

We focus our study on (i) long-term linear mass variation rates; (ii) mean mass anomalies
per calendar month; and (iii) monthly mass anomalies. We investigate the impact of
the parameterization on these estimates and select the best parameterization in each
case. We conduct the analysis at the level of drainage systems. To that end, we divide
Greenland into five regions, which approximately follow the geometry of the drainage
systems defined in (*van den Broeke et al.*, 2009). The geometries of different drainage
systems, which are aggregated from mascons, are also shown in Fig. 6.1. Note that it is
not possible to make the geometries of the five drainage systems (as shown in Fig. 6.1
with different colours) to be the same for different parameterizations. The impact of
the differences between the resulting geometries is, however, minor, since we compare
estimates over each drainage system with the "true" value based on the same geometry.
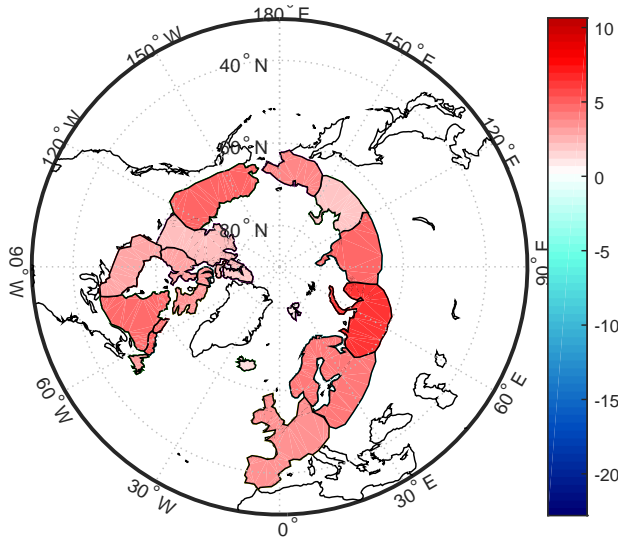
Figure 6.5: The annual amplitude of mass change for the mascons outside Greenland, which are introduced to simulate leakage (EWH: cm).

6

Recovery of long-term linear trends

After summing up the recovered mass anomalies over all mascons within each drainage system, we extract the linear trend of mass change in Gt/yr, co-estimated with bias, annual and semi-annual terms. The true linear trend at the drainage system scale is estimated from the true mass anomaly time-series computed from the synthetic mass anomalies over 20×20 km patches inside the territory of each drainage system. As quality measure, we use the RMS difference between estimated and true linear trends. This RMS difference is referred to as the "total RMS error" if all error sources are switched on, and computed as

$$\text{RMS}_\text{t} = \sqrt{\frac{\sum_{n=1}^{5}(\text{t}_n^{\text{recovered}} - \text{t}_n^{\text{true}})^2}{5}}. \tag{6.1}$$

If only a single noise c.q. error source is considered, the corresponding RMS difference is referred to as RMS AOD error, RMS leakage error, RMS parameterization error, and RMS random error. All computations are done using two estimators: i) a weighted least-squares estimator where the weight matrix is set equal to the inverse data noise covariance matrix of June 2008, and ii) the ordinary least-squares estimator. The corresponding solutions are referred to as solutions with and without data weighting, respectively.

The total RMS error is shown in Fig. 6.6. When using data weighting, the smallest total RMS error (8 Gt) is obtained for 36 mascons. Without data weighting, the smallest total RMS error (5 Gt) is obtain when using 23 mascons, though there is little difference to the total RMS error for 54 mascons.
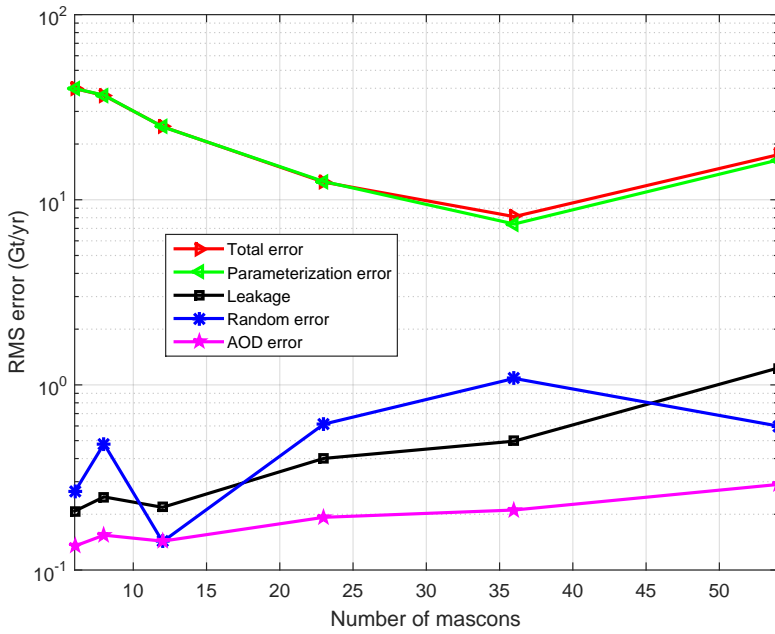
As far as each of the individual error sources of Section 6.3.1 is concerned, we repeated the numerical experiments, where in each run the data are only contaminated by one error source. Figure 6.6 reveals that the RMS parameterization error is the dominant error source no matter whether data weighting is used nor not. In both cases, it has a minimum at 36 (with data weighting) and 23 (without data weighting) mascons, respectively. One would expect to see a decrease in the RMS parameterization error when using more mascons, which, however, is not the case. We explain this by the higher condition number (Fig. 6.7) and associated data noise amplification.

The RMS random error is rather small, ~1 Gt/yr and ~ 2 Gt/yr with data weighting and without data weighting, respectively. This is one to two orders of magnitude smaller than the RMS parameterization error, depending on the number of mascons. The RMS leakage error and the RMS AOD error are either smaller or comparable to the RMS random error.

Figure 6.6b also reveals that the total RMS error is smaller than the RMS parameterization error when using 54 mascons. We explain this by a partial compensation of parameterization error and leakage error due to their anti-correlation in the considered study. It is very likely that this anti-correlation reflects the specific set-up of the conducted experiment. Therefore, we do not consider the parameterization of Greenland with 54 mascons as a plausible option when using no data weighting.

Based on the results shown in Fig. 6.6, we conclude that if the target quantity is the long-term linear trend at drainage system scale, data weighting is not necessary. The ordinary least-squares estimator may even provide slightly better results than the weighted least-squares estimator. This is to be expected if other error sources than random noise are present and have magnitudes comparable or larger than the random noise.

We repeat the above experiments, now for the linear trend of entire Greenland. The results are shown in Fig. 6.8. First of all, we notice that the total RMS error decreases with increasing number of mascons. The minimum is attained for the maximum number of mascons considered in this study (i.e., 54 mascons) no matter whether data weighting is used (0.8 Gt/yr) or not (2.0 Gt/yr). If not enough mascons are used, the total RMS error may be very large, in particular when no data weighting is used. For instance, when using just 6 mascons, the total RMS error is ~6 Gt/yr (with data weighting) and ~40 Gt/yr (without data weighting), respectively. Responsible for the large errors is the parameterization error, whereas all other error sources are negligible. From this we conclude, that when estimating a linear trend for entire Greenland, one needs to take care of that enough mascons (e.g., 54) are used to reduce the parameterization error. Using a sufficiently high number of mascons is more important when using the ordinary least-squares estimator. The highest quality is obtained when using a weighted least-squares estimator in combination with a sufficiently high number of mascons.

(a)
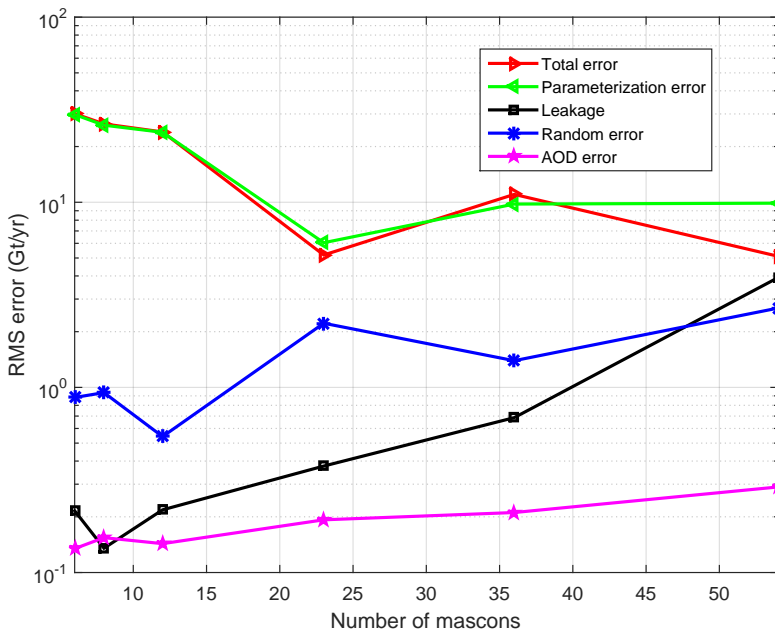
(b)

Figure 6.6: Total RMS error and RMS error of individual error sources of linear trends at drainage system scale in units of Gt/yr. Weighted least-squares estimator (a) versus ordinary least-squares estimator (b), as a function of the number of mascons.
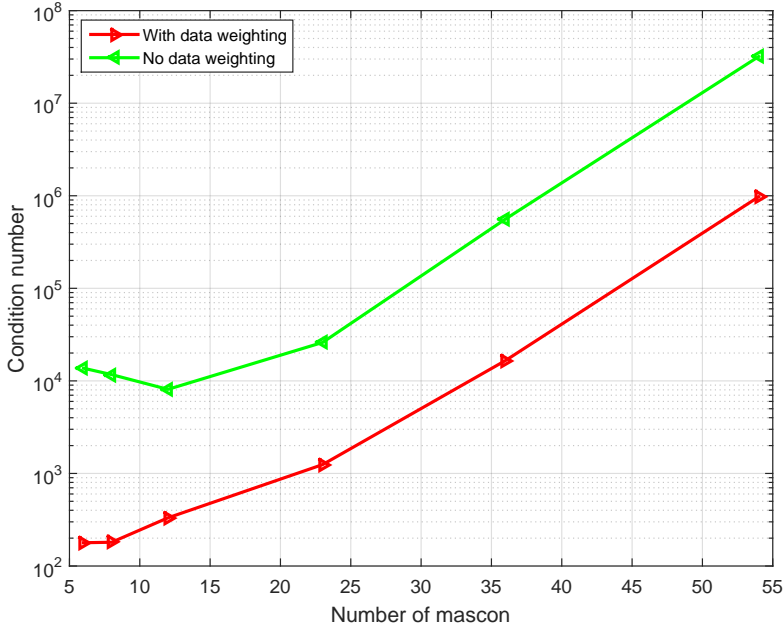
Figure 6.7: Condition numbers of the normal matrices when using the ordinary least-squares estimator (green) and weighted least-squares estimator (red), respectively, as a function of the number of mascons. Note that no regularization is used when computing the least-squares estimates.

Recovery of mass anomalies per calendar month

Mean mass anomalies per calendar month are useful to study the mean seasonal cycle of mass anomalies over Greenland. Here, we examine the impact of the parameterization on the accuracy of estimates of mean mass anomalies per calendar month.

First, we compute for each mascon the mean mass anomalies per calendar month, $\overline{\widehat{m}}^i$ (i=1, 2, $\cdots$, 12). This is done using the functional model

$$\widehat{m}^{i,j} = \overline{\widehat{m}}^i + b^j, \tag{6.2}$$

where $\{\widehat{m}^{i,j} : i = 1\dots12, \ j = 1\dots J\}$ is the mass anomaly of month i and year j, and b^j is the mean anomaly of year j, which accounts for the long-term variability. We add the constraint

$$\sum_{i=1}^{12} \overline{\widehat{m}}^i = 0, \tag{6.3}$$

to guarantee that the sum over all 12 calendar months of the mean mass anomalies per calendar month is equal to zero. The $12 + J$ parameters per mascon are estimated using ordinary least-squares. The corresponding mean mass anomalies per calendar months
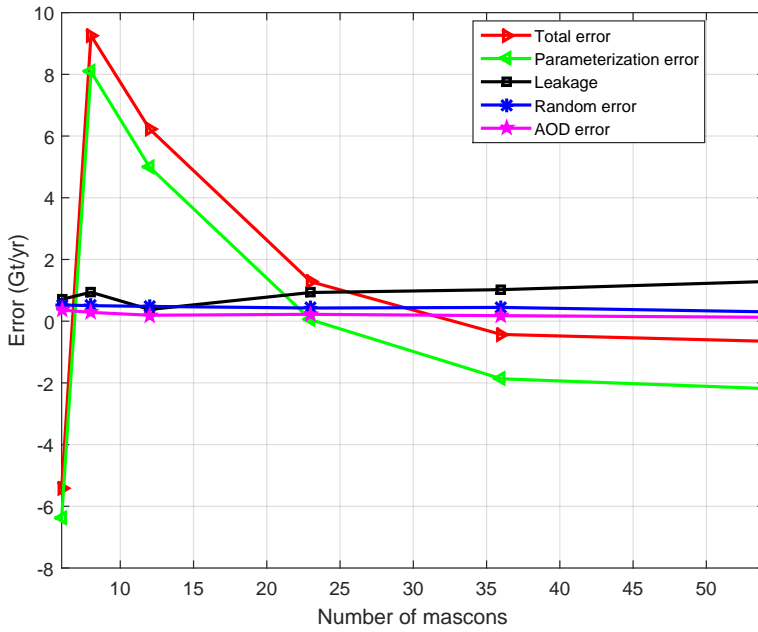
(a)
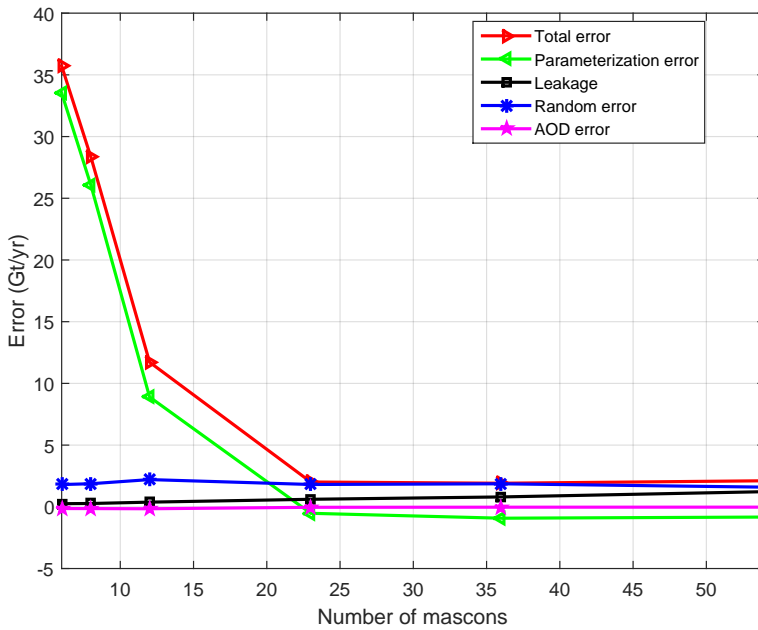
(b)

Figure 6.8: Errors in the linear trend (in Gt/yr) over entire Greenland when using a weighted least-squares estimator (a) and an ordinary least-squares estimator (b), respectively, as a function of the number of mascons.

for each drainage system is simply obtained by summing up over the mascons inside the drainage system. As an example, Fig. 6.9 shows the mean SMB mass anomalies per calendar month of the Northern (N) drainage system when using a parameterization comprising 8 mascons.
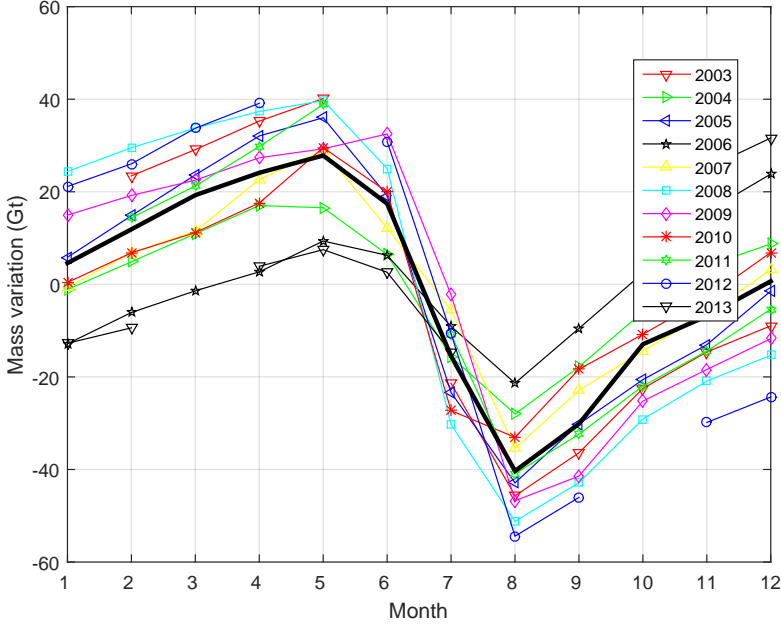
Figure 6.9: Mean SMB mass anomalies per calendar month of Greenland, $\overline{\widehat{m}}^{i}$ (thick black curve). The thin curves represent monthly mass anomalies of different years after removing the mean yearly mass anomalies, b^{j}

The RMS error per drainage system, τ_k, is computed as the RMS difference between estimated and "true" mean mass anomalies for all 12 months, i.e.,

$$\tau_k = \sqrt{\frac{\sum_{n=1}^{12}(\overline{m}_{k,n}^{\text{recovered}} - \overline{m}_{k,n}^{\text{true}})^2}{12}}, \tag{6.4}$$

where $\overline{m}_{k,n}^{\text{recovered}}$ and $\overline{m}_{k,n}^{\text{true}}$ are the estimated and true mean mass anomalies of the k-th drainage system at month n, respectively.

Then, the RMS error of mean mass anomalies per calendar month is computed by averaging the errors over 5 drainage systems:

$$\text{RMS}_{\overline{m}} = \sqrt{\frac{\sum_{k=1}^{5}\tau_k^2}{5}}. \tag{6.5}$$

The RMS error of mean mass anomalies per calendar month of Eq. (6.5) is computed as total RMS error and as RMS error per error source for the ordinary least-squares estimator and the weighted least-squares estimator, respectively. The results are shown in Fig. 6.10 as function of the chosen parameterization. Obviously, using data weighting provides a smaller total RMS error than no data weighting, 8 Gt versus 13 Gt. In the former case, this minimum is attained for 23 mascons, whereas in the latter case, it is attained for 8 mascons.

As far as the RMS error per error source is concerned, we notice that no matter whether data weighting is used or not, the parameterization error decreases and the random error and leakage error increase with increasing number of mascons, whereas the AOD error shows a minor sensitivity to the number of mascons. For a low number of mascons, the parameterisation error is the dominant error source, whereas for finer parameterizations, the random error becomes dominant. The crossing point of both error sources depends on the estimator; it is at 12 mascons if the ordinary least-squares estimator is used and above 23 mascons if the weighted least-squares estimator is used. We also notice that no matter how many mascons are used, the random error for solutions computed with data weighting is almost smaller than for solutions without data weighting. For solutions using 54 mascons the difference is maximum: 30 Gt versus 50 Gt in favour of using data weighting. From this, we conclude that data weighting always provides more accurate mean mass anomalies per calendar month than no data weighting.

6

Recovery of monthly mass anomalies

In this section, we analyse the impact of the parameterization on the accuracy of monthly mass anomalies at the drainage system scale. To do so, we de-trend both the estimated time series and the true time series of monthly mass anomalies, and compute the total RMS error and the RMS errors per error source as the RMS difference between the two de-trended time series, i.e.,

$$\text{RMS} = \sqrt{\frac{\sum_{n=1}^{N}(m_n^{\text{recovered}} - m_n^{\text{true}})^2}{N}} \tag{6.6}$$

where m_n is the mass anomaly of month n and N is the number of months.

Figure 6.11 shows the results. When data weighting is used, the total RMS error attains a minimum of 13 Gt when 8 mascons are used. If more mascons are used the total RMS error increases monotonously, and attains its largest value of about 100 Gt when 54 mascons are used. Without data weighting, the smallest total RMS error of 24 Gt is obtained for 12 mascons. Thereafter it increases monotonously up to about 200 Gt for 54 mascons. It is important to note that the total RMS error is smaller with data weighting compared to no data weighting, no matter what parameterization is chosen.

When looking at the individual error sources, we notice that the random error dominates the error budget. Except the single case of 6 mascons in combination with data
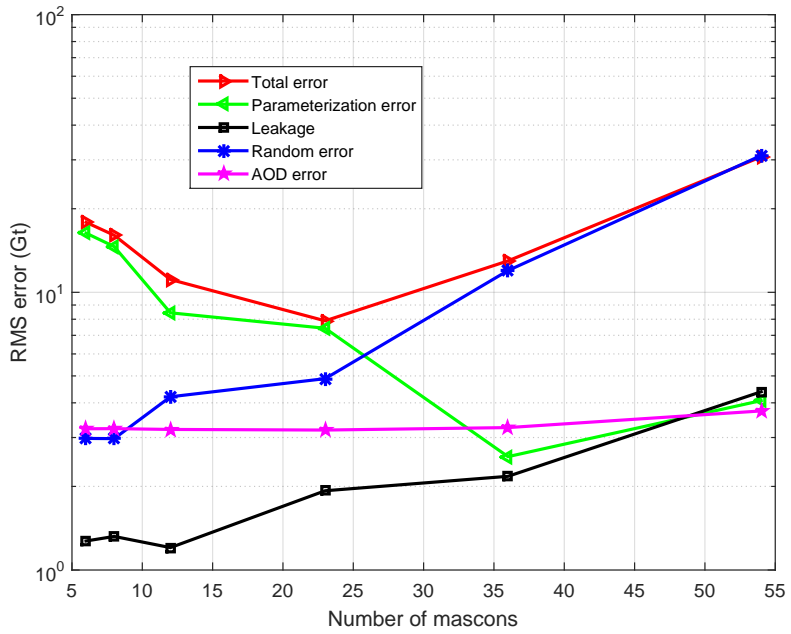
(a)
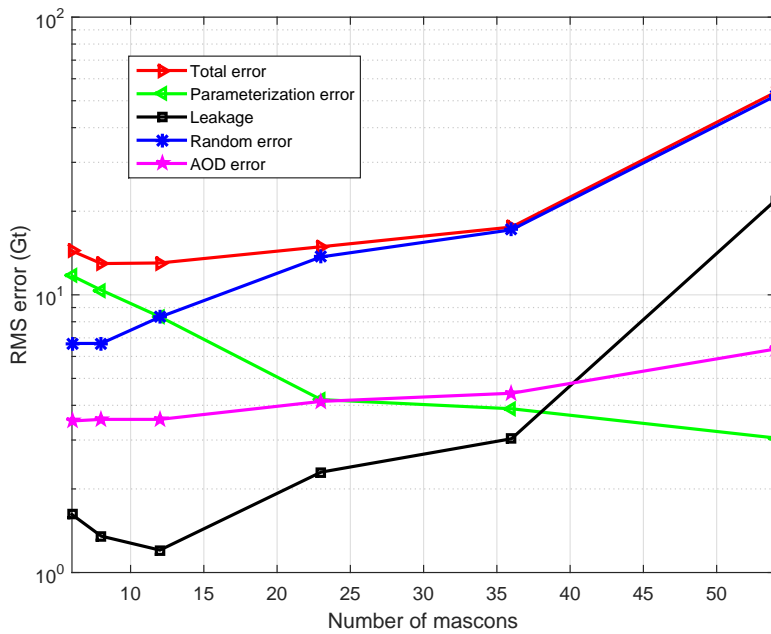
(b)

Figure 6.10: The RMS errors in mean mass anomalies per calendar month estimated with (a) and without (b) data weighting at drainage system scale as a function of the number of mascons (Gt).
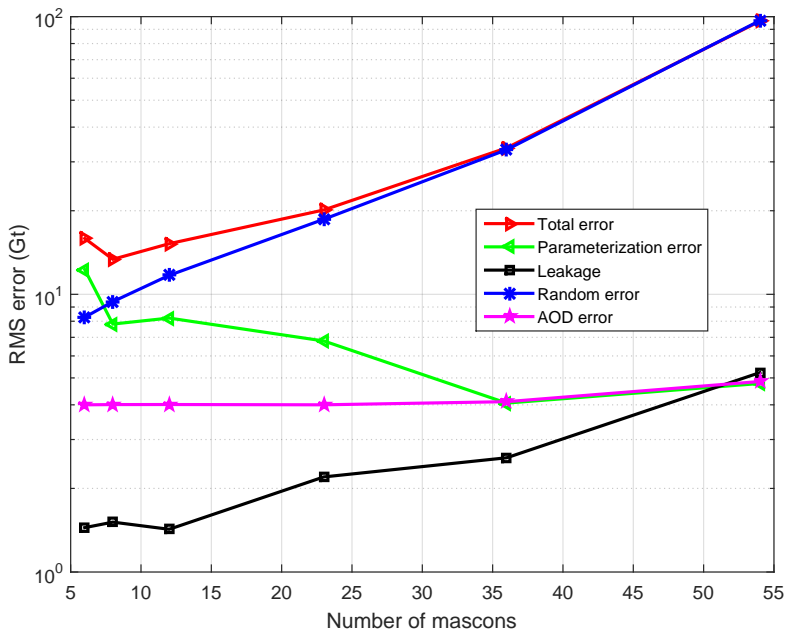
(a)
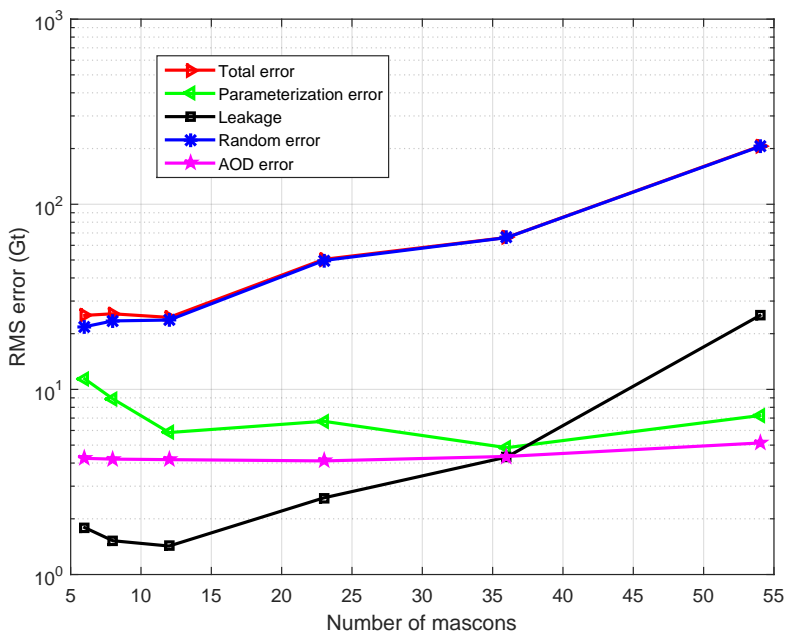
(b)

Figure 6.11: Total RMS error and RMS error of individual error sources of monthly mass anomalies at drainage system scale in units of Gt. Ordinary least-squares estimator (a) versus weighted least-squares estimator (b), as a function of the number of mascons.

weighting, all other error sources are negligible.

Compared with the mean mass anomalies per calendar month, the random noise in the time-series of monthly mass anomalies plays an even larger role, making the optimal data weighting even more beneficial.

6.4. Analysis based on real GRACE data

In this section, we investigate the impact of the parameterization on Greenland mass anomaly estimates using real GRACE data. We use the RL05 GRACE monthly gravity field solutions from the Center for Space Research (CSR) at the University of Texas as input to compute mass anomalies. Each solution is provided as a set of spherical harmonic coefficients complete to degree 96, and supplied with a full noise covariance matrix. The considered time interval is Jan 2003 – Dec 2013. Since data for 9 months are missing, the set comprises 123 months. Due to the strong noise in the C_{20} coefficients, we replaced them with available estimates based on satellite laser ranging (*Cheng et al.*, 2013). The degree-one coefficients, which are missing in the GRACE products, are taken from *Swenson et al.* (2008). The GRACE solutions are corrected for Glacial Isostatic Adjustment (GIA) using the model from *A et al.* (2013).

For each chosen parameterization, a time-series of mass anomalies per mascon is estimated. We first investigate the impact of parameterization on the long-term linear trend estimates. Note that because of the lack of the truth or reliable independent trend estimates at the drainage system scale, it is problematic to evaluate the trends at the drainage system scale. Therefore, we only evaluate the long-term trend estimates integrated over entire Greenland. To begin with, we sum up the mass anomalies per mascon over entire Greenland and extract the linear trend, co-estimating the bias, as well as the annual and semi-annual terms.

The estimated trends are shown in Fig. 6.12. We notice that the trend estimates both with and without data weighting converge to a value between −280 to −285 Gt/yr when the number of mascons increases. Interestingly, the sensitivity of the estimated trend to the chosen parameterization is much stronger when no data weighting is used; it changes from -242 Gt/yr for 6 mascons to -282 Gt/yr for 54 mascons. This is a change of 40 Gt/yr or almost 15% of the total trend. When using data weighting, the sensitivity is significantly reduced to 12 Gt/yr or 4%. This finding is consistent with the numerical study of Section 6.3.2 (cf. Fig. 6.8), demonstrating that data weighting makes the trend estimates for entire Greenland less sensitive to the dominant parameterization errors.

In line with the findings of Section 6.3.2 based on synthetic data, we consider the trend estimates obtained with the largest number of mascons as the most realistic and accurate ones. These estimates, i.e., −284 Gt/yr with data weighting and −281 Gt/yr without data weighting, are consistent with trends over the same period (i.e., 2003-2013) published in the literature (e.g., -280 ± 58 Gt/yr for *Velicogna et al.* (2014) and -278 ± 19

Gt/yr for *Schrama et al.* (2014)).

In addition, we investigate the impact of the parameterization on mass anomaly estimates at the intra-annual scale, i.e., mean mass anomalies per calendar month. For this purpose, we compare the estimates of the mean mass anomalies per calendar month from real GRACE data with the output of RACMO2.3 model (*Noël et al.*, 2015), by assuming the seasonality of mass variations observed by GRACE is dominated by SMB (*van den Broeke et al.*, 2009). GRACE measures total mass variations, which are mostly triggered by ice discharge and SMB. Ice discharge mainly manifest itself as a long-term trend. Therefore, we de-trend the mass estimates from both GRACE and SMB to make them comparable. Then, the RMS difference between GRACE and RACMO-based mean mass anomaly estimates per month is computed. The results are shown in Fig. 6.13.

Without data weighting, the RMS difference stays at a nearly constant level when the number of mascons ranges from 6 to 12, followed by a sharp increase for 23 or more mascons. With data weighting, the RMS differences show little variation between 6 to 36 mascons. Beyond 36, they increase comparable to the increase without data weighting. These findings are slightly different from the ones based on synthetic data (cf. Fig. 6.10). This might be caused by (i) different ways to process the estimates, since the estimates from real data are de-trended unlike the estimates in the numerical study; (ii) the computed RMS differences reflect not only noise in GRACE data, but also errors in SMB estimates, as well as the contribution of processes not related to SMB.

Finally, the impact of the parameterization on the monthly mass anomaly estimates from real GRACE data is analyzed. Again, to remove the effect of ice discharge, we de-trend both GRACE- and SMB-based time-series. Then, we analyze the RMS difference between the time-series at the drainage system scale, as shown in Fig. 6.14. With data weighting, the smallest RMS difference is observed when using 8 mascons; more mascons let the RMS differences increase exponentially. Without data weighting, the RMS differences are comparable between solutions using 6–12 mascons. In absolute terms, the RMS differences are about 20% larger than those with data weighting. All these findings are consistent with the ones based on simulated data and errors presented in Section 6.3.2. We consider this as an indication that the simulation study gives a reasonable impression on the GRACE error budget at monthly time scales.

6

6.5. Conclusions

In this study, we analyzed the impact of the chosen parameterization on the mass anomaly estimates from GRACE both with and without data weighting. We analyzed the impact at different temporal scales, i.e., monthly, intra-annual and multi-year scales. Both synthetic and real GRACE data were considered.

In the numerical study, four error sources (i.e., parameterization error, random error, leakage and AOD error) were considered. In this way, we found that the parameterization
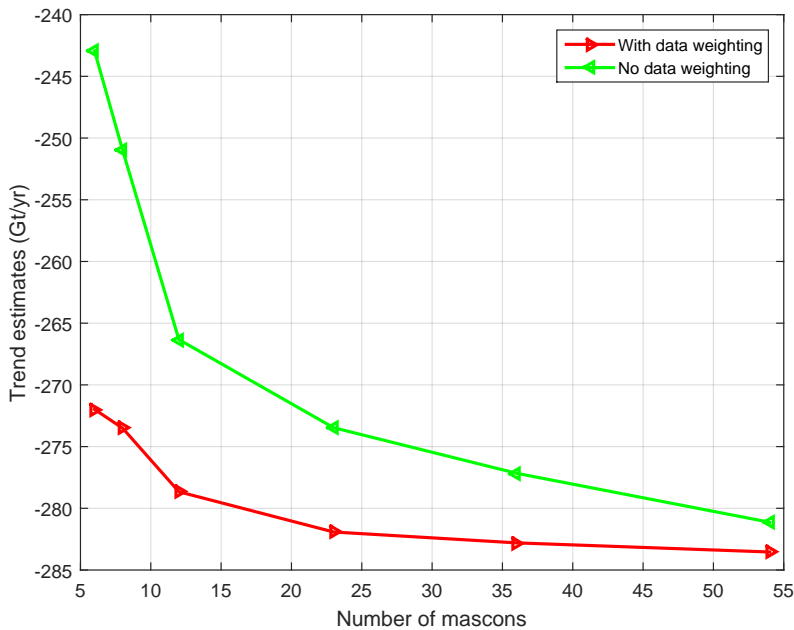
Figure 6.12: Mass anomaly trends over the period 2003–2013 estimated with and without data weighting from real GRACE data and integrated over entire Greenland, as a function of the number of mascons (Gt/yr).

error and the random error are the two major contributors to the overall error budget of the estimates produced both with and without data weighting. For long-term linear trend estimates, the parameterization error is dominant for any number of mascons. This is due to a significant reduction of the random noise when estimating a linear trend from a larger number of monthly solutions. For mean mass anomalies per calendar month, the parameterization error is dominant when the number of mascons is small; when increasing the number of mascons, the random error becomes dominant. When focusing on monthly mass anomalies, the random error is the most critical error source for almost all parameterizations, except the one with only 6 mascons, where the parameterization error is the largest error source. The AOD error and the leakage error are minor contributors to the overall error budget no matter what temporal scales are considered. To summarize, the parameterization error dominates the error budgets of estimates at a large spatial scale, whereas the random error plays a major role in the estimates at a short temporal scale.

We also investigated the impact of the parameterization using real GRACE data. First, the long-term linear trend estimates over the period 2003–2013 for whole Greenland converge with increasing number of mascons to a value of about −280 Gt/yr when using 54 mascons. This number agrees well with earlier trend estimates in *Velicogna et al.*
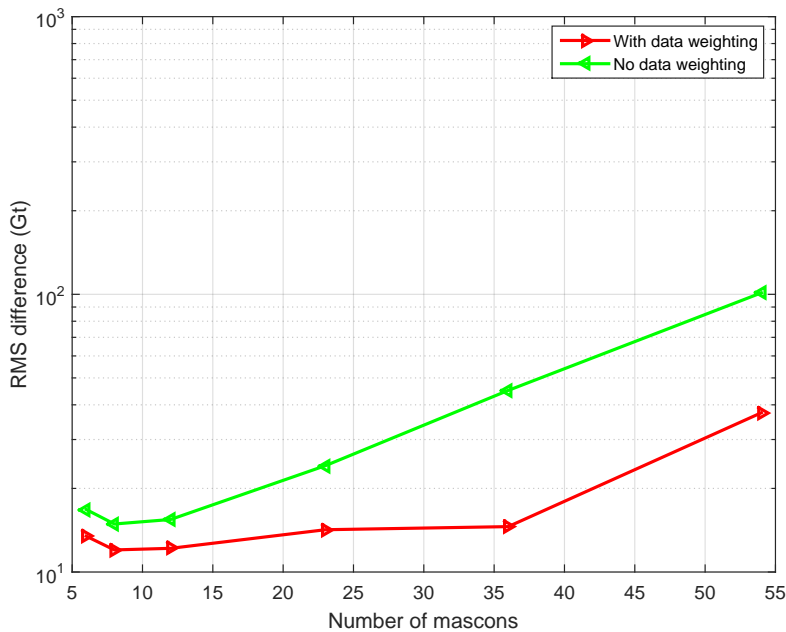
Figure 6.13: The RMS difference between mean mass anomaly estimates per calendar month from real GRACE data and SMB output, as a function of the number of mascons (Gt).

(2014) and *Schrama et al.* (2014). From the numerical study involving synthetic data and errors, we found that the converged estimates for entire Greenland agree well with the true trend with little errors (i.e., 0.8 Gt/yr with data weighting and 2 Gt/yr without data weighting). We also showed that the smallest RMS difference between mean mass anomalies per calendar month estimated from GRACE and SMB is attained when using data weighting in combination with 8 mascons. This finding is different from the study based on synthetic data and errors, where the smallest RMS difference is attained for 23 mascons. The mismatch is caused by the different ways to compute the RMS error. In the simulation study, the true mass anomalies were known, whereas they were unknown in real data analysis. Moreover, errors in the SMB estimates may also have an impact on the results using real data. Finally, the time-series of monthly mass anomalies were analyzed. The smallest RMS difference between de-trended monthly mass anomalies from GRACE and SMB is observed in the case of a large number of mascons, which is consistent with the findings of the simulation study.

In summary, we demonstrated that the parameterization of Greenland indeed has a large impact on mass anomaly estimates. The best choice of parameterization depends on the target quantity. If one is interested in the long-term trend estimates at the drainage system scale, we recommend use a relatively large number of mascons (e.g.,
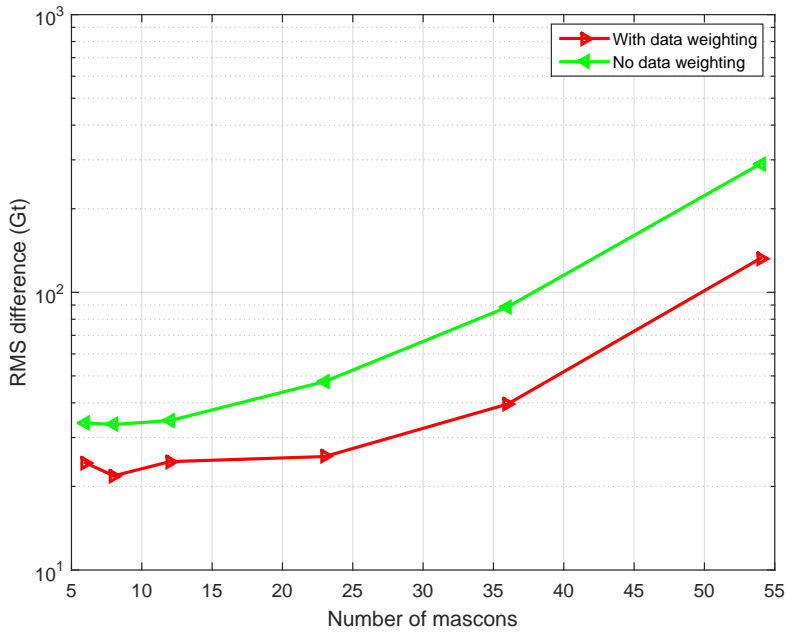
Figure 6.14: The RMS difference between traditional monthly mass anomaly in de-trended time-series from GRACE and SMB output, as a function of the number of mascons (Gt).

23) in combination with the ordinary least-squares estimator. When long-term trend estimates over entire Greenland are the target, a large number of mascons should be combined with a weighted least-squares estimator. For mean mass variations per calendar month, a medium-size parameterization involving 12–23 mascons is to be preferred in combination with a weighted least-squares estimator. Finally, if the target are monthly mass anomalies, we recommend to use a limited number of mascons (e.g., 8) in combination with a weighted least-squares estimator.

7

Conclusions and Recommendations

The primary goal of this thesis was to continue investigation of the Greenland ice sheet (GrIS) mass balance using multiple data sources. The major objectives are two-fold: (i) development of a more accurate GRACE data processing scheme; (ii) an illustration of the potential of combining GRACE-based mass estimates, ice discharge observations and regional climate model output, complemented by simple physical constraints, to better understand the GrIS mass variations at various time scales. Improving the estimates of (natural and forced) mass variations associated with individual processes is of key importance for robust projections of future GrIS mass changes and its contribution to sea level rise.

In Section 7.1 we provide a short summary. The recommendations for further research are the subject of Section 7.2.

7.1. Summary

1. A new variant of the mascon approach was developed in this study. It can be considered as a improvement upon the computational procedure proposed by *Forsberg and Reeh* (2007) and *Baur and Sneeuw* (2011). The approach consists of two major steps. In the first step, time series of gravity disturbances are computed using time series of GRACE spherical harmonic models. The data points are located at a mean satellite altitude (here, 500 km), and are homogeneously distributed over an area including Greenland and a surrounding buffer zone. Importantly, instead of using scaled unit matrices to model the noise in gravity disturbance as done in (*Forsberg and Reeh*, 2007; *Baur and Sneeuw*, 2011), we use full noise covariance matrices. In the second step, the synthesized gravity disturbances are used as observations to estimate mascon mass anomalies using weighted-least squares.

   (a) The main methodological developments are the following.
      - We take into account the full noise variance-covariance matrices $\mathbf{C_d}$ of gravity disturbances. They are propagated from the full noise covariance matrices of spherical harmonic coefficients using the law of covariance propagation. Because the matrices $\mathbf{C_d}$ appear to be ill-conditioned, with a gradually decreasing eigenvalue spectrum, we developed a methodology to approximately invert them.

- We developed refined parameterizations of entire Greenland comprising equal-area mascons and taking into account the geometry of the coastal line.

- We developed an approach to achieve spectral consistency between data and model, and demonstrated its importance. Monthly GRACE solutions and gravity disturbances synthesized from these solutions are bandlimited to the maximum spherical harmonic degree. Mascons, however, are strictly spoken not bandlimited. Without making data and model spectrally consistent, the estimated mascons are biased towards zero, in particular if a weighed least-squares estimator is used with the inverse data noise covariance matrix as the weight matrix. The bias is more pronounced the more eigenvalues of the noise covariance matrix are retained when computing an approximate inverse.

(b) Based on simulation experiments where parameterization error, random error, leakage and AOD error were considered, a set of optimal data processing parameters has been selected, to estimate mass anomalies of the GrIS over a one-year interval: this set comprises a buffer zone of 800 km, retaining the 600 largest eigenvalues of the noise covariance matrix when computing an approximate inverse, and using 23 mascons each of a size of about $90,000$ km^2 to parameterize entire Greenland. We also showed that estimating monthly mass anomalies or a long-term linear trend requires a different set of processing parameters.

(c) Using a weighted least-squares estimator, mass anomalies per mascon were estimated over the period February 2003 until December 2013 from CSR RL05 monthly GRACE solutions. By integrating mass anomalies per mascon over entire Greenland, the long-term linear trend of mass loss is estimated as -286 ± 21 Gt/yr. This value is in agreement with earlier estimates: -280 ± 58 Gt/yr (*Velicogna et al.*, 2014) over the period January 2003 until December 2013 and -278 ± 19 Gt/yr (*Schrama et al.*, 2014) over the period February 2003 until June 2013. We used a temporal regularization method by *Ditmar et al.* (2016) to evaluate the random noise level of the estimates per drainage system. In this way, we found that data weighting may suppress random noise by a factor of 1.5 to 3.0, depending on the drainage system.

(d) The mass anomalies derived from GRACE comprise SMB and ice discharge. According to *van den Broeke et al.* (2009), ice discharge manifests itself mostly as a long-term trend, whereas the seasonal mass variations are largely attributed to surface processes. Therefore the seasonal SMB provided by the model RACMO 2.3 was used to validate seasonal signals estimated from GRACE data. In particular, we used RACMO 2.3 to compare the weighted least-squares estimator with the ordinary least-squares estimator. We found that the former improves upon the latter in the range from 24% to 47% depending on the drainage system, whereas the improvement is minor for entire Greenland. We explained the latter by a significant reduction of random errors, but also by the meltwater retention signal, which for entire

Greenland likely dominates the difference between GRACE-based and SMB-based mass anomalies.

2. We analyzed the Greenland mass budget at various temporal and spatial scales, by combining GRACE data, SMB model output, and ice discharge estimates from other data. This is new compared to earlier studies, which focus on the GrIS, which covers only ~81% of the territory of Greenland (the remaining 19% are tundra and isolated glaciers, which also contribute to mass variations estimated with GRACE, in particular at the intra-annual scale). We considered two different data sets of ice discharge estimates. The first set was already presented in *Enderlin et al.* (2014). It was used to reconstruct the 2003–2012 multi-year mass trends and accelerations, as well as to separate the contributions from SMB and ice discharge, and covers 178 outlet glaciers with annual resolution. The second data set, which is used to examine intra-annual variations of ice discharge, was computed in this thesis and covers 55 marine-terminating glaciers with sub-annual resolution for the period 2009–2013. Ice discharge observations of these glaciers at monthly scale were estimated by multiplying ice flow velocities (provided by *Moon et al.* (2014)) with ice thickness values (*Morlighem et al.*, 2015). We made the analysis at the drainage system scale. Similar to *van den Broeke et al.* (2009), we divided Greenland into 5 drainage systems. We referred to these drainage systems as: (a) North (N); (b) Northwest (NW); (c) Southeast (SE); (d) Southwest (SW); and (e) Northeast (NE).

   (a) According to RACMO 2.3, the SMB accumulates mass with a mean rate of 231±122 Gt/yr over the period 2003–2012. Contrary to previous studies (*van den Broeke et al.*, 2009; *Velicogna et al.*, 2014), we computed the absolute SMB accumulation and not a relative accumulation with respect to an assumed equilibrium over the period 1960–1990.

   (b) We denote the difference between non-detrended monthly GRACE- and SMB-based mass anomaly estimates as "Total-SMB" ("Total minus SMB"). The trend of Total-SMB is -508±124 Gt/yr over the period 2003–2012, which is consistent with the ice discharge estimate of 520±31 Gt/yr in *Enderlin et al.* (2014). By combining the GRACE-based estimates, the SMB model and ice discharge, we closed the budget of the long-term trend of Greenland mass variations. At the drainage system scale, the budget is closed except for the SE and N drainage systems. The mis-closure is likely caused deficiencies of RACMO 2.3, which overestimates precipitation in the SE drainage system and underestimates precipitation in the N drainage systeml.

   (c) We also closed the budget of the long-term acceleration of mass variations over Greenland. Our estimates of accelerations in SMB-related (-29.7±2.7 Gt/yr^2), ice discharge-related (2.5±1.5 Gt/yr^2), and total (-31.1±8.1 Gt/yr^2) mass anomalies are consistent: the residual does not exceed 1 Gt/yr^2, which is well within the error bar. The two largest contributors to the observed acceleration are the SW and NW drainage systems.

   (d) By analyzing the ice discharge at the monthly time scale, we found that the ice discharge in the NW drainage system shows a noticeable seasonal

variations (~10%), whereas the seasonality of ice discharge in the SE drainage system is negligible.

(e) To analyze the mean annual cycle of total (GRACE) and cumulative SMB (RACMO2.3) mass anomalies over the period 2003–2013, we divided the entire period into eleven overlapping 13-month time intervals, each of which starts in December of the previous year and ends in December of the current year. Then, the mean mass anomaly for each calendar month was estimated by linear regression. A remarkable seasonal cycle was observed in the "Total-SMB" residuals, which could not be attributed to ice discharge, because the ice discharge could not be zero or could not increase in summer. We suggested that seasonal variations of non-SMB mass anomalies ("Total-SMB") may be caused by a delayed meltwater runoff. To estimate the instantaneous amount of meltwater subject to runoff, we fitted the Total-SMB residuals in two periods before and after the flat feature (April-May and September-November) with a linear function. In this way, we found that meltwater is retained in Greenland between May and October, with a maximum in the month of July of about 100 Gt.

3. In order to understand the impact of the parameterization on the mass anomaly estimates, we performed a simulation study over the period 2003–2013. The signal was generated by combining the altimetry trend over the period 2003–2009 from ICESat and de-trended SMB mass anomalies from RACMO2.3. To make the simulation more realistic, all relevant error sources (i.e., parameterization error, leakage, AOD error and random error) were taken into account. Thereafter, we did a similar analysis using real GRACE data. We found that the parameterization has a strong effect on the estimates at different temporal scales.

(a) We showed that the parameterization error and the random error are the two major contributors to the overall error budget of the estimates produced both with and without data weighting. An exception are estimates of the long-term linear trend. Here, the parameterization error is the dominant error source for any number of mascons. We explained this by the fact that in this case random noise is significantly reduced due to the large number of months used in the estimate. As for the mean mass anomalies per calendar month, we found that the random error plays a major role only when the size of the mascons is small, whereas the parameterization error dominates when mascons of large sizes are used. For monthly mass anomalies, we found that the random error dominates the error budget when the number of mascons ranges from 8 to 54, whereas the parameterization error plays an important role only when using just 6 mascons. The AOD errors and leakage are minor for estimates at different temporal scales. When using real GRACE data, we found that most findings of the simulation study are confirmed.

(b) We showed that the optimal parameterization depends on the target. If one is interested in the long-term trend at the drainage system scale, a large number of mascons should be used in combination with the ordinary least-squares estimator. When the long-term trend estimates over entire Greenland is

targeted, a large number of mascons and data weighting should be used. For mean mass variations per calendar month, we found that it is better to divide Greenland into 12-23 mascons in combination with data weighting. Finally, when the target are monthly mass anomalies, large-size mascons (e.g., 8 mascons) in combination with data weighting provides the best results.

7

7.2. Recommendations

A number of follow-up activities are recommended as a continuation of this study.

1. The variant of the mascon approach developed in this study implies that the mass variation within each mascon is uniform. This is not realistic. An attempt to conquer this problem has been made by *Sasgen et al.* (2010), who used ice discharge velocities to define a spatially varying pattern of mass variations inside each mascon. Further work, however, is needed to adjust the mascon approach in order to allow for spatially varying signals inside each mascon.

2. Though this study focussed on Greenland, we expect that data weighting may also improve the quality of mass anomaly estimates for other applications, such as ice mass loss over Antarctica or monitoring groundwater storage variations.

3. As shown in Fig. 4.18, the residual time series of de-trended GRACE- and SMB-based estimates of GrIS mass variations show a noticeable multi-year signal. This may, among others, indicate accelerated ice discharge and/or long-term meltwater retention. Further studies are needed to explain this signal.

4. The meltwater retention at the drainage system scale and the entire ice-sheet scale has been estimated in this study. Further studies, however, are needed to understand the underlying mechanisms and to describe the spatial distribution of meltwater retention.

A

Eigenvalue decomposition of the noise covariance matrix $\mathbf{C_d}$

A statistically-optimal inversion of gravity disturbances into mass anomalies per mascon requires the inversion of the noise covariance matrix $\mathbf{C_d}$. Since this matrix is ill-conditioned some type of regularization is needed. Here, we use an eigenvalue decomposition

$$\mathbf{C_d} = \mathbf{Q}\Lambda\mathbf{Q}^T, \tag{A.1}$$

To minimize the loss of significant digits during the computations, we do not compute explicitly the noise covariance matrix but apply the following procedure.

We start with Eq. (4.2) in matrix-vector form:

$$\mathbf{d} = \mathbf{F}\delta\mathbf{p}, \tag{A.2}$$

where the vector $\delta\mathbf{p}$ comprises the SHCs of a monthly GRACE solution (ΔC_{lm}, ΔS_{lm}), and $\mathbf{F}$ is the matrix of spherical harmonic synthesis that maps SHCs into gravity disturbances. If the noise covariance matrix of the SHCs is $\mathbf{C}_{\delta\mathbf{p}}$ and no constraints are applied when estimating the SHCs,

$$\mathbf{C}_{\delta\mathbf{p}} = \mathbf{N}^{-1}, \tag{A.3}$$

where $\mathbf{N}$ is the normal matrix exploited in the computation of SHCs from GRACE level-1b data. The Cholesky decomposition of this matrix is:

$$\mathbf{N} = \mathbf{LL}^T. \tag{A.4}$$

According to the law of covariance propagation, the noise covariance matrices $\mathbf{C}_{\delta\mathbf{p}}$ and $\mathbf{C_d}$ are related to each other as

$$\mathbf{C_d} = \mathbf{F}\mathbf{C}_{\delta\mathbf{p}}\mathbf{F}^T. \tag{A.5}$$

A substitution of Eqs. (A.3) and (A.4) in Eq. (A.5) gives

$$\mathbf{C_d} = \mathbf{F}\left(\mathbf{LL}^T\right)^{-1}\mathbf{F}^T = \mathbf{F}\left(\mathbf{L}^{-1}\right)^T\mathbf{L}^{-1}\mathbf{F}^T = \mathbf{HH}^T, \tag{A.6}$$

where

$$\mathbf{H} = \mathbf{F}\left(\mathbf{L}^{-1}\right)^T. \tag{A.7}$$

Let

$$\mathbf{H} = \mathbf{U}\Sigma\mathbf{V}^T, \tag{A.8}$$

be the SVD of the matrix **H**, where Σ is the matrix of singular values, and **U** and **V** is the matrix of left and right singular vectors, respectively. Equation (A.8) and the equality

$$\mathbf{V}^T \mathbf{V} = \mathbf{I}. \tag{A.9}$$

allow Eq. (A.6) to be re-written as

$$\mathbf{C_d} = \mathbf{U}\Sigma\mathbf{V}^T\mathbf{V}\Sigma^T\mathbf{U}^T = \mathbf{U}\Sigma\Sigma^T\mathbf{U}^T. \tag{A.10}$$

It is easy to see that $\Sigma\Sigma^T$ is a square diagonal matrix with elements λ_i defined as

$$\lambda_i = \sigma_i^2 \qquad (i = 1,...N_d), \tag{A.11}$$

where σ_i are the singular values forming the matrix Σ and N_d is the number of data points. Therefore, the representation of matrix **C$_d$** given by Eq. (A.10) satisfies the properties of the eigendecomposition, so that λ_i are the eigenvalues of **C$_\mathbf{d}$**,

$$\mathbf{Q} = \mathbf{U}, \qquad \text{and} \qquad \Lambda = \Sigma\Sigma^T. \tag{A.12}$$

Thus, the operations prescribed by Eqs. (A.4), (A.7), (A.8), and (A.12) provide the eigenvalue decomposition of the matrix **C$_\mathbf{d}$** without the need to compute this matrix explicitly.

In order to demonstrate the superior stability of the proposed computational procedure, we perform the following experiment. We use the normal equation matrix for the monthly GRACE solution of August 2006 from DMT. We compute explicitly the noise covariance matrix **C**$_d$ and perform an eigenvalue decomposition of this matrix. Alternatively, we follow the procedure outlined before. Figure A.1 shows the eigenvalues of **C**$_d$ for both procedures. The direct computation of the eigenvalues of **C**$_d$ provides only the first 900 eigenvalues. The flattening of the eigenvalue spectrum beyond an index of about 900 is caused by numerical roundoff errors, and is at the level of the largest eigenvalue times machine epsilon for IEEE double precision arithmetic. Using the proposed procedure allows to compute the first 1400 eigenvalues before numerical roundoff errors become dominant. From this we conclude that the proposed procedure is numerically more stable, and therefore better suited to deal with ill-conditioned noise covariance matrices when computing a weighted least-squares solution.
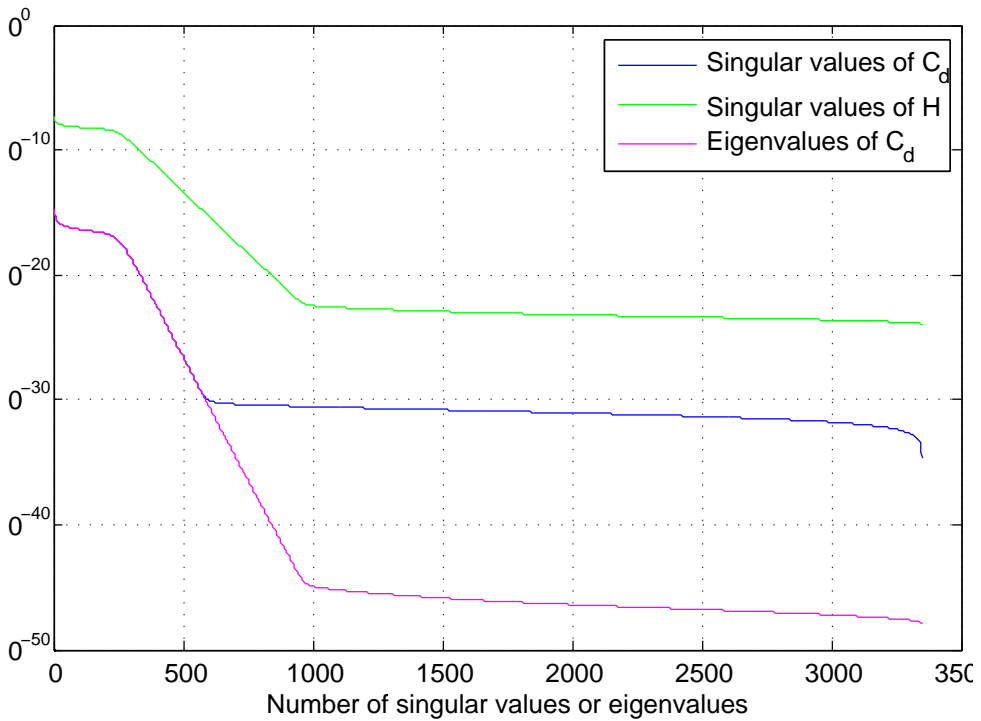
A

Figure A.1: Eigenvalues of the matrix **C_d** computed directly (blue) and using the procedure suggested in this study (red). The singular values of the matrix **H** are shown in green.

.

B

Robustness of GRACE-based estimates at the intra-annual time scale

In this appendix, we investigate the robustness of GRACE-based estimates of mass anomalies at the intra-annual time scale. In this way, we want to understand to what extent they could be interpreted as signal or noise. The mean annual cycle of "Total-SMB" differences shows three periods of almost null month-to-month variations (nearly flat segments in Fig. 5.11): February–March, May–July, and November–December. If we assume that the main contributor to Total-SMB variations is ice discharge, these flat features are unphysical: ice discharge cannot stop. Therefore, they should be explained either by melt water retention or by errors in RACMO2.3- and GRACE-based estimates.

To assess a possible impact of errors in RACMO2.3 and in GRACE-based mass anomalies, we estimate mass anomalies from GRACE data using different processing parameters. This includes: i) the use of a weighted least-squares estimator with the inverse of the noise covariance matrix $\mathbf{C_d}$ as the weight matrix or the use of the ordinary least-squares estimator; ii) to retain a different number of eigenvalues of $\mathbf{C_d}$ when computing a weighted least-squares estimate of the mass anomalies (i.e., 200, 400 and 600 eigenvalues, respectively); iii) a different handling of the surrounding ocean (i.e., parameterization with one patch, parameterization with four patches (cf. Fig. B.1), and no parameterization, respectively); iv) a different choice of spherical harmonic degree-one coefficients (i.e., from *Swenson et al.* (2008), *Cheng et al.* (2013), and *Sun et al.* (2016), respectively). Note that only one parameter varies at a time, while the other parameters are defined as in the primary data processing scheme. To make the investigation more comprehensive, we also compare Total-SMB annual cycles derived from different GRACE-based estimates (i.e., from estimates computed in this study, from *Wouters et al.* (2008), and from *Watkins et al.* (2015), respectively).

The results are depicted in Figs. B.1-B.5. Obviously, the presence and appearance of the quasi-null Total-SMB month-to-month variations during February-March and November–December varies from case to case. For instance, when the surrounding ocean is parameterized with four patches, the February-March feature becomes less flat; when using an ordinary least-squares estimator, the November-December flat feature is not significant either, similarly to the estimates of *Wouters et al.* (2008). The flat features of February–March and November–December do not appear in the Total-SMB differences obtained with the JPL mascon solutions of *Watkins et al.* (2015). On the other hand, the flat feature of May-July persists, no matter what processing parameters are
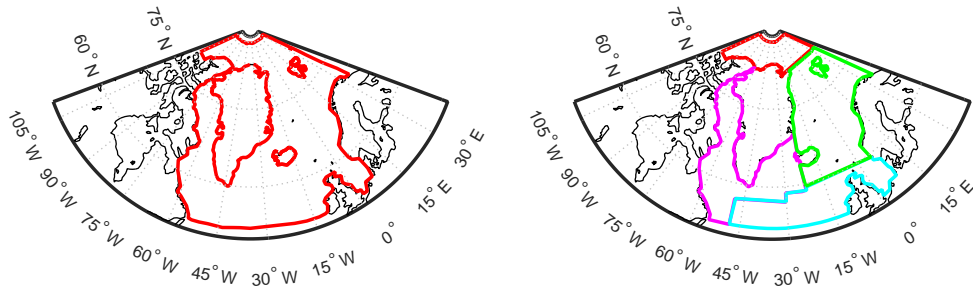
Figure B.1: Parameterization of the ocean area around Greenland with one (left) and four (right) patches.

chosen and which GRACE product is utilized. Therefore, we suggest that the May-June feature is not triggered by noise in the estimates, but is likely physical. Most probably, this signal is caused by meltwater retention.

(a)

(b)

(c)

(d)
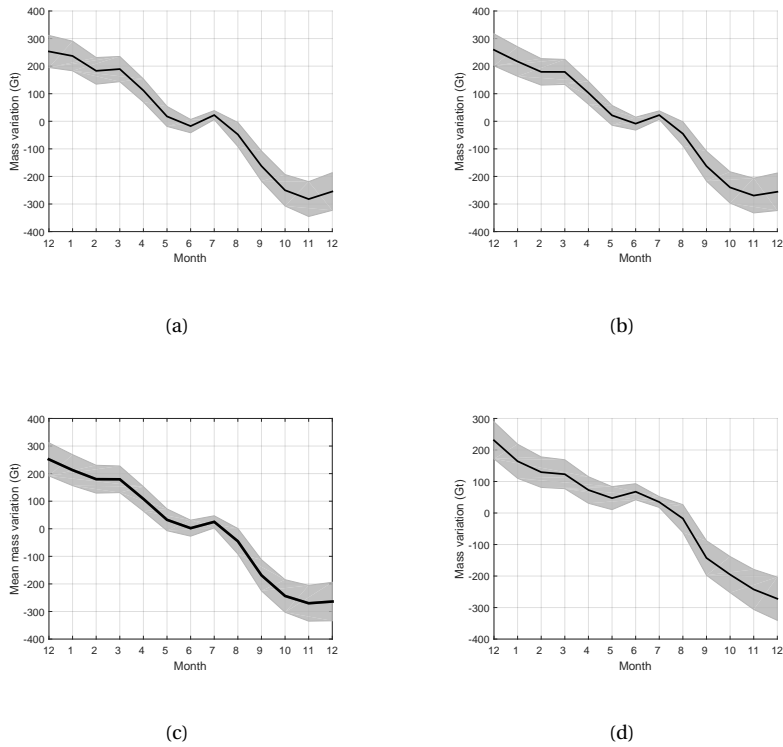
Figure B.2: Mean annual cycle of "Total-SMB" mass anomalies estimated using different approaches to data weighting and inversion of the matrix $\mathbf{C_d}$: data weighting based on matrix $\mathbf{C_d}$ where 200 (a), 400 (b), or 600 (c) eigenvalues are retained; no data weighting (d).

(a)

(b)

(c)
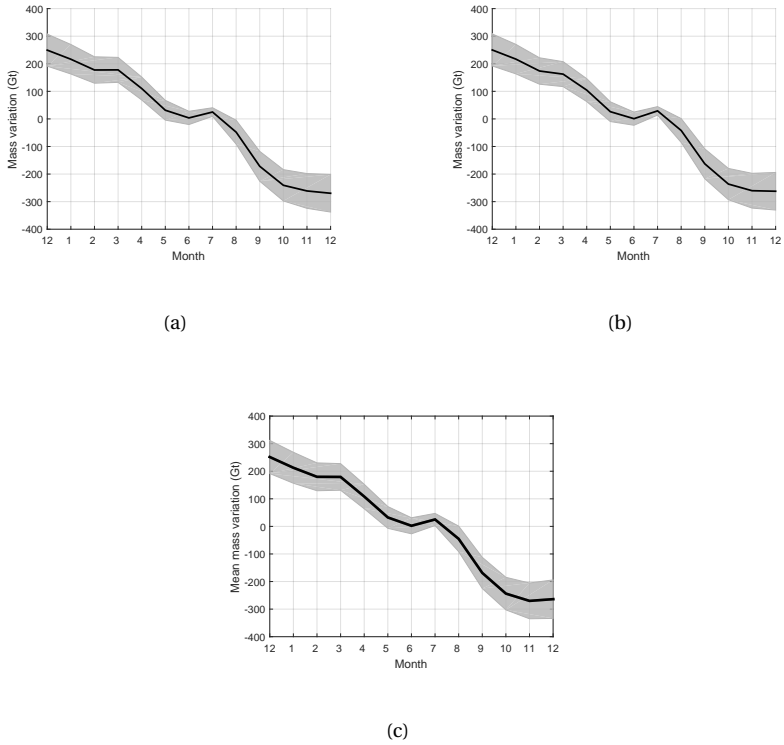
Figure B.3: Mean annual cycle of "Total-SMB" mass anomalies estimated using different parameterizations of the ocean surrounding the GrIS: one patch (a), four patches (b), and no parameterization (c).

(a)

(b)

(c)

Figure B.4: Mean annual cycle of "Total-SMB" mass anomalies estimated with different degree-one coefficients: from *Swenson et al.* (2008) (a), *Cheng et al.* (2013) (b), *Sun et al.* (2016) (c).

(a)

(b)

Figure B.5: Mean annual cycle of "Total-SMB" mass anomalies using the GRACE-based mass anomalies from *Wouters et al.* (2008) (a) and *Watkins et al.* (2015).

Bibliography

A, G., J. Wahr, and S. Zhong (2013), Computations of the viscoelastic response of a 3-d compressible earth to surface loa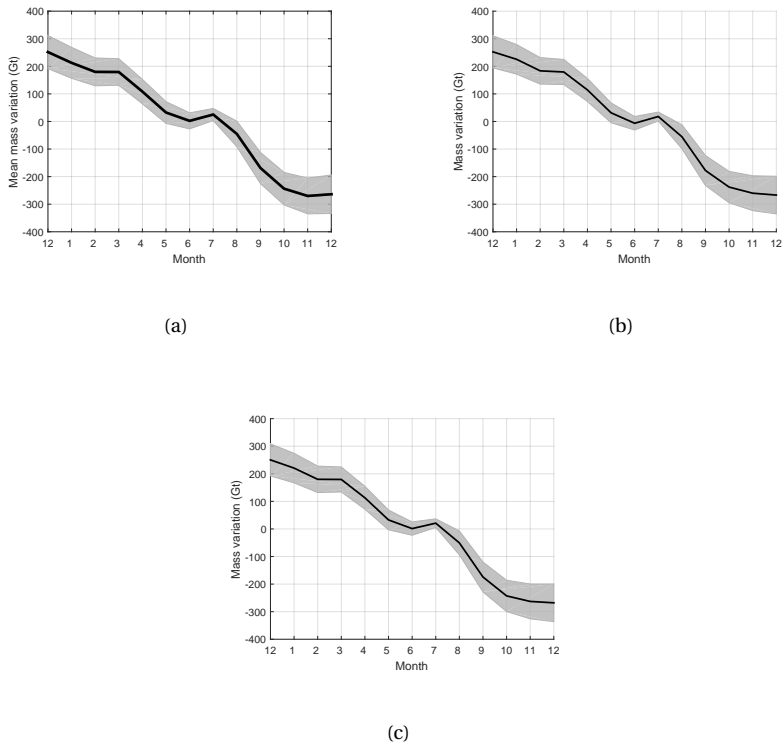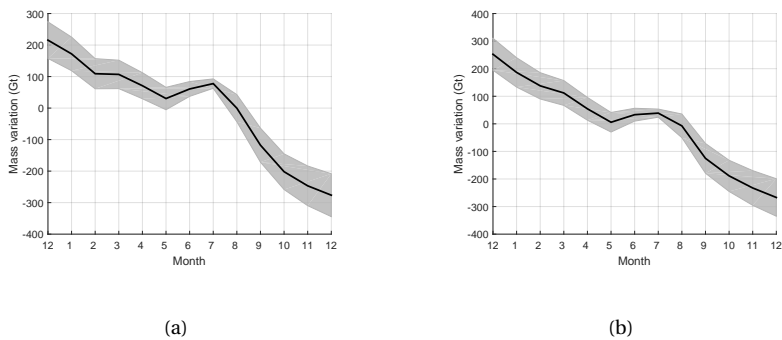ding: an application to glacial isostatic adjustment in antarctica and canada, *Geophysical Journal International*, *192*(2), 557–572, doi:10.1093/gji/ggs030.

Baur, O. (2013), Greenland mass variation from time-variable gravity in the absence of GRACE, *Geophysical Research Letters*, *40*(16), 4289–4293, doi:10.1002/grl.50881.

Baur, O., and N. Sneeuw (2011), Assessing Greenland ice mass loss by means of point-mass modeling: A viable methodology, *Journal of Geodesy*, *85*(9), 607–615, doi:10.1007/s00190-011-0463-1.

Beighley, R. E., R. L. Ray, Y. He, H. Lee, L. Schaller, K. M. Andreadis, M. Durand, D. E. Alsdorf, and C. K. Shum (2011), Comparing satellite derived precipitation datasets using the hillslope river routing (hrr) model in the congo river basin, *Hydrological Processes*, *25*(20), 3216–3229, doi:10.1002/hyp.8045.

Bettadpur, S. (2012), UTCSR Level-2 Processing Standards Document for Level-2 Product Release 0005, GRACE 327–742, CSR Publ. GR-12-xx, Rev. 4.0, University of Texas at Austin, *Tech. rep.*

Bonin, J., and D. Chambers (2013), Uncertainty estimates of a GRACE inversion modelling technique over Greenland using a simulation, *Geophysical Journal International*, *194*(1), 212–229, doi:10.1093/gji/ggt091.

Chandler, D., J. Wadham, G. Lis, T. Cowton, A. Sole, I. Bartholomew, J. Telling, P. Nienow, E. Bagshaw, D. Mair, et al. (2013), Evolution of the subglacial drainage system beneath the greenland ice sheet revealed by tracers, *Nature Geoscience*, *6*(3), 195–198.

Chen, J., M. Rodell, C. Wilson, and J. Famiglietti (2005), Low degree spherical harmonic influences on gravity recovery and climate experiment (grace) water storage estimates, *Geophysical Research Letters*, *32*(14).

Chen, J. L., C. R. Wilson, and B. D. Tapley (2006), Satellite gravity measurements confirm accelerated melting of Greenland ice sheet, *Science*, *313*(5795), 1958–1960, doi:10.1126/science.1129007.

Cheng, M., B. D. Tapley, and J. C. Ries (2013), Deceleration in the Earth's oblateness, *Journal of Geophysical Research: Solid Earth*, *118*(2), 740–747, doi:10.1002/jgrb.50058, 00011.

Christensen, J. H., O. B. Christensen, P. Lopez, E. Van Meijgaard, and M. Botzet (1996), The hirham4 regional atmospheric climate model, *DMI Scientific report*, *4*, 51.

Dahle, C., F. Flechtner, C. Gruber, D. König, R. König, G. Michalak, and K.-H. Neumayer (2012), GFZ GRACE level-2 processing standards document for level-2 product release 0005, *Tech. rep.*, doi:10.2312/GFZ.b103-1202-25.

Davis, C. H. (1998), Elevation Change of the Southern Greenland Ice Sheet, *Science*, *279*(5359), 2086–2088, doi:10.1126/science.279.5359.2086.

Ditmar, P., J. Teixeira da Encarnação, and H. Hashemi Farahani (2012), Understanding data noise in gravity field recovery on the basis of inter-satellite ranging measurements acquired by the satellite gravimetry mission grace, *Journal of Geodesy*, *86*(6), 441–465, doi:10.1007/s00190-011-0531-6.

Ditmar, P., N. Tangdamrongsub, J. Ran, and R. Klees (2016), Mass anomaly time-series based on satellite gravimetry data: regularization and noise quantification, manuscript submitted for Journal of Geodesy.

Dobslaw, H., F. Flechtner, I. Bergmann-Wolf, C. Dahle, R. Dill, S. Esselborn, I. Sasgen, and M. Thomas (2013), Simulating high-frequency atmosphere-ocean mass variability for dealiasing of satellite gravity observations: AOD1B RL05, *Journal of Geophysical Research: Oceans*, *118*(7), 3704–3711, doi:10.1002/jgrc.20271.

Enderlin, E. M., I. M. Howat, S. Jeong, M.-J. Noh, J. H. van Angelen, and M. R. van den Broeke (2014), An improved mass budget for the greenland ice sheet, *Geophysical Research Letters*, *41*(3), 866–872, doi:10.1002/2013GL059010, 2013GL059010.

Ettema, J., M. R. van den Broeke, E. van Meijgaard, W. J. van de Berg, J. L. Bamber, J. E. Box, and R. C. Bales (2009a), Higher surface mass balance of the Greenland ice sheet revealed by high-resolution climate modeling, *Geophysical Research Letters*, *36*(12), L12,501, doi:10.1029/2009GL038110.

Ettema, J., M. R. van den Broeke, E. van Meijgaard, W. J. van de Berg, J. L. Bamber, J. E. Box, and R. C. Bales (2009b), Higher surface mass balance of the Greenland ice sheet revealed by high-resolution climate modeling, *Geophysical Research Letters*, *36*(12), L12,501, doi:10.1029/2009GL038110.

Felikson, D., T. J. Urban, N. Pie, B. C. Gunter, R. Harpold, and B. E. Schutz (2016), Comparison of elevation change detection methods from ICESat altimetry over the Greenland and Antarctic Ice Sheets, manuscript submitted for Transactions on Geoscience and Remote Sensing.

Fettweis, X., H. Gallée, F. Lefebre, and J.-P. Van Ypersele (2005), Greenland surface mass balance simulated by a regional climate model and comparison with satellite-derived data in 1990–1991, *Climate Dynamics*, *24*(6), 623–640.

Forsberg, R., and N. Reeh (Eds.) (2007), *Mass change of the Greenland Ice Sheet from GRACE*, vol. 73, Gravity Field of the Earth – 1st meeting of the International Gravity Field Service, Harita Dergisi, Ankara.

Forsberg, R., L. Sørensen, and S. Simonsen (2017), Greenland and antarctica ice sheet mass changes and effects on global sea level, *Surveys in Geophysics*, *38*(1), 89–104, doi: 10.1007/s10712-016-9398-7.

Forster, R. R., M. R. van den Broeke, C. Miège, E. W. Burgess, J. H. van Angelen, J. T. Lenaerts, L. S. Koenig, J. Paden, C. Lewis, S. P. Gogineni, et al. (2014), Extensive liquid meltwater storage in firn within the greenland ice sheet, *Nature Geoscience*, *7*(2), 95–98.

Gent, P. R., G. Danabasoglu, L. J. Donner, M. M. Holland, E. C. Hunke, S. R. Jayne, D. M. Lawrence, R. B. Neale, P. J. Rasch, M. Vertenstein, P. H. Worley, Z. L. Yang, and M. Zhang (2011), The community climate system model version 4, *Journal of Climate*, *24*(19), 4973–4991, doi:10.1175/2011JCLI4083.1.

González, Á. (2010), Measurement of Areas on a Sphere Using Fibonacci and Latitude-Longitude Lattices, *Mathematical Geosciences*, *42*(1), 49–64, doi:10.1007/s11004-009-9257-x.

Jacob, T., J. Wahr, W. Pfeffer, and S. Swenson (2012), Recent contributions of glaciers and ice caps to sea level rise, *Nature*, *482*(7386), 514–8, doi:10.1038/nature10847.

Jekeli, C. (1981), Modifying Stokes' function to reduce the error of geoid undulation computations, *Journal of Geophysical Research*, *86*(B8), 6985–6990.

Joughin, I., R. B. Alley, and D. M. Holland (2012), Ice-sheet response to oceanic forcing, *Science*, *338*(6111), 1172–1176, doi:10.1126/science.1226481.

Khan, S. A., A. Aschwanden, A. A. Bjørk, J. Wahr, K. K. Kjeldsen, and K. H. Kjaer (2015), Greenland ice sheet mass balance: a review, *Reports on Progress in Physics*, *046801*, 1–26, doi:10.1088/0034-4885/78/4/046801.

Koch, K.-R., and J. Kusche (2002), Regularization of geopotential determination from satellite data by variance components, *Journal of Geodesy*, *76*(5), 259–268, doi:10.1007/s00190-002-0245-x.

Korona, J., E. Berthier, M. Bernard, F. Rémy, and E. Thouvenot (2009), Spirit. spot 5 stereoscopic survey of polar ice: reference images and topographies during the fourth international polar year (2007–2009), *ISPRS Journal of Photogrammetry and Remote Sensing*, *64*(2), 204–212.

Larour, E., H. Seroussi, M. Morlighem, and E. Rignot (2012), Continental scale, high order, high spatial resolution, ice sheet modeling using the ice sheet system model (issm), *Journal of Geophysical Research: Earth Surface*, *117*(F1), n/a–n/a, doi:10.1029/2011JF002140, f01022.

Longuevergne, L., B. R. Scanlon, and C. R. Wilson (2010), Grace hydrological estimates for small basins: Evaluating processing approaches on the high plains aquifer, usa, *Water Resources Research*, *46*(11), W11,517, doi:10.1029/2009WR008564.

Luthcke, S. B., H. J. Zwally, W. Abdalati, D. D. Rowlands, R. D. Ray, R. S. Nerem, F. G. Lemoine, J. J. McCarthy, and D. S. Chinn (2006a), Recent Greenland ice mass loss by drainage system from satellite gravity observations., *Science (New York, N.Y.)*, *314*(October), 1286–1289, doi:10.1126/science.1130776.

Luthcke, S. B., D. D. Rowlands, F. G. Lemoine, S. M. Klosko, D. Chinn, and J. J. McCarthy (2006b), Monthly spherical harmonic gravity field solutions determined from GRACE inter-satellite range-rate data alone, *Geophysical Research Letters*, *33*(2), L02,402, doi: 10.1029/2005GL024846.

Luthcke, S. B., T. J. Sabaka, B. D. Loomis, A. A. Arendt, J. J. McCarthy, and J. Camp (2013), Antarctica, Greenland and Gulf of Alaska land-ice evolution from an iterated GRACE global mascon solution, *Journal of Glaciology*, *59*(216), 613–631, doi:10.3189/2013JoG12J147.

Miège, C., R. R. Forster, L. Brucker, L. S. Koenig, D. K. Solomon, J. D. Paden, J. E. Box, E. W. Burgess, J. Z. Miller, L. McNerney, N. Brautigam, R. S. Fausto, and S. Gogineni (2016), Spatial extent and temporal variability of greenland firn aquifers detected by ground and airborne radars, *Journal of Geophysical Research: Earth Surface*, *121*(12), 2381–2398, doi:10.1002/2016JF003869, 2016JF003869.

Moon, T., I. Joughin, B. Smith, and I. Howat (2012), 21st-century evolution of Greenland outlet glacier velocities., *Science (New York, N.Y.)*, *336*(6081), 576–8, doi:10.1126/science.1219985.

Moon, T., I. Joughin, B. Smith, M. R. Van Den Broeke, W. J. Van De Berg, B. Noël, and M. Usher (2014), Distinct patterns of seasonal Greenland glacier velocity, *Geophysical Research Letters*, *41*(20), 7209–7216, doi:10.1002/2014GL061836.

Morlighem, M., E. Rignot, J. Mouginot, H. Seroussi, and E. Larour (2015), Icebridge bedmachine greenland, version 2, *NASA DAAC at the National Snow and Ice Data Center, Boulder, Colorado, USA (doi: 10.5067/AD7B0HQNSJ29)*.

Mouginot, J., E. Rignot, B. Scheuchl, I. Fenty, A. Khazendar, M. Morlighem, A. Buzzi, and J. Paden (2015), Fast retreat of zachariæ isstrøm, northeast greenland, *Science*, *350*(6266), 1357–1361.

Muller, P. M., and W. L. Sjogren (1968), Mascons: lunar mass concentrations., *Science (New York, N.Y.)*, *161*(3842), 680–684.

Noël, B., W. J. van de Berg, E. van Meijgaard, P. Kuipers Munneke, R. S. W. van de Wal, and M. R. van den Broeke (2015), Evaluation of the updated regional climate model racmo2.3: summer snowfall impact on the greenland ice sheet, *The Cryosphere*, *9*(5), 1831–1844, doi:10.5194/tc-9-1831-2015.

Ramillien, G., A. Cazenave, and O. Brunau (2004), Global time variations of hydrological signals from grace satellite gravimetry, *Geophysical Journal International*, *158*(3), 813–826.

Rennermalm, A. K., L. C. Smith, V. Chu, J. Box, R. R. Forster, M. Van den Broeke, D. Van As, and S. E. Moustafa (2013a), Evidence of meltwater retention within the greenland ice sheet, *The Cryosphere*, *7*, 1433–1445.

Rennermalm, A. K., L. C. Smith, V. W. Chu, J. E. Box, R. R. Forster, M. R. Van den Broeke, D. Van As, and S. E. Moustafa (2013b), Evidence of meltwater retention within the greenland ice sheet, *The Cryosphere*, *7*(5), 1433–1445, doi:10.5194/tc-7-1433-2013.

Rowlands, D. D., S. B. Luthcke, S. M. Klosko, F. G. R. Lemoine, D. S. Chinn, J. J. McCarthy, C. M. Cox, and O. B. Anderson (2005), Resolving mass flux at high spatial and temporal resolution using GRACE intersatellite measurements, *Geophysical Research Letters*, *32*(4), 1–4, doi:10.1029/2004GL021908.

Rowlands, D. D., S. B. Luthcke, J. J. McCarthy, S. M. Klosko, D. S. Chinn, F. G. Lemoine, J.-P. Boy, and T. J. Sabaka (2010), Global Mass Flux Solutions from GRACE: A Comparison of Parameter Estimation Strategies - Mass Concentrations Versus Stokes Coefficients, *115*, 1–19, doi:10.1029/2009JB006546.

Sasgen, I., Z. Martinec, and J. Bamber (2010), Combined GRACE and InSAR estimate of West Antarctic ice mass loss, *Journal of Geophysical Research: Earth Surface*, *115*(4), F04,010, doi:10.1029/2009JF001525.

Savcenko, R., and W. Bosch (2010), EOT11a—Empirical ocean tide model from multi-mission satellite altimetry, *Tech. Rep. Report No 89*, doi:10013/epic.43894.d001.

Save, H., S. Bettadpur, and B. D. Tapley (2016), High-resolution csr grace rl05 mascons, *Journal of Geophysical Research: Solid Earth*, *121*(10), 7547–7569, doi:10.1002/2016JB013007, 2016JB013007.

Schlegel, N.-J., D. N. Wiese, E. Y. Larour, M. M. Watkins, J. E. Box, X. Fettweis, and M. R. van den Broeke (2016), Application of grace to the evaluation of an ice flow model of the greenland ice sheet, *The Cryosphere Discussions*, *2016*, 1–35, doi:10.5194/tc-2015-224.

Schrama, E. J. O., and B. Wouters (2011), Revisiting Greenland ice sheet mass loss observed by GRACE, *Journal of Geophysical Research: Solid Earth*, *116*(2), B02,407, doi:10.1029/2009JB006847.

Schrama, E. J. O., B. Wouters, and R. Rietbroek (2014), A mascon approach to assess ice sheet and glacier mass balances and their uncertainties from GRACE data, *Journal of Geophysical Research: Solid Earth*, *119*(7), 6048–6066, doi:10.1002/2013JB010923.

Selmes, N., T. Murray, and T. James (2011), Fast draining lakes on the greenland ice sheet, *Geophysical Research Letters*, *38*(15).

Shepherd, A., E. R. Ivins, G. A, V. R. Barletta, M. J. Bentley, S. Bettadpur, K. H. Briggs, D. H. Bromwich, R. Forsberg, N. Galin, M. Horwath, S. Jacobs, I. Joughin, M. a. King, J. T. M. Lenaerts, J. Li, S. R. M. Ligtenberg, A. Luckman, S. B. Luthcke, M. McMillan, R. Meister, G. Milne, J. Mouginot, A. Muir, J. P. Nicolas, J. Paden, A. J. Payne, H. Pritchard, E. Rignot,

H. Rott, L. S. Sørensen, T. a. Scambos, B. Scheuchl, E. J. O. Schrama, B. Smith, A. V. Sundal, J. H. van Angelen, W. J. van de Berg, M. R. van den Broeke, D. G. Vaughan, I. Velicogna, J. Wahr, P. L. Whitehouse, D. J. Wingham, D. Yi, D. Young, and H. J. Zwally (2012), A reconciled estimate of ice-sheet mass balance., *Science*, *338*(6111), 1183–9, doi:10.1126/science.1228102.

Siemes, C., P. Ditmar, R. E. M. Riva, D. C. Slobbe, X. L. Liu, and H. H. Farahani (2013), Estimation of mass change trends in the Earth's system on the basis of GRACE satellite data, with application to Greenland, *Journal of Geodesy*, *87*(1), 69–87, doi:10.1007/s00190-012-0580-5.

Simpson, M. J., G. A. Milne, P. Huybrechts, and A. J. Long (2009), Calibrating a glaciological model of the greenland ice sheet from the last glacial maximum to present-day using field observations of relative sea level and ice extent, *Quaternary Science Reviews*, *28*(17), 1631–1657.

Slater, D., P. Nienow, T. Cowton, D. Goldberg, and A. Sole (2015), Effect of near-terminus subglacial hydrology on tidewater glacier submarine melt rates, *Geophysical Research Letters*, *42*(8), 2861–2868.

Slobbe, D., P. Ditmar, and R. Lindenbergh (2009), Estimating the rates of mass change, ice volume change and snow volume change in greenland from icesat and grace data, *Geophysical Journal International*, *176*(1), 95–106.

Sørensen, L., S. B. Simonsen, K. Nielsen, P. Lucas-Picher, G. Spada, G. Adalgeirsdottir, R. Forsberg, and C. Hvidberg (2011), Mass balance of the greenland ice sheet (2003–2008) from icesat data–the impact of interpolation, sampling and firn density, *The Cryosphere*, *5*, 173–186.

Stedinger, J. R., and G. D. Tasker (1986), Regional hydrologic analysis, 2, model-error estimators, estimation of sigma and log-pearson type 3 distributions, *Water Resources Research*, *22*(10), 1487–1499.

Stocker, T. F., D. Qin, G.-K. Plattner, M. Tignor, S. K. Allen, J. Boschung, A. Nauels, Y. Xia, V. Bex, and P. M. Midgley (2013), Climate change 2013: The physical science basis, *Tech. rep.*, 1535 pp.

Sun, Y., P. Ditmar, and R. Riva (2016), Observed changes in the earth's dynamic oblateness from grace data and geophysical models, *Journal of Geodesy*, *90*(1), 81–89, doi:10.1007/s00190-015-0852-y.

Swenson, S. (2012), Grace monthly land water mass grids netcdf release 5.0. ver. 5.0., *PO. DAAC, CA, USA. Dataset accessed [2016-12-01] at http://dx.doi.org/10.5067/TELND-NC005*, *10*.

Swenson, S., and J. Wahr (2006), Post-processing removal of correlated errors in GRACE data, *Geophysical Research Letters*, *33*(8), L08,402, doi:10.1029/2005GL025285.

Swenson, S., D. Chambers, and J. Wahr (2008), Estimating geocenter variations from a combination of grace and ocean model output, *Journal of Geophysical Research: Solid Earth*, *113*(B8), n/a–n/a, doi:10.1029/2007JB005338, b08410.

Tapley, B. D., S. Bettadpur, J. C. Ries, P. F. Thompson, and M. M. Watkins (2004), GRACE measurements of mass variability in the Earth system., *Science (New York, N.Y.)*, *305*(5683), 503–505, doi:10.1126/science.1099192.

Thomas, R., T. Akins, B. Csatho, M. Fahnestock, P. Gogineni, C. Kim, and J. Sonntag (2000), Mass balance of the greenland ice sheet at high elevations, *Science*, *289*(5478), 426–428, doi:10.1126/science.289.5478.426.

Thompson, P. F., S. Bettadpur, and B. D. Tapley (2004), Impact of short period, non-tidal, temporal mass variability on GRACE gravity estimates, *Geophysical Research Letters*, *31*(6), L06,619, doi:10.1029/2003GL019285.

Van Angelen, J., M. Van den Broeke, B. Wouters, and J. Lenaerts (2014), Contemporary (1960–2012) evolution of the climate and surface mass balance of the greenland ice sheet, *Surveys in geophysics*, *35*(5), 1155–1174.

van den Broeke, M., J. Bamber, J. Ettema, E. Rignot, E. Schrama, W. J. van de Berg, E. van Meijgaard, I. Velicogna, and B. Wouters (2009), Partitioning recent Greenland mass loss., *Science (New York, N.Y.)*, *326*(5955), 984–6, doi:10.1126/science.1178176.

van den Broeke, M. R., E. M. Enderlin, I. M. Howat, and B. P. Noël (2016), On the recent contribution of the greenland ice sheet to sea level change, *The Cryosphere*, *10*(5), 1933.

Velicogna, I. (2009), Increasing rates of ice mass loss from the Greenland and Antarctic ice sheets revealed by GRACE, *Geophysical Research Letters*, *36*(19), L19,503, doi:10.1029/2009GL040222.

Velicogna, I., and J. Wahr (2005), Greenland mass balance from GRACE, *Geophysical Research Letters*, *32*(18), 1–4, doi:10.1029/2005GL023955.

Velicogna, I., and J. Wahr (2006), Acceleration of Greenland ice mass loss in spring 2004., *Nature*, *443*(7109), 329–331, doi:10.1038/nature05168.

Velicogna, I., and J. Wahr (2013), Time-variable gravity observations of ice sheet mass balance: Precision and limitations of the grace satellite data, *Geophysical Research Letters*, *40*(12), 3055–3063, doi:10.1002/grl.50527.

Velicogna, I., T. C. Sutterley, and M. R. V. D. Broeke (2014), Regional acceleration in ice mass loss from Greenland and Antarctica using GRACE time-variable gravity data, (January 2003), 8130–8137, doi:10.1002/2014GL061052.Received.

Wahr, J., M. Molenaar, and F. Bryan (1998), Time variability of the earth's gravity field: Hydrological and oceanic effects and their possible detection using grace, *Journal of Geophysical Research: Solid Earth*, *103*(B12), 30,205–30,229, doi:10.1029/98JB02844.

Wahr, J., D. Wingham, and C. Bentley (2000), A method of combining icesat and grace satellite data to constrain antarctic mass balance, *Journal of Geophysical Research: Solid Earth*, *105*(B7), 16,279–16,294, doi:10.1029/2000JB900113.

Watkins, M. M., D. N. Wiese, D.-N. Yuan, C. Boening, and F. W. Landerer (2015), Improved methods for observing earth's time variable mass distribution with grace using spherical cap mascons, *Journal of Geophysical Research: Solid Earth*, *120*(4), 2648–2671, doi:10.1002/2014JB011547, 2014JB011547.

Wingham, D., A. Ridout, R. Scharroo, R. Arthern, and C. Shum (1998), Antarctic elevation change from 1992 to 1996, *Science*, *282*(October), 1996–1999, doi:10.1126/science.282.5388.456.

Wouters, B., D. Chambers, and E. J. O. Schrama (2008), GRACE observes small-scale mass loss in Greenland, *Geophysical Research Letters*, *35*(20), L20,501, doi:10.1029/2008GL034816.

Wouters, B., J. L. Bamber, M. R. van den Broeke, J. T. M. Lenaerts, and I. Sasgen (2013), Limits in detecting acceleration of ice sheet mass loss due to climate variability, *Nature Geoscience*, *6*(8), 613–616, doi:10.1038/ngeo1874.

Xu, G. (2010), *Sciences of Geodesy-I: Advances and Future Directions*, Springer Science & Business Media.

Zwally (2002), ICESat's laser measurements of polar ice, atmosphere, ocean and land, *Journal of Geodynamics*, *34*, 405–445.

Zwally, H. J., M. B. Giovinetto, M. A. Beckley, and J. L. Saba (2012), Antarctic and greenland drainage systems, gsfc cryospheric sciences laboratory, *Available at ic esat4. gsfc. nasa. gov/cryo_data/ant_grn_drainage_systems.php.*, *1*, 2015.

Samenvatting

De Groenlandse ijskap verliest tegenwoordig massa als gevolg van complexe ijs-klimaatinteracties, die moeten worden begrepen voor betrouwbare voorspellingen van toekomstige zeespiegelstijging. Dit proefschrift richt zich op het schatten van massa-afwijkingen op Groenland met behulp van data van de GRACE satellietgravimetrie missie. Maandelijkse oplossingen van het GRACE gravitatieveld worden bewerkt met een nieuwe variant van de "masconmethode". De Groenlandse regio is gesplitst in verschillende "mascons", waarbij we aannemen dat de massa-afwijkingen daarbinnen lateraal homogeen zijn.

Zwaartekrachtsverstoringen op the gemiddelde satelliethoogte worden gesynthetiseerd vanuit de GRACE sferisch harmonische coëfficiënten. Ze worden gebruikt als pseudo-observaties om the massa-afwijkingen te schatten voor de mascons met behulp van kleinste-kwadraten technieken. Er wordt geen regularisatie toegepast. De volledige ruiscovariantiematrix van de zwaartekrachtsverstoringen wordt gepropageerd vanuit de volledige ruiscovariantiematrix van de sferische harmonische coëfficiënten met behulp van de propagatiewetten. Deze matrices vertegenwoordigen een volledige stochastische beschrijving van de ruis in de data op voorwaarde dat deze normaal verdeeld is. De inverse van de ruiscovariantiematrix wordt gebruikt als weging in de kleinste-kwadratenschatting van de massa-afwijkingen in de mascons. Het beperkte spectrale bereik wordt meegenomen door het toepassen van een laagdoorlaatfilter op de ontwerpmatrix, zodat het functionele model spectraal consistent is met de data.

Met numerieke experimenten, van gesimuleerde signalen en data, demonstreren we het belang van de dataweging en de spectrale consistentie tussen het masconmodel en de pseudo-observaties. De ontwikkelde methode wordt vervolgens toegepast op de maandelijke zwaartekrachtsveldoplossingen van GRACE CSR RL05 met hun volledige ruiscovariantiematrices. We hebben vijf drainagesystemen geïdentificeerd. De geschatte massa-afwijkingen per mascon worden geïntegreerd over de individuele drainagesystemen en over heel Groenland. Onze bevindingen laten zien dat de onzekerheid van de geschatte massa-afwijkingen tussen 1.5 en 3.0 keer wordt gereduceerd, afhankelijk van het drainagesysteem. Daarnaast vergelijkingen we tijdreeksen van massa-afwijkingen, waarvan de trend is afgetrokken, met vergelijkbare tijdreeksen van het Regional Atmospheric Climate Model (RACMO 2.3), die de oppervlaktemassabalans beschrijft. We laten zien dat de statistisch optimaal gewogen GRACE data de verschillen met 24–47 % reduceert.

Vervolgens combineren we GRACE, de gemodelleerde oppervlaktemassabalans en ijsafvoerdata om de massabalans van Groenland systematisch te analyseren op verschillende tijd- en ruimteschalen. We laten onder andere een opslag van smeltwater zien van 100 ± 20 Gt, die piekt in juli. Smeltwateropslag is met name groot in de noordelijke, noordwestelijke en zuidoostelijke drainagesystemen. Een analyse van de afvoergletsjer-

snelheden laat zien dat de bijdrage van gletsjerafvoer klein is; op het niveau van enkele Gt. Daarnaast stellen wij een simpele methode voor om GRACE data te gebruiken om oppervlaktemassabalansschattingen in de winter te valideren, gebaseerd op het feit dat deze niet negatief kunnen zijn.

Uiteindelijk gebruiken we numerieke simulaties en echte data om de optimale bewerkingsstrategie voor GRACE data te bepalen (voornamelijk mascongrootte) voor een bepaalde temporale schaal: maandelijkse massa-afwijkingen, gemiddelde massa-afwijkingen per kalendermaand en trends over langere periodes. We demonstreren de twee grote bijdragers voor de fout willekeurige fouten en parametrisatiefouten zijn, waarvan de laatste voortkomen uit ruimtelijke verschillen van massa-afwijkingen binnen de mascons. Onze bevindingen laten zien dat de fouten in de trendschattingen voornamelijk voortkomen uit parametrisatiefouten, zodat deze schattingen moeten worden gemaakt met behulp van kleine mascons met behulp van de ongewogen kleinste-kwadratenmethode. De fouten in de gemiddelde massa-afwijkingen per kalendermaand worden gedomineerd door parametrisatiefouten als de mascons te groot zijn en bij te kleine mascons door willekeurige fouten. Daarom moeten deze schattingen geproduceerd worden met behulp van mascons met gemiddelde grootte en de gewogen kleinste-kwadratenmethode. Uiteindelijk, laten onze bevinden zien dat willekeurige fouten de fouten in de maandelijkse massa-afwijkingen domineren. Daarom adviseren wij in dit geval grote mascons te gebruiken met de gewogen kleinste-kwadratenmethode.

Onze nieuwe variant van de masonmethode en de resultaten van deze thesis kunnen gebruikt worden in vervolgstudies naar de Groenlandse ijskap betreffende de hydrologie, gletsjerdynamica en oppervlaktemassabalans en hun onderlinge interacties.

Curriculum Vitae

Jiangjun Ran was born in Chongqing, People's Republic of China on May 08, 1986. In September 2004, he enrolled at SouthWest JiaoTong University (SWJTU), China. He received the B.Sc. in Surveying and Mapping Engineering from SWJTU in June 2008. In September 2008, he started the study for a M.Sc. degree at University of Chinese Academy of Sciences (UCAS) in Beijing. From September 2009 to February 2011, he had worked for the numerical analysis of Chinese satellite gravity mission at Institute of Geodesy and Geophysics, Chinese Academy of Sciences (IGG, CAS). After this, he started to process GRACE Level 1B data at National Chiao Tung University in Taiwan, including the orbit determination of GRACE satellites using GNSS data. From November 2011, he worked as a Ph.D. candidate in the group of Physical and Space Geodesy at Delft University of Technology, aiming to analyze the mass variations in Greenland.

Acknowledgements

This is not the final destination, but a fresh start.

Before moving forward, I would like to write down my gratitude to everyone who helped me in the PhD study. Accomplishing this PhD study would not have been possible without the support of many people. The first one who comes to my mind is my daily supervisor, Dr. Pavel Ditmar. Without his help, I will never reach this far. I would like to give him my greatest gratitude because of his remarkable patience and solid knowledge. I also want to thank my promotor, Prof. Roland Klees, for providing me the opportunity to pursue my PhD study in Physical and Space Geodesy (PSG) at Delft University of Technology. His critical comments and constructive recommendations guided this research.

The members of the doctoral committee are acknowledged for their evaluations and valuable comments. Prof. M.R. van den Broeke and colleagues from Institute for Marine and Atmospheric Research of Utrecht University are grateful for providing RACMO 2.3 and SNOWPACK. Dr. Twila Moon from National Snow and Ice Data Center is thanked for providing ice velocity observations of outlet glaciers in Greenland. I also want to thank Dr. Ellyn M. Enderlin from University of Maine for her ice discharge estimates of outlet glaciers. In particular, Miren, Prof. M.R. van den Broeke and Dr. Bert Wouters are appreciated for their valuable discussions. Many thanks go to the secretaries of the Department of Geoscience and Remote Sensing, and the colleagues for their help. For instance, Riccardo and Marcel are thanked for the rehearsal and translating the summary to Dutch, respectively.

I would like to thank my former Chinese supervisors Prof. Xu and Prof. Zhong from the Institute of Geodesy and Geophysics, Chinese Academy of Sciences, for their support over the past several years. I also want to thank Prof. Li from China Spacesat Co., Ltd., Prof. Zhou and Prof. Luo from Huazhong University of Science and Technology for their concern of my research. Prof. Hwang from National Chiao Tung University in Taiwan and Dr. Liu in Fugro Intersite B.V. are also thanked for their valuable discussions.

Last but not least, I would like to thank my family for their love and encouragement, which inspire me in my life.

Jiangjun Ran
Delft
July 6, 2017

List of Publications

Journals:

1. **Jiangjun Ran**, Pavel Ditmar, Roland Klees. 2017. Statistically optimal estimation of Greenland Ice Sheet mass variations from GRACE monthly solutions using an improved mascon approach, Journal of Geodesy. Under review

2. **Jiangjun Ran**, Pavel Ditmar, Roland Klees. 2017. Optimal mascon geometry in estimating mass anomalies within Greenland from GRACE. Submitted to Geophysical Journal International

3. **Jiangjun Ran** Miren Vizcaino, Pavel Ditmar, Michiel R. van den Broeke, Twila Moon, Ellyn M. Enderlin, Bert Wouters and Roland Klees. 2017. Seasonal mass variations show timing and magnitude of meltwater storage in the Greenland ice sheet, The Cryosphere. To be submitted

4. Pavel Ditmar, Natthachet Tangdamrongsub, **Jiangjun Ran** (✉), Roland Klees. 2017. Mass anomaly time-series based on satellite gravimetry data: regularization and noise quantification. To be submitted

Conference Proceedings:

1. Pavel Ditmar, **Jiangjun Ran**, Roland Klees. 2016. Regularization of GRACE mass anomaly time-series and quantifying random noise in it (Oral), International Symposium on Gravity, Geoid and Height Systems. Thessaloniki, Greece

2. Pavel Ditmar, Roland Klees, R. Riva, C. Slobbe, Miren Vizcaino, Marcel Kleinherenbrink, Thomas Frederikse, **Jiangjun Ran**, Olga Didova, Natthachet Tangdamrongsub, and Hassan Farahani. 2016. Studying global water re-distribution in the Earth's system with satellite gravimetry and other remote sensing techniques (Oral). The Netherlands Center for Geodesy and Geo-informatics (NCG) symposium. Enschede, the Netherlands

3. **Jiangjun Ran**, Pavel Ditmar, Roland Klees, Miren Vizcaino. 2015. Advanced analysis of mass balance of the Greenland Ice Sheet from GRACE and surface mass balance modeling (Oral). The International Union of Geodesy and Geophysics. Prague, Czech Republic

4. **Jiangjun Ran**, Pavel Ditmar, Roland Klees. 2014. Towards improved post-processing of GRACE monthly gravity fields to estimate regional mass variations of the Greenland Ice Sheet (Oral), GRACE Science Team Meeting 2014. Potsdam, Germany